The role of myeloid-derived growth factor (MYDGF) as an angiocrine signal for hepatocyte proliferation

Inaugural-Dissertation

zur Erlangung des Doktorgrades
der Mathematisch-Naturwissenschaftlichen Fakultät
der Heinrich-Heine-Universität Düsseldorf

vorgelegt von

Paula Follert
aus Wien

Düsseldorf, März 2024

aus dem Institut für Stoffwechselphysiologie
der Heinrich-Heine-Universität Düsseldorf

Gedruckt mit der Genehmigung der
Mathematisch-Naturwissenschaftlichen Fakultät der
Heinrich-Heine-Universität Düsseldorf

Berichterstatter:

1. Prof. Dr. Eckhard Lammert

2. Prof. Dr. Axel Gödecke

Tag der mündlichen Prüfung: 15. Juli 2024

Table of Contents

I. Annotations to this thesis

Parts of this thesis were published in (Große-Segerath and Follert et al., 2024) in particular parts of the "Material and Methods" section and figures including figure legends in the "Results" section.

Author contributions adapted from the manuscript (Große-Segerath and Follert et al., 2024)

L.G. and P.F. performed most of the experiments; L.G. performed stretch experiments with human hepatic ECs, EdU proliferation and apoptosis assays with 2D hepatocyte cultures, and established 3D organoid cultures. P.F. performed stretch experiments for flow cytometric analysis of cell viability, PH3 and EdU proliferation staining with 2D hepatocyte cultures and HepG2 cells and caspase-3 staining with 2D hepatocyte cultures, proliferation assays of daily treated 3D organoid cultures, and Western blot experiments with human hepatocytes and liver lysates. P.K. helped P.F. with the analysis of cell viability via flow cytometry. M.K.-K. and K.C.W. provided MYDGF KO mice. T.B., K.B. and J.E. performed partial hepatectomy in mice. T.B. worked under the guidance of B.L., and K.B. and J.E. worked under the guidance of J.S. The mice were then monitored by L.G., P.F. and D.E., and their livers were isolated and analyzed by L.G. and P.F.; L.G. and P.F. performed tail vein injections in mice. S.Ha. and S.L. performed the LC-MS/MS experiment following discussions on the experimental design with H.A.-H.; D.E. participated in discussions, data management and statistical evaluations. N. L.-T. and W.T.K. performed in-situ split liver surgery and provided human blood serum samples. S.He. performed liver resection and provided human blood plasma samples. E.L. supervised and guided L.G. and P.F. during their experiments. L.G. wrote the manuscript together with E.L. and with the help from P.F. All authors read and contributed to the manuscript.

P.F. contributed experimentally about 50% to the manuscript.

Parts of this thesis were adapted from my master thesis “Functional characterization of a novel angiocrine signal in hepatocytes” that was conducted between 2019-2020 at the “Institute of metabolic physiology” at Heinrich Heine University Düsseldorf.

II. List of abbreviations

A

AAV	Adeno-associated virus
AdDMEM	Advanced Dulbecco's Modified Eagle Medium
AFP	Alpha-fetoprotein
AKT	Serine-threonine protein kinase
A.m.	Ante meridiem
ANOVA	Analysis of variance
Arg	Arginase

B

Bax	Bcl-2-associated X protein
Bad	Bcl-2 antagonist of cell death
BCA	Bicinchoninic acid
BD	Bile ducts
BMI	Body mass index
BSA	Bovine serum albumin

C

C19orf10	Chromosome 19 open reading frame 10
Ca^{2+}	Calcium
CCl4	Carbon tetrachloride
cDNA	Complementary deoxyribonucleic acid
CHRM	Cryopreserved hepatocyte recovery medium
CO_2	Carbon dioxide
COD	Cause of death
Ctrl	Control
CXCR2	C-X-C chemokine receptor type 2
CXCR4	C-X-C chemokine receptor type 4
CXCR7	C-X-C chemokine receptor type 7

D

DAPI	4′,6-diamidino-2-phenylindole
dH_2O	Distilled water
DKD	Diabetic kidney disease
DNA	Deoxyribonucleic acid
dNTP mix	Deoxynucleotide mix

E

EC	Endothelial cell
ECM	Extracellular matrix
EdU	5-ethynyl-2'-deoxyuridine
EGF	Epidermal growth factor
EGFR	Epidermal growth factor receptor
ELISA	Enzyme-linked immunosorbent assay
ERK	Extracellular signal-regulated kinase
ET-1	Endothelin-1

F

FBS	Fetal bovine serum
FGF	Fibroblast growth factor
FGFR1	Fibroblast growth factor receptor 1
Fiji	Fiji is just imageJ

G

g	Gram
GAPDH	Glycerinaldehyd-3-phosphat-dehydrogenase
GC	Genome copies
GFP	Green fluorescent protein
GH	Growth hormone
GLP-1	Glucagon-like peptide-1
Glul	Glutamate-ammonia ligase
GPCR	G protein-coupled receptor
gp130	Glycoprotein 130

H

h	Hours
HA	Hepatic artery
Hamp	Hepcidin
HCAEC	Human coronary artery endothelial cell
HCC	Hepatocellular carcinoma
HEPES	4-(2-hydroxyethyl)-1-piperazineethanesulfonic acid
HGF	Hepatocyte growth factor
HNF4α	Hepatocyte nuclear factor 4 alpha
HPRT	Hypoxanthine-phosphoribosyltransferase
HRP	Horseradish peroxidase
HSC	Hepatic stellate cell
HV	Hepatic venule

I

ICAM	Intercellular adhesion molecule
Id1	Inhibitor of DNA binding 1
IGF-1	Insulin growth factor 1
IL-6	Interleukin-6
Igfbp	Insulin-like growth factor-binding protein

J

JAK	Janus kinase

K

KCl	Potassium chloride
KC	Kupffer cell
kDa	Kilodalton
KO	Knockout

L

LC-MS/MS	Liquid chromatography tandem-mass spectrometry
LDL	Low-density lipoproteins
LSEC	Liver sinusoidal endothelial cell
LSM	Laser scanning microscope

M

M	Molar
MACS	Magnetic activated cell sorting
MAPK	Mitogen-activated protein kinase
MAPKK	Mitogen-activated protein kinase kinase
MAPKKK	Mitogen-activated protein kinase kinase kinase
MAFLD	Metabolic dysfunction-associated fatty liver disease
$MgCl_2$	Magnesium chloride
MI	Myocardial infarction
Min	Minute
ml	Milliliter
mM	Millimolar
mmHg	Millimetre of mercury
MMPs	Matrix metalloproteinases
MT1	Metallothionein 1
MYDGF	Myeloid-derived growth factor

N

NaCl	Sodium chloride
NAFLD	Non-alcoholic fatty liver disease
NDS	Normal donkey serum
NF-κB	Nuclear factor kappa-light-chain-enhancer of activated B cells
ng	Nanogram
nm	Nanometer
NO	Nitric oxide

O

Oat	Ornithine aminotransferase
o/n	Over night

P

PBS	Phosphate-buffered saline
Pck	phosphoenolpyruvate carboxykinase
PFA	Paraformaldehyde
PH3	Phospho-Histone H3
PHx	Partial hepatectomy
PI3K	Phosphatidylinositol 3-kinase
p.m.	Post meridiem
POD	Postoperative day
PPARα	Peroxisome proliferator-activated receptor alpha
PV	Portal vein

Q

qPCR	Quantitative real time polymerase chain reaction

R

RNA	Ribonucleic acid
rpm	Revolutions per minute
RPLP0	Ribosomal protein lateral stalk subunit P0
RSPO	R-Spondin
RT	Room temperature
RTK	Receptor tyrosine kinase

S

s	Seconds
SEM	Standard error of mean
SLT	Split liver transplantation
STAT3	Signal transducer and activator of transcription 3

T

T2D	Type 2 diabetes
TBG	Thyroxine binding globulin
TGF-α	Transforming growth factor-alpha
TGF-β1	Transforming growth factor-beta 1
TGF-βR	Transforming growth factor-beta receptor
TLR	Toll-like receptor
TNF-α	Tumor necrosis factor-alpha

U

uPA	Urokinase plasminogen activator

V

VEGF	Vascular endothelial growth factor
VEGFR	Vascular endothelial growth factor receptor

W

WB	Western blot
WI	Wntless

Special characters

β2M	Beta-2-microglobulin
µg	Microgram
µl	Microliter
µm	Micrometer
µM	Micromolar
%	Percentage
°C	Degree Celsius
2D	Two-dimensional
3D	Three-dimensional

1. Summary

The liver is the largest detoxifying organ in the human body and has a remarkable ability to regenerate. When two-thirds of the liver is surgically dissected, a process called partial hepatectomy (PHx), the liver mass restores within 5-7 days in mice and within 14 days in humans. The process of liver regeneration is initiated by increased blood flow in the remaining one third of the liver. This causes vasodilation of hepatic blood vessels, which results in mechanical stretching of hepatic endothelial cells (hepatic ECs) that line the inside of the blood vessels and triggers the secretion of angiocrine signals. The latter promote the proliferation and survival of hepatocytes to restore the original liver mass.

In this study, we described the role of myeloid-derived growth factor (MYDGF) as an angiocrine signal for hepatocyte proliferation and thus liver regeneration. Previous experiments in our laboratory have shown that MYDGF is secreted by mechanically stretched primary human hepatic ECs and has a proliferation- and survival-promoting effect on primary human hepatocytes. Here we demonstrated that our stretching conditions, which have been shown to trigger the release of MYDGF, do not lead to increased cell death of mechanically stretched primary human hepatic ECs. Subsequently, we verified our previous results that MYDGF induces proliferation and prevents apoptosis of 2D cultured primary human hepatocytes. We also showed that daily MYDGF treatment triggers the growth and proliferation of primary human hepatocyte organoids. In addition, we reported that phosphorylation of mitogen-activated protein kinase (MAPK) and signal transducer and activator of transcription 3 (STAT3) is involved in MYDGF-induced hepatocyte proliferation. Next, we analyzed the expression kinetics of MYDGF in humans and mice and revealed that MYDGF levels are elevated at an earlier timepoint after liver surgery compared to the known angiocrine signal: hepatocyte growth factor (HGF). Finally, we investigated the effect of MYDGF on liver regeneration after two-thirds PHx. Our results showed that overexpression of MYDGF in the liver significantly increased hepatocyte proliferation and improved liver regeneration after two-thirds PHx in mice, and a knockout (KO) of MYDGF significantly abolished hepatocyte proliferation after two-thirds PHx.

In conclusion, our results showed that MYDGF is an angiocrine signal that enhances the proliferation and survival of primary human hepatocytes *in vitro*. *In vivo*, MYDGF increases in the first hours after liver surgery and represents a promoting factor for liver regeneration. Thus, our results provide a basis for further investigation of MYDGF as a potential therapeutic drug to stimulate liver regeneration after liver surgery.

2. Zusammenfassung

Die Leber ist das größte Entgiftungsorgan des menschlichen Körpers und besitzt eine bemerkenswerte Regenerationsfähigkeit. Wenn zwei Drittel der Leber chirurgisch entfernt werden, was als partielle Hepatektomie (PHx) bezeichnet wird, stellt sich die Lebermasse bei Mäusen innerhalb von 5-7 Tagen und beim Menschen innerhalb von 14 Tagen wieder her. Der Prozess der Leberregeneration wird durch einen erhöhten Blutfluss im verbleibenden Drittel der Leber eingeleitet. Dieses führt zu einer Vasodilatation in den Leberblutgefäßen, was eine mechanische Streckung der Leberendothelzellen (hepatischen ECs) zur Folge hat, die das Innere der Blutgefäße auskleiden, und die Ausschüttung von angiokrinen Signalen auslöst. Letztere fördern die Proliferation und das Überleben von Hepatozyten, um die ursprüngliche Lebermasse wiederherzustellen.

In dieser Studie haben wir die Rolle des myeloid-derived growth factor (MYDGF) als angiokrines Signal für die Proliferation von Hepatozyten und damit für die Leberregeneration beschrieben. Frühere Experimente in unserem Labor haben gezeigt, dass MYDGF von mechanisch gedehnten primären menschlichen hepatischen ECs sezerniert wird und eine proliferations- und überlebensfördernde Wirkung auf primäre menschliche Hepatozyten hat. Hier konnten wir zeigen, dass unsere Dehnungsbedingungen, die nachweislich die Freisetzung von MYDGF auslösen, nicht zu einem erhöhten Zelltod von mechanisch gedehnten primären humanen hepatischen ECs führen. Anschließend bestätigten wir unsere früheren Ergebnisse, dass MYDGF die Proliferation induziert und die Apoptose von in 2D kultivierten primären humanen Hepatozyten verhindert. Wir zeigten auch, dass eine tägliche MYDGF-Behandlung das Wachstum und die Proliferation primärer menschlicher Hepatozyten-Organoide auslöst. Darüber hinaus berichteten wir, dass die Phosphorylierung der mitogen-aktivierten Proteinkinase (MAPK) und des Signal Transducers und Aktivators der Transkription 3 (STAT3) an der MYDGF-induzierten Hepatozytenproliferation beteiligt ist. Als Nächstes analysierten wir die Expressionskinetik von MYDGF bei Menschen und Mäusen und stellten fest, dass MYDGF im Vergleich zu dem bekannten angiokrinen Signal, dem hepatocyte growth factor (HGF), zu einem früheren Zeitpunkt nach einer Leberoperation erhöht ist. Schließlich untersuchten wir die Wirkung von MYDGF auf die Leberregeneration nach einer Zweidrittel-PHx. Unsere Ergebnisse zeigten, dass die Überexpression von MYDGF in der Leber die Hepatozytenproliferation signifikant erhöhte und die Leberregeneration nach einer Zweidrittel-PHx bei Mäusen verbesserte, während ein Knockout (KO) von MYDGF die Hepatozytenproliferation nach einer Zweidrittel-PHx signifikant aufhob.

Zusammenfassend zeigten unsere Ergebnisse, dass MYDGF ein angiokrines Signal ist, das *in vitro* die Proliferation und das Überleben menschlicher Hepatozyten fördert. *In vivo*

steigt MYDGF in den ersten Stunden nach der Leberoperation an und ist ein fördernder Faktor für die Leberregeneration. Unsere Ergebnisse bilden somit eine Grundlage für die weitere Untersuchung von MYDGF als potenzielles therapeutisches Mittel zur Stimulierung der Leberregeneration nach einer Leberoperation.

3. Introduction

3.1 Liver

3.1.1 Anatomy

The liver is a brownish organ with smooth external surface, which is conserved in all vertebrates (Sibulesky, 2013, Trefts et al., 2017). The organ makes up nearly 2% of the human adult body weight and is located in the right upper quadrate of the abdomen (Sibulesky, 2013, Abdel-Misih and Bloomston, 2010). Ligamentous attachments ensure the position of the liver in the upper abdomen next to the diaphragm, while the falciform ligament morphologically separates the human liver in a left and right lobe (Abdel-Misih and Bloomston, 2010). In general, the human liver can be divided into four different liver lobes, consisting of right, left, quadrate, caudate lobe (**Figure 1a**) (Kruepunga et al., 2019). These lobes can be further separated into eight segments according to Couinaud's classification (Couinaud, 1954). This classification is widely used in liver surgery and subdivides the liver lobes based on their vascular and biliary relationships (Couinaud, 1954, Mahadevan, 2020). In mice the liver is located in the entire subdiaphragmatic region of the body and is divided into four lobes: left, right, median, and caudate liver lobe (**Figure 1b**) (Rogers and Dintzis, 2018, Kruepunga et al., 2019). Compared to the human liver, the mouse liver has a larger left liver lobe, whereas in humans it is the right liver lobe (Rogers and Dintzis, 2018). Due to its many structural similarities to the human liver (e.g., cell types of the liver, hepatic lobules), the mouse serves as a model organism for studying the function and regenerative capacity of the liver (Rogers and Dintzis, 2018).

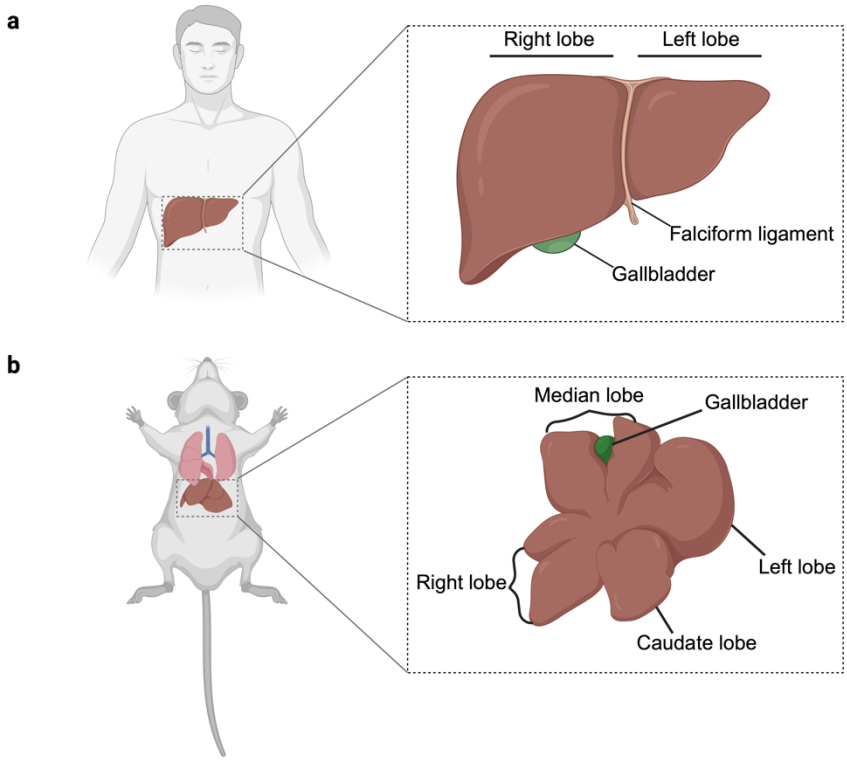

Figure 1: Location and anatomy of the human and mouse liver.
(**a**) Location of the liver in the human body, with a magnified view of the right and left liver lobe separated by the falciform ligament, as well as location of the gallbladder. The quadrate and caudate lobes are not visible due to their dorsal position. (**b**) Location of the liver in the mouse body and magnified view of the four liver lobes: median, left, caudate and right lobe; as well as location of the gallbladder. Figure was created with BioRender.com by Paula Follert according to (Rogers and Dintzis, 2018, Mitchell and Willenbring, 2008).

In addition to its morphological anatomy, the liver also has a functional unit made up of the hepatic lobules, whose architecture is similar in humans and mice (Ishibashi et al., 2009, Si-Tayeb et al., 2010, Rogers and Dintzis, 2018). Hepatic lobules have a hexagonal structure with a hepatic venule in the center and are surrounded by six portal triads (Si-Tayeb et al., 2010, Ishibashi et al., 2009). Portal triads are composed of bile ducts, lymphatics, branches of the hepatic artery and branches of the portal vein (**Figure 2**) (Ishibashi et al., 2009, Vekemans and Braet, 2005). Portal triads and the hepatic venule are connected by small blood vessels, called liver sinusoids (Vollmar and Menger, 2009, Si-Tayeb et al., 2010). As the structure of the hepatic lobules indicates, the liver is characterized by a dual blood supply (Abdel-Misih and Bloomston, 2010). 25-30% of the liver blood supply is provided by the hepatic artery, which delivers oxygen-rich blood from the heart (Abdel-Misih and Bloomston, 2010). The remaining 70-75% of the blood supply occurs via the portal vein, which carries deoxygenated but nutrient-rich blood from the gastrointestinal tract (Abdel-Misih and Bloomston, 2010, Alamri, 2018, Häussinger, 2014, Eipel et al., 2010). Both blood vessels branch into the sinusoids, where deoxygenated and oxygenated blood mixes and leaves through the hepatic venule (Trefts et al., 2017). Due to

its dual blood supply, the liver has different blood pressure levels in the vessels (Eipel et al., 2010). Blood enters the liver through the hepatic artery at a pressure of 90 mmHg (same pressure rate as in the aorta) and through the portal vein at a pressure of 5-10 mmHg (Eipel et al., 2010, Rocha, 2012, Corsini et al., 2022). In the sinusoids, blood mixes at a pressure of 2-4 mmHg and leaves the liver via the inferior vena cava (Eipel et al., 2010, Rocha, 2012, Grosse-Segerath and Lammert, 2021).

Due to its location in the body and its dual blood supply, the liver plays a central role in metabolic homeostasis and detoxification of the body.

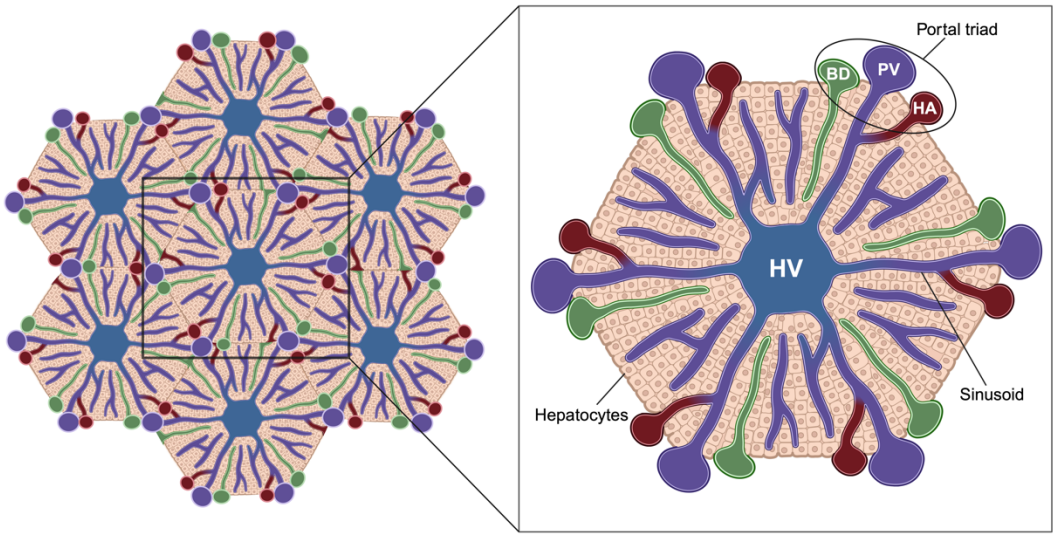

Figure 2: Structure of a hepatic lobule.
Illustration of hepatic lobules with a magnified view of a single lobule. Hepatic lobules have a hexagonal structure with a portal triad at each corner and a hepatic venule (HV) in the center, connected by sinusoids. Portal triad consists of bile ducts (BD), lymphatics (not shown), branches of the portal vein (PV) and branches of the hepatic artery (HA). Figure was created with BioRender.com by Paula Follert according to (Ishibashi et al., 2009).

3.1.2 Metabolic relevance

The liver is an important organ for maintaining plasma protein synthesis, nutrient metabolism, urea synthesis, bile formation, detoxification, and is part of the innate immune system (Häussinger, 2014, Ishibashi et al., 2009). One of the metabolic functions of the liver is to synthesize 85-90% of the circulating protein volume, including albumin, apolipoproteins, and acute phase proteins (Ishibashi et al., 2009, Si-Tayeb et al., 2010, Häussinger, 2014, Trefts et al., 2017).

Furthermore, the location of the liver and its direct connection to the gastrointestinal tract via the portal vein enables primary contact with nutrients and toxins absorbed in the intestine (Michalopoulos, 2007, Häussinger, 2014). Following food intake, glucose is absorbed in the intestine and transported to the liver via the portal vein (Abdel-Misih and Bloomston, 2010, Trefts et al., 2017). In the liver, glucose is either converted to energy through glycolysis or to glycogen via glycogenesis (Trefts et al., 2017, Alamri, 2018). Both processes are stimulated by increased insulin levels. Additionally, fatty acids from food can be used to generate energy through β-oxidation or stored as triglycerides in the liver (Trefts et al., 2017). During a fasting state, glycogenolysis occurs. Glycogen is broken down into glucose, which is then used in glycolysis to provide energy for the body's tissues, such as skeletal muscle or the brain (Alamri, 2018, Häussinger, 2014). If the liver's glycogen storage is exhausted, amino acids, lactate, and fatty acids can be converted to glucose (Trefts et al., 2017). Both glycogenolysis and gluconeogenesis are stimulated by an increase in glucagon and decreased insulin levels (Häussinger, 2014, Alamri, 2018). During a longer fasting period, the liver can produce ketones from fatty acids and proteins to provide energy to vital organs, such as the brain (Trefts et al., 2017, Alamri, 2018). Since the degradation of free amino acids produces ammonia, which is toxic to the human body, the liver converts ammonia to urea through the urea cycle, which is excreted in the urine through the kidneys (Trefts et al., 2017, Alamri, 2018).

The liver also has an exocrine function, which includes the production and secretion of bile (Si-Tayeb et al., 2010, Abu Rmilah et al., 2019). Bile contains liver substances that aid in the absorption and digestion of fats and fat-soluble vitamins, such as vitamins A, D, E, and K, in the intestine (Abu Rmilah et al., 2019). As the largest detoxifying organ, the liver also helps to remove toxic waste products from internal and external sources, such as metabolites of nutrients, medications, or alcohol (Abu Rmilah et al., 2019, Alamri, 2018). To maintain all these various functions of the liver, different cell types are necessary.

3.2 Cell types of the liver

Liver tissue is composed of parenchymal and non-parenchymal cell types. 78% of the liver tissue is made up of parenchymal cells and 6% of non-parenchymal cells. The remaining tissue volume (~16%) is filled by extracellular space, called space of Disse (**Figure 3**) (Ishibashi et al., 2009).

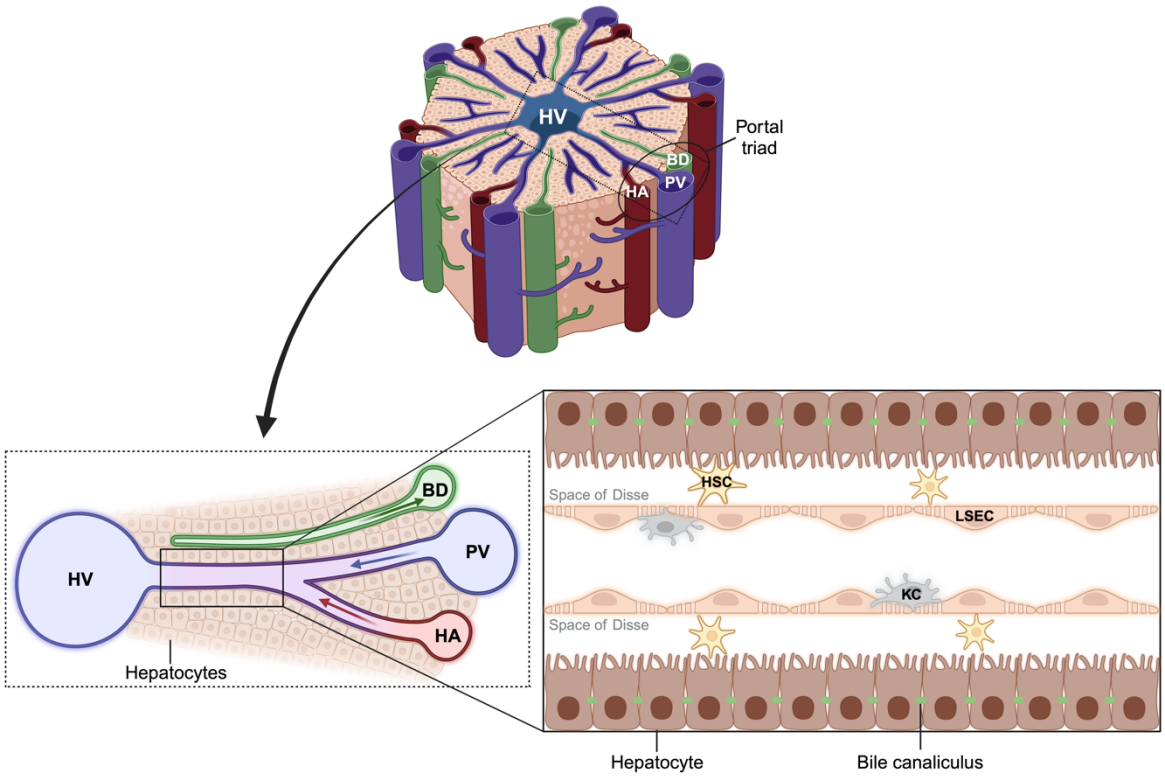

Figure 3: Structure of the hepatic lobule and therewith associated different cell types of the liver.
Overview of the hexagonal structure of the hepatic lobule with a magnified view of a lobule segment. The lobule segment includes the portal triad, containing bile ducts (BD), branches of the portal vein (PV), lymphatics (not shown), and branches of the hepatic artery (HA). Sinusoids, located between hepatocytes, pass blood from the portal triad to the hepatic venule (HV). Arrows show bile (green) and blood flow (blue: deoxygenated blood; red: oxygenated blood). Enlarged view of a sinusoidal section, showing the different cell types of the liver. Liver sinusoidal endothelial cell (LSEC), Kupffer cell (KC), Hepatic stellate cell (HSC). Figure was created with BioRender.com by Paula Follert according to (Häussinger, 2014, Lorenz et al., 2018).

3.2.1 Parenchymal cells

The liver parenchyma is composed of hepatocytes, the main cell type of the liver (Ishibashi et al., 2009, Si-Tayeb et al., 2010). Hepatocytes are polar cells whose basolateral surface faces the hepatic endothelial cells, while the apical surface between two hepatocytes is connected by gap and tight junctions (Si-Tayeb et al., 2010, Kojima et al., 2003, Häussinger, 2014). Gap junctions between hepatocytes control intercellular communication, while tight junctions form bile ducts (bile canaliculus) and built the barrier between the bile and the circulating blood (Kojima et al., 2003, Si-Tayeb et al., 2010). Bile produced by the hepatocytes is secreted into the bile ducts and transported in the opposite direction of the blood flow to the gallbladder, where it is stored (Ishibashi et al., 2009). However, a gallbladder is not present in all vertebrates (e.g., in rats) (Kruepunga et al., 2019, Michalopoulos and Bhushan, 2021).

Besides their production of bile, hepatocytes are also important for the production of albumin, clotting factors, and serum proteins, as well as for the detoxification of the body (Stanger, 2015). However, depending on their location along the sinusoids and the associated oxygen and nutrient concentrations, hepatocytes have different metabolic functions and can therefore be divided into three different metabolic zones (metabolic zonation) (Martini et al., 2023). The latter is mediated by Wnt-β-catenin signaling, whereby the signaling activity is promoted by the availability of R-Spondin and Wnt (RSPO) (Burke et al., 2009, Leibing et al., 2018, Hu et al., 2022a, Martini et al., 2023). While RSPO-LGR4/5-ZNRF3/RNF43 module regulates Wnt-β-catenin activity and spatial metabolic zonation (Planas-Paz et al., 2016), EC-specific deletion of *Wnts*, such as *Wnt2* and *Wnt9b,* results in impaired liver zonation (Hu et al., 2022a). In addition, metabolic function and the localization of distinct liver cell types is based on their different gene expression patterns (Halpern et al., 2017, Ben-Moshe et al., 2019, Hildebrandt et al., 2021, Inverso et al., 2021, Hu et al., 2022a, Martini et al., 2023, Gomez-Salinero et al., 2022). Thus, hepatocytes located in zone one, are closer to the portal triad and are mainly involved in gluconeogenesis, urea production and β-oxidation of fatty acids and mainly express genes such as *phosphoenolpyruvate carboxykinase 1* (*Pck*) and *arginase 1* (*Arg1*) (Trefts et al., 2017, Stanger, 2015, Gilgenkrantz and Collin de l'Hortet, 2018, Martini et al., 2023). Zone two describes the area between zones one and three and contains hepatocytes between the portal tract and the hepatic venule. In this zone, hepatocytes have a strong proliferative capacity rather than metabolic activity and express genes such as *hepcidin* (*Hamp*) and *insulin-like growth factor-binding protein 2* (*Igfbp2*) (Martini et al., 2023). Hepatocytes in zone three are closer to the hepatic venule and are important for glycolysis, glutamine synthetase, lipogenesis and detoxification processes and express genes such as

glutamate-ammonia ligase (*Glul*) and *ornithine aminotransferase* (*Oat*) (Trefts et al., 2017, Stanger, 2015, Gilgenkrantz and Collin de l'Hortet, 2018, Martini et al., 2023).

In addition to parenchymal cells, the liver also contains non-parenchymal cells that are essential for other liver functions.

3.2.2 Non-parenchymal cells

Non-parenchymal cells represent 6% of the total liver volume and include hepatic endothelial cells (3%), Kupffer cells (2%), and hepatic stellate cells (1%) (Ishibashi et al., 2009).

Liver sinusoidal endothelial cells (LSECs) make up 15-20% of liver cells, but account for only 3% of the total liver volume (Poisson et al., 2017). The cells, lining the inside of the hepatic sinusoids, have a unique characteristic, which was first described by Wisse in 1970 (Wisse, 1970). The basal lamina of LSECs has numerous fenestrae, with diameters ranging from 50-180 nm in humans and 50-280 nm in mice, which can be clustered together to form so-called sieve plates (Sorensen et al., 2015, Trefts et al., 2017). Therefore, LSECs form a semi-permeable barrier between the blood and the liver parenchyma, allowing passage of particles smaller than the fenestrae size, such as soluble molecules or chylomicrons (30-80 nm), while preventing the passage of larger particles (e.g., red blood cells, 8-9 µm) (Sorensen et al., 2015, Poisson et al., 2017, Diez-Silva et al., 2010). Next to the passive transport mechanism, LSECs also have a high endocytic and lysosomal capacity (Koch et al., 2021). Endocytic and scavenger receptors of LSECs mediate the removal of smaller particles such as macromolecules and nanoparticles from the blood (Poisson et al., 2017, DeLeve and Maretti-Mira, 2017, Koch et al., 2021). Thus, LSECs are required for the exchange of fluids, solutes, and particles between liver parenchyma and sinusoidal blood (Vekemans and Braet, 2005). In addition, LSECs cooperate with hepatic stellate cells, to regulate the hepatic vascular tone by secreting vasoconstrictors, such as endothelin-1 (ET-1) and vasodilators, such as nitric oxide (NO) (Koch et al., 2021).

Hepatic stellate cells (HSCs), also called Ito or fat-storing cells are located in the presinusoidal space of Disse, which is located at the abluminal surface of LSECs (Ishibashi et al., 2009, Si-Tayeb et al., 2010). HSCs can exist in both an inactive and an active form. In the dormant form, the cells store vitamin A and lipid droplets (Ishibashi et al., 2009, Trefts et al., 2017). When the cells are activated, as a result of liver injury, they start synthesis and secretion of extracellular matrix (ECM) proteins such as collagen (Vekemans and Braet, 2005, Ishibashi et al., 2009). HSCs are also responsible for the development of cirrhosis, as excessive secretion of collagen can lead to scarring of the liver tissue (Trefts et al., 2017).

Kupffer cells (KCs) are attached to the apical surface of endothelial cells, with a preferably localization in the periportal zone of the liver lobule (Vekemans and Braet, 2005). KCs are the macrophages of the liver, which phagocytose larger particles from the blood and act as antigen presenting cells (Vekemans and Braet, 2005, Sato et al., 2016). During liver injury Kupffer cells get activated and release active substances like cytokines, NO, or chemokines (Ishibashi et al., 2009).

In summary, the liver tissue is composed of different cell types that enable various metabolic functions. In addition, these cell types also play a crucial role in maintaining the high regenerative capacity of the liver.

3.3 Liver regeneration and hemodynamic changes

The liver is an organ with a remarkable regenerative capacity. After surgical removal of parts of the liver, the remaining liver grows until the original liver-to-body weight ratio is restored (Michalopoulos and DeFrances, 1997, Taub, 2004, Fausto et al., 2006). In general, the liver size is adjusted to maintain a liver to body weight ratio of 100% (Michalopoulos and Bhushan, 2021). For example, liver size increases during pregnancy, and decreases with weight loss (Bartlett et al., 2021). The rapid re-growth of the liver to its original size is a particular advantage in liver transplants as well as in the surgical removal of liver tumors. It is therefore possible to split a donor liver and transplant it into two patients (Pichlmayr et al., 1988, Bismuth et al., 1989, Broering et al., 2004). In addition, the high regenerative capacity of the liver also allows the removal of primarily irresectable liver tumors. In cases where the patient's remaining healthy liver volume is considered too small (less than 25%), an in-situ split liver surgery can be performed, which involves two surgeries (Lang et al., 2014, Knoefel et al., 2013). In the first surgery (stage 1), the diseased right part of the liver is separated from the healthy left part by a right portal vein ligation (Knoefel et al., 2013, Lang et al., 2014). This results in hypertrophy of the left liver lobe, which then increases in volume within nine days. During the subsequent second surgery (stage 2), the diseased right lobe of the liver can be dissected since the remaining left liver lobe is now sufficient to maintain liver function (Knoefel et al., 2013, Lang et al., 2014).

To study the process of liver regeneration in more detail, the most widely used method is the two-thirds partial hepatectomy (PHx). This method was first described in 1931 by Higgins and Anderson (Higgins, 1931). They demonstrated that if two-thirds of a rodent liver is surgically dissected, the remaining liver lobes restore the original liver mass within one week (Michalopoulos, 2007). To restore the liver mass, mature hepatocytes undergo hypertrophy (1.5-fold increase in cell size) and hyperplasia (1.6-fold increase in cell number)

after exactly two-thirds PHx (2.4-fold increase in total) (Abu Rmilah et al., 2019, Miyaoka and Miyajima, 2013). If less than two-thirds of the liver is surgically dissected, hypertrophy is sufficient to restore the dissected liver mass (Miyaoka and Miyajima, 2013). More than two-thirds of the liver can hardly be surgically dissected, as then the remaining part of the liver is too small to maintain liver function and restore liver volume (Demetriou et al., 1988). In addition to the mechanical model, a chemically induced liver regeneration model exists. In this model, liver tissue is injured by treatment with hepatoxic chemicals such as carbon tetrachloride (CCl4), which stimulates inflammation response followed by liver regeneration (Michalopoulos, 2007). In contrast to mechanically induced regeneration, which leaves the remaining tissue intact, chemically induced regeneration injures the entire liver (Ding et al., 2010, Huang et al., 2021).

In general, liver regeneration after PHx is associated with massive hemodynamic changes (Michalopoulos, 2007). In a healthy human liver 1.25 liters per minute of blood flow through the liver, while after PHx the same amount of blood flows through the remaining smaller part of the liver (Grosse-Segerath and Lammert, 2021). This causes an increased blood flow through the portal vein, so that the pressure in the portal vein exceeds the pressure in the hepatic artery. As a results the hepatic artery contracts, a phenomenon known as the “hepatic arterial buffer response” (Lautt and Greenway, 1987, Eipel et al., 2010). In addition, increased portal blood flow leads to mechanical stretching of LSECs, causing secretion of urokinase plasminogen activator (uPA) as well as cytokines (e.g., tumor necrosis factor-alpha (TNF-α), interleukin-6 (IL-6)) and growth promoting angiocrine signals (e.g., hepatocyte growth factor (HGF)) (Sokabe et al., 2004, Lorenz et al., 2018). Cytokine secretion induces the recruitment of neutrophils (e.g., leukocytes) into the space of Disse, which is enabled by interactions between CD44 (present on the neutrophil surface) and sinusoidal hyaluronan or by toll-like receptors (TLRs) (Shetty et al., 2018, McDonald et al., 2008, Moles et al., 2014). Leukocytes secrete matrix metalloproteinases (MMPs), such as MMP9, which are important for ECM remodeling (Kim et al., 2000). As a part of ECM remodeling, inactive hepatocyte growth factor (pro-HGF) is released from the ECM and converted to its active form by uPA (Stolz et al., 1999). This process occurs during the first minutes after PHx and is part of the priming phase (Michalopoulos, 2007). The priming phase is the first step of liver regeneration and occurs within the first few minutes after PHx (Gilgenkrantz and Collin de l'Hortet, 2018). During this phase, quiescent hepatocytes convert from G_0 to G_1 of the cell cycle, and more than 100 genes (e.g., *c-fos* and *c-jun*) are activated (Taub, 2004, Su et al., 2002). Liver regeneration can generally be divided into three phases: priming, proliferation, and termination (Tao et al., 2017).

After the priming phase, the proliferation phase begins, which starts with the proliferation of hepatocytes (Michalopoulos, 2007). In a healthy liver, the basal hepatocyte proliferation rate

is typically less than 0.1% (Michalopoulos and DeFrances, 1997). During liver regeneration, hepatocyte proliferation reaches its peak 36-48 hours after PHx in mice (Michalopoulos and DeFrances, 1997). This process is induced by growth factors and their receptors, like HGF, c-Met, epidermal growth factor (EGF), epidermal growth factor receptor (EGFR), and transforming growth factor-alpha (TGF-α), but also by cytokines like IL-6 and TNF-α (Michalopoulos and Bhushan, 2021, Murtha-Lemekhova et al., 2021). Thus, these factors play an important role in liver regeneration. For example, deletion of the HGF receptor *c-Met* in adult mice results in reduced hepatocyte proliferation and consequently impaired liver regeneration (Borowiak et al., 2004, Huh et al., 2004), while homozygous deletion of *Hgf* or its receptor *c-Met* in mice causes embryonic lethality at embryonic days 13.5 and 16.5 and defects in liver development (Schmidt et al., 1995, Bladt et al., 1995, Uehara et al., 1995, Dietrich et al., 1999). In contrast, continuous injection of HGF via the portal vein results in liver enlargement in mice (Patijn et al., 1998), and treatment with recombinant human HGF inhibits hepatocyte death in mice with acute liver failure, as well as Fas-induced apoptosis in primary human hepatocytes (Motoi et al., 2019). *In vitro* administration of recombinant HGF or EGF to rat or human hepatocytes initiates DNA synthesis (Strain et al., 1991, Gómez-Lechón et al., 1995, Richman et al., 1976). In contrast, transgenic mice overexpressing the growth factor TGF-α show liver hypertrophy at a young age, while older mice develop liver tumors (Lee et al., 1992, Takagi et al., 1992). But liver regeneration is also mediated by cytokines. For example, deletion of *Il-6* in mice results in impaired liver regeneration after PHx (Cressman et al., 1996). However, this impaired liver regeneration can be almost restored by a single injection of IL-6 into *Il-6*-deficient mice prior to PHx (Cressman et al., 1996). Furthermore, treatment with IL-6, HGF and EGF enables long-term expansion of *in vitro* cultured primary mouse hepatocytes (Guo et al., 2022).

A few hours after hepatocyte proliferation, cholangiocytes and Kupffer cells start to proliferate (Michalopoulos and DeFrances, 1997, Ait Ahmed et al., 2021). Hepatic stellate cells begin to proliferate 1-2 days later than hepatocytes, while hepatic ECs start to proliferate 2-3 days and complete the process 4-5 days after PHx (Michalopoulos, 2007). The proliferation of hepatic ECs is stimulated by factors such as Angiopoetin-2 or vascular endothelial growth factor (VEGF) and promotes the formation of new blood vessels (angiogenesis) to cover the metabolic demands of the growing liver (Ross et al., 2001, Poisson et al., 2017, Rafii et al., 2016).

When the liver-to-body weight ratio is fully restored, the termination phase occurs as the last step of liver regeneration. In this step, the proliferation of hepatic cells is inhibited by activation of growth-inhibitory cytokines and ECM remodeling, to prevent a liver overgrowth (Michalopoulos, 2007). The most prominent termination factor is the cytokine transforming growth factor-beta 1 (TGF-β1), which is predominantly secreted by non-parenchymal cells,

including activated hepatic stellate cells, endothelial cells, and Kupffer cells (Fausto et al., 1986, Braun et al., 1988, Schon and Weiskirchen, 2014). Expression of TGF-β1 starts 4 hours and reaches its peak 72 hours after PHx (Braun et al., 1988). Additionally, its receptor, transforming growth factor beta receptor (TGF-βR), is predominantly increased during a later stage of liver regeneration (Nishikawa et al., 1998). TGF-β1 promotes the production of ECM proteins and facilitates ECM remodeling (Roberts et al., 1992). Furthermore, TGF-β1 suppresses uPA expression and the activation of HGF (Mars et al., 1996). Thus, reduced liver regeneration can be observed in rats that received an intravenous injection of porcine platelet-derived TGF-β1 before and after PHx (Russell et al., 1988).

Accordingly, liver regeneration is a complex process involving hemodynamic changes and the secretion of various growth factors and cytokines. However, the entire mechanism of liver regeneration is not yet fully understood. Furthermore, liver regeneration is based on the activation of various signaling pathways.

3.3.1 Signaling pathways in liver regeneration

During liver regeneration several signaling pathways are activated to promote proliferation of parenchymal and non-parenchymal cells. Three of the main signaling pathways during liver regeneration, including Ras/Raf/MEK/ERK, JAK/STAT3 and PI3K/AKT, have also been linked to MYDGF in recent years and are therefore described below (**Figure 4**).

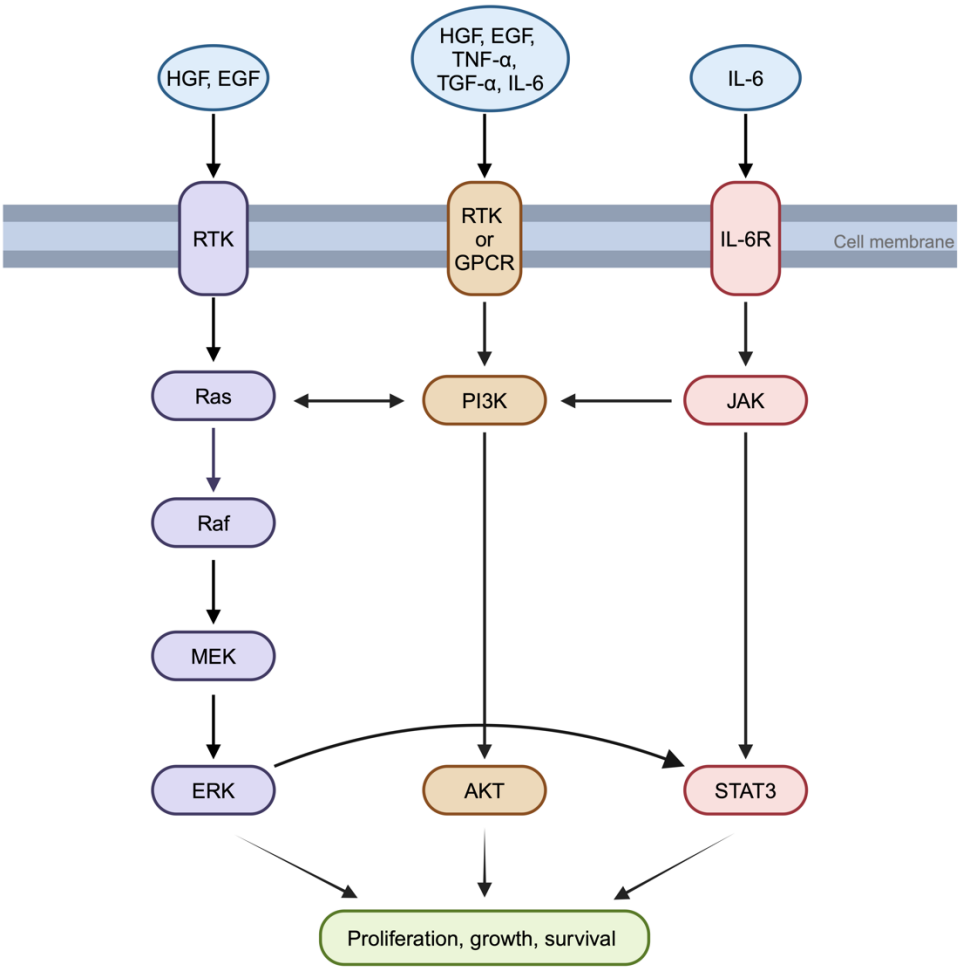

Figure 4: Signaling pathways during liver regeneration.
Schematic illustration of the three main signaling pathways associated with liver regeneration. HGF: Hepatocyte growth factor, EGF: Epidermal growth factor; TNF-α: Tumor necrosis factor-alpha, TGF-α: Transforming growth factor-alpha, IL-6: Interleukin-6, RTK: Receptor tyrosine kinase; GPCR: G-protein coupled receptor. Figure was created with BioRender.com by Paula Follert according to (Yagi et al., 2020).

The Ras/Raf/MEK/ERK signaling pathway is mainly associated with the G_1/S and G_2/M cell cycle progression during liver regeneration (Talarmin et al., 1999, Guegan et al., 2012, Wen et al., 2022). Activation of this signaling pathway occurs through the binding of ligands, such as HGF or EGF, to receptor tyrosine kinases (RTKs) (Zhang and Liu, 2002, Yagi et al.,

2020). This leads to the activation of the Ras protein which further stimulates and activates Raf kinase (also known as mitogen-activated protein kinase kinase kinase, MAPKKK) (Talarmin et al., 1999). The latter phosphorylates and thus activates the mitogen-activated protein kinase kinase (MAPKK, also known as MEK), promoting the activation and phosphorylation of MAPK on threonine (T202) and tyrosine (Y204) residues, also known as extracellular signal-regulated kinase 1 (ERK1) and extracellular signal-regulated kinase 2 (ERK2) (Talarmin et al., 1999). The relevance of MAPK (ERK1/2) signaling in liver regeneration is demonstrated by the fact that injection of a specific MEK inhibitor, PD98059, into mice after PHx results in a lack of DNA replication in isolated and cultured primary hepatocytes (Talarmin et al., 1999). Similarly, DNA replication and the increased phosphorylation of MAPK (ERK1/2) within the first 5 minutes in primary cultured hepatocytes treated with EGF plus sodium pyruvate can be prevented by additional treatment with PD98059 (Talarmin et al., 1999). Furthermore, mice with a mutation of *Met* (gene encoding the HGF receptor c-Met) show a lack of MAPK (ERK1/2) signaling activation and a G_2/M cell cycle arrest associated with impaired liver regeneration after PHx (Borowiak et al., 2004, Factor et al., 2010). Similarly, mice with a deletion of the growth hormone (GH) receptor or the insulin growth factor 1 (IGF-1) receptor exhibit impaired MAPK (ERK1/2) activation and liver regeneration (Zerrad-Saadi et al., 2011, Desbois-Mouthon et al., 2006). Diminished MAPK (ERK1/2) activation and impaired liver regeneration after PHx can also be observed in mice in which senescent cells were eliminated by the senolytic drug ABT263, resulting in impaired IL-6 and C-X-C chemokine receptor type 2 (CXCR2) ligand secretion (Cheng et al., 2022).

In addition, activation of MAPK (ERK1/2) is also associated with the Janus kinase (JAK)/STAT3 signaling pathway, which promotes tasks such as cell proliferation and survival during liver regeneration (Chung et al., 1997, Yagi et al., 2020). The JAK/STAT3 signaling pathway is classically activated by the binding of IL-6 to its receptor IL-6R. This IL-6/IL-6R complex dimerizes glycoprotein 130 (gp130), leading to the activation of JAK (Schmidt-Arras and Rose-John, 2016). In addition to this classical IL-6 signaling, the IL-6 trans-signaling exists. Here, IL-6 forms a complex with the soluble form of IL-6R (sIL-6R), which binds to gp130 and also activates JAK (Fazel Modares et al., 2019). The latter then activates the transcription factor STAT3 through phosphorylation of tyrosine 705 (Y705) residue (Tesoriere et al., 2021). This post-translational modification of STAT3 allows its translocation to the nucleus, to act as a transcription factor (Tesoriere et al., 2021). Furthermore, the activation of STAT3 can also occur through phosphorylation of serine 727 (S727) residue by Ras/RAF/MEK/ERK signaling pathway, without the activation of JAK (Chung et al., 1997, Korf-Klingebiel et al., 2015, Xu et al., 2022). Thus, phosphorylation of S727 is stimulated by kinases in cell- and stimuli-specific manner (Tesoriere et al., 2021).

That the activation of STAT3 is crucial for liver regeneration has been shown in IL-6 or IL-6R KO mice for example. Deletion of IL-6 signaling in mice results in impaired liver regeneration associated with absence of STAT3 activation and reduced DNA synthesis in hepatocytes (Cressman et al., 1996). IL-6R deficient mice also show significantly reduced STAT3 activation and decreased survival rate after PHx (Fazel Modares et al., 2019). Furthermore, IL-6 trans-signaling alone was shown to be sufficient to regulate liver regeneration after PHx, by activating the STAT3 signaling (Fazel Modares et al., 2019). In addition, increased IL-6/STAT3 activation and enhanced hepatocyte proliferation can also be observed in myeloid-specific peroxisome proliferator-activated receptor alpha (*PPARα)*-deficient mice after PHx (Xie et al., 2022).

Next to the aforementioned signaling pathways, the phosphatidylinositol 3-kinase (PI3K)/AKT pathway is also involved in liver regeneration (Hong et al., 2000, Murata et al., 2007, Jackson et al., 2008). PI3K is a kinase that is activated by binding of ligands such as HGF, EGF, TNF-α, TGF-α, IL-6 to RTK or G protein-coupled receptors (GPCRs) (Yagi et al., 2020). Furthermore, PI3K and Ras can interact to activate each other (Zhang and Liu, 2002). Activation of PI3K leads to phosphorylation of AKT (also known as protein kinase B), which promotes the expression of genes important for cell growth, proliferation, and survival (Jackson et al., 2008, Yagi et al., 2020). When the PI3K/AKT pathway is inhibited using wortmannin (a potent PI3K inhibitor), liver regeneration in mice is delayed by inhibiting the priming of hepatocytes (Jackson et al., 2008). Similarly, liver-specific deletion of *Akt* results in impaired liver regeneration and increased mortality in mice after PHx (Pauta et al., 2016). Furthermore, PI3K/AKT also has a compensatory effect on the JAK/STAT3 signaling pathway, as liver-specific knockout of *Stat3* in mice results in increased activation of the PI3K/AKT signaling pathway, which induces hepatocyte hypertrophy and thus supports liver regeneration after PHx (Haga et al., 2005).

In summary, several signaling pathways are required to promote cell proliferation and survival during liver regeneration. These pathways can be activated by signals from cells such as hepatic stellate cells, but also by angiocrine signals.

3.3.2 Angiocrine signals in liver regeneration

Angiocrine signals are paracrine factors that are secreted by endothelial cells and play a crucial role in the regulation of vascular tone and organ regeneration (Rafii et al., 2016, Kostallari and Shah, 2016).

Regulation of the vascular tone plays a central role during liver regeneration (Grosse-Segerath and Lammert, 2021). After PHx, hepatic ECs in the remaining smaller part of the liver are exposed to shear stress due to increased blood flow and to mechanical stretch due to increased blood pressure (Schoen et al., 2001, Urner et al., 2018). This activates the endothelial cell-specific transcription factor Kruppel-like factor 2, leading to upregulation of the vasodilator NO and downregulation of the vasoconstrictor ET-1 (Schoen et al., 2001, Parmar et al., 2006). Furthermore, the unchanged blood flow velocity but increased blood volume in the remaining liver leads to mechanical stretching of hepatic ECs, resulting in activation of β1 integrin and vascular endothelial growth factor receptor (VEGFR) 3 and secretion of HGF as a growth-promoting signal for hepatocytes (Lorenz et al., 2018). Thus, the secretion of angiocrine signals initiates proliferation-promoting processes during liver regeneration (Rafii et al., 2016).

In the early phase of liver regeneration, the transcription factor inhibitor of DNA binding 1 (Id1) is upregulated in LSECs in a VEGFR2/AKT-dependent manner, resulting in increased secretion of HGF and Wnt2 by LSECs (Rafii et al., 2016). Furthermore, the activation of Id1 is also associated with the presentation of C-X-C chemokine receptor type 7 (CXCR7) on the surface of LSECs (Ding et al., 2014). During acute liver injury (e.g., after CCl4 treatment), C-X-C chemokine receptor type 4 (CXCR4) is upregulated on the surface of LSECs, activating fibroblast growth factor receptor 1 (FGFR1) and causing fibrosis (Ding et al., 2014). Thus, CXCR7 and CXCR4 are antagonists and represent the balance between liver regeneration and fibrosis (Koch et al., 2021). Since the Id1 upregulation in LSECs occurs in a VEGFR2/AKT-dependent manner, LSEC-specific ablation of *Vegfr2* in mice results in decreased hepatocyte proliferation and hepatic vascular mass and inhibited *Id1* upregulation, whereas *Id1*-deficient mice show defects in liver regeneration and decreased expression of HGF and Wnt2 (Ding et al., 2010). Also, LSEC-specific ablation of *Hgf* impairs the ability of the liver to regenerate. Mice show a delayed liver regeneration and reduced HGF/c-Met signaling (Zhang et al., 2020). The deletion of *c-Met* in adult mice results in reduced hepatocyte proliferation and impaired liver regeneration (Huh et al., 2004, Borowiak et al., 2004). As aforementioned, investigation of homozygous deletion of *Hgf* or *c-Met* on liver regeneration is not possible, due to embryonic lethality (Schmidt et al., 1995, Bladt et al., 1995, Uehara et al., 1995, Dietrich et al., 1999). Mice with an EC-specific deletion of *Wnt2* and *Wnt9b* show significantly abolished hepatocyte proliferation and thus

impaired liver regeneration 40 hours after PHx (Hu et al., 2022a). Similarly, mice with an EC-specific deletion of *Wntless* (*Wl*), required for Wnt secretion, exhibit reduced hepatocyte proliferation 40 hours after PHx, which increases 72 hours after PHx (Preziosi et al., 2018).

Next to the upregulation of Id1 in the early phase of liver regeneration, angiopoietin-2 is downregulated, which is accompanied by a downregulation of TGF-β (inhibits hepatocyte proliferation) in LSECs (Hu et al., 2014, Koch et al., 2021). 4-8 days after PHx, angiopoietin-2 levels in LSECs returns to normal levels and VEGFR2 expression is upregulated through autocrine stimulation of Tie2 (Koch et al., 2021). In addition, hepatocytes secrete VEGF, which leads to the proliferation of LSECs necessary for the formation of new blood vessels (angiogenesis) and to cover the metabolic demands of the enlarged liver (Koch et al., 2021, Rafii et al., 2016). Angiocrine signals are also important for the termination of liver regeneration. For example, the release of TGF-β1 from LSECs at the end of liver regeneration inhibits hepatocyte proliferation and prevents liver overgrowth (Michalopoulos, 2007).

In conclusion, angiocrine signals are important for liver development and regeneration. To date, not all angiocrine signals that can promote or terminate liver regeneration have been identified. Therefore, it is of great interest to discover new angiocrine signals to better understand the process of liver regeneration and to promote regeneration in medical applications.

3.4 Myeloid-derived growth factor (MYDGF)

3.4.1 Identification of SF20/IL-25 / C19orf10

MYDGF, initially named SF20/IL-25, was first described in 2001 by Tulin et al. during a screen of ST2 stromal cells from mouse bone marrow. Here, the authors demonstrated that SF20/IL-25 promotes the proliferation of mutant mouse Ba/F3 pro-B cells (Tulin et al., 2001). However, this work was rejected in 2003 due to the inability to reproduce the proliferation data (Tulin et al., 2003). In addition, SF20/IL-25 was described as a secreted factor from mouse 3T3-L1 adipocytes (Wang et al., 2004). Until then, no function could be assigned to SF20/IL-25. Thus, in the following years it was named chromosome 19 open reading frame 10 (C19orf10) due to its chromosomal localization and described in the following cell types: human fibroblast-like synoviocytes (Weiler et al., 2007), human eosinophils (Straub et al., 2009), murine macrophages (Bailey et al., 2011) and human cholangiocarcinoma cells (Weeraphan et al., 2012). C19orf10 has also been identified in alpha-fetoprotein-negative hepatocellular carcinoma (HCC) cell lines, where an overexpression of *C19orf10* leads to increased proliferation, while a knockdown of *C19orf10* results in reduced cell proliferation (Sunagozaka et al., 2011).

3.4.2 Renaming of C19orf10 to MYDGF

In 2015, Korf-Klingebiel et al. identified C19orf10 as a novel paracrine-acting protein that is produced by bone marrow-derived monocytes and macrophages and named it myeloid-derived growth factor (MYDGF) (Korf-Klingebiel et al., 2015). MYDGF is localized in the endoplasmic reticulum, in the Golgi apparatus, and extracellularly (Bortnov et al., 2018, Ebenhoch et al., 2019). Interestingly, the structure of MYDGF is highly asymmetric and has no connections to other cytokines or growth factors but shows a strong homology between human and mouse (Ebenhoch et al., 2019, Korf-Klingebiel et al., 2015). The protein has a theoretical molecular mass of around 16 kilodalton (kDa) and consists of ten antiparallel β-strands forming two β-sheets (Bortnov et al., 2018, Ebenhoch et al., 2019). However, a receptor for MYDGF has not yet been identified; only an interaction between MYDGF and synthetic anticancer macromolecules, such as guanidium-functionalized polycarbonates, has been detected (Sim et al., 2024). Since, MYDGF is expressed in nearly 140 human tissues and cell lines, as reported by ProteomicsDB (Bortnov et al., 2018), its function has been recently described in different tissues (heart, kidney, liver), organisms (human, mouse, zebrafish larvae), and in relation to the malignant stage of some cancers (bladder cancer, HCC) (Xu et al., 2023b).

3.4.3 The role of MYDGF in the heart

MYDGF was first described in the heart, where it promotes cardiac repair after myocardial infarction (MI) by enhancing cardiac myocyte survival and angiogenesis (Korf-Klingebiel et al., 2015). While a deletion of *Mydgf* has no phenotype under baseline conditions, post-MI MYDGF KO mice show increased scar size and contractile dysfunction in the heart compared to wild-type mice (Korf-Klingebiel et al., 2015). This effect can be reversed by treatment with recombinant MYDGF, which significantly reduced infarct size and contractile dysfunction in MYDGF KO mice (Korf-Klingebiel et al., 2015). In neonatal mouse hearts MYDGF also promotes cardiomyocyte proliferation and improves cardiac function after cardiac injury (Wang et al., 2020b). *In vitro* MYDGF treatment protects cardiac myocytes from apoptosis by promoting phosphorylation of AKT on threonine 308 (T308) and serine 473 (S473) and enhances human coronary artery endothelial cell (HCAEC) proliferation by causing rapid phosphorylation of MAPK (ERK1/2) on threonine (T202) and tyrosine 204 (Y204) and STAT3 on serine 727 (S727) (Korf-Klingebiel et al., 2015, Zhao et al., 2020). In addition, MYDGF reduces hypoxia/reoxygenation-induced apoptosis in *in vitro* cultured cardiac microvascular endothelial cells (Wang et al., 2022) and prevents pressure overload-induced heart failure through crosstalk between MYDGF and inflammatory cells and cardiomyocytes (Korf-Klingebiel et al., 2021).

MYDGF also represents a potential treatment strategy for restenosis after angioplasty in the heart. Restenosis describes a re-narrowing of the arterial lumen characterized by aberrant dedifferentiation of vascular smooth muscle cells and often occurs after percutaneous coronary interventions (e.g., bypass grafting or stent implantation) in patients with obstructive coronary artery disease. Exogenous administration of MYDGF around the damaged vessel after a vascular injury reduces the narrow endovascular diameter and collagen deposition, improves hemodynamics, and inhibits vascular smooth muscle cell dedifferentiation (Yang et al., 2023).

Thus, treatment with MYDGF in the heart has numerous beneficial effects and leads to improved repair of the heart after cardiac injury.

3.4.4 The role of MYDGF as a potential therapeutic drug in metabolic diseases

In recent years, MYDGF has also been described as a potential therapeutic drug in relation to various metabolic diseases, such as type 2 diabetes (T2D) (Wang et al., 2020a), diabetic kidney disease (DKD) (He et al., 2020), osteoporosis (Xu et al., 2022), atherosclerosis (Meng et al., 2021, Xu et al., 2023a), and non-alcoholic fatty liver disease (NAFLD) (Ding et al., 2023). All these metabolic diseases (T2D, DKD, atherosclerosis or NAFLD) are associated with a reduced MYDGF blood plasma (3.3 ng/ml in healthy humans) or serum levels in humans and mice (Polten et al., 2019, Wang et al., 2020a, He et al., 2020, Meng et al., 2021, Xu et al., 2023a, Ding et al., 2023). Furthermore, diabetic mice with a deletion of MYDGF, show diminished production of glucagon-like peptide-1 (GLP-1) and impaired glucose homeostasis (Wang et al., 2020a). Restoration of MYDGF in these mice promotes intestinal GLP-1 production and improves glucose and lipid metabolism (Wang et al., 2020a). In addition, mice with DKD and deletion of MYDGF show increased podocyte injury, including podocyte apoptosis and more severe glomerular injury (He et al., 2020). Bone marrow transplantation from wild-type mice in these MYDGF KO mice ameliorates glomerular injury and improves glucose metabolism (He et al., 2020). This protective effect may be due to the fact that MYDGF prevents the accumulation of podocytes in the S phase of the cell cycle, thereby preventing the mitotic catastrophe (cell death during mitosis) of these cells (Zhan et al., 2022). Further, MYDGF represents a potential therapeutic drug for bone metabolism disorders such as osteoporosis. When MYDGF is deleted in a myeloid cell-specific manner, bone mass and strength are reduced in both young and old mice. However, this phenotype can be prevented by restoring MYDGF (Xu et al., 2022).

Recent publications have shown that MYDGF also plays a decisive role in preventing inflammation in zebrafish larvae and mammals. In zebrafish larvae MYDGF acts as a

damage signal that serves as an endogenous inhibitor of neutrophil inflammation in response to tissue damage (Houseright et al., 2021). In mice with atherosclerosis, restoration of MYDGF results in a reduction in vascular inflammation and endothelial injury (Meng et al., 2021). This protection against atherosclerosis is achieved by inhibiting the first step of atherosclerosis, namely the transcytosis of low-density lipoproteins (LDLs). During LDL transcytosis, LDLs accumulate in the subendothelial space and promote atherosclerosis (Xu et al., 2023a). Treatment with MYDGF also reduces ischemic acute kidney injury caused by renal ischemia/reperfusion, which often occurs after kidney transplantation. For example, intraperitoneal injection of recombinant human MYDGF into mice prior to renal ischemia/reperfusion significantly improves renal function and reduces oxidative stress, apoptosis, and inflammation (Wang et al., 2023). In addition, MYDGF also regulates the inflammatory response in gingival fibrosis. Overexpression of MYDGF in high glucose-induced gingival fibrosis reduces apoptosis and oxidative stress of fibroblasts and inhibits the secretion of cytokines (Gao et al., 2023). Last year, MYDGF was described for the first time in relation to the liver. It was shown that NAFLD patients and mice have reduced serum MYDGF levels, which negatively correlate with the severity of NAFLD and several serum inflammatory factors (Ding et al., 2023). However, transplantation of bone marrow from wild-type mice into high-fat diet-induced NAFLD MYDGF KO mice shows a beneficial effect on lipogenesis, hepatic steatosis, and decreases levels of inflammatory factors in isolated hepatocytes, Kupffer cells, and serum (Ding et al., 2023).

In summary, MYDGF represents an interesting novel factor with beneficial effects on various diseases occurring in different tissues. Since MYDGF has a positive effect on the cardiac repair after MI and on NAFLD, MYDGF may also play a crucial role in liver regeneration.

3.5 Aim of this thesis

The liver is an organ with a remarkable regenerative capacity (Michalopoulos and DeFrances, 1997, Taub, 2004, Fausto et al., 2006). During the regenerative process after two-thirds PHx, angiocrine signals secreted by hepatic ECs play a crucial role to restore the original liver mass (Michalopoulos, 2007, Lorenz et al., 2018, Grosse-Segerath and Lammert, 2021). In previous experiments, we identified MYDGF as an angiocrine signal in the supernatant of mechanically stretched primary human hepatic ECs with a proliferation- and survival-promoting effect on primary human hepatocytes (Große-Segerath 2020, Große-Segerath and Follert et al., 2024).

The aim of this thesis was to investigate the role of MYDGF on hepatocyte proliferation. First, we aimed to confirm our hypothesis that MYDGF is secreted by human hepatic ECs and is not present in increased amounts in the supernatants of stretched primary human hepatic ECs due to cell lysis. Next, we aimed to verify our previous results that MYDGF has a proliferation- and survival-promoting effect on primary human hepatocytes using an additional proliferation and apoptosis marker. In addition, we tested whether MYDGF has an effect on the growth and proliferation of human hepatocyte organoids. Furthermore, we aimed to uncover the underlying signaling pathway of MYDGF that is required to induce hepatocyte proliferation.

Since it is unknown whether MYDGF levels are altered after liver surgery, we aimed to analyze the expression kinetics of MYDGF in humans and mice after liver surgery and to compare it with the expression kinetics of HGF. Furthermore, we aimed to determine the role of MYDGF in liver regeneration by performing gain- and loss-of-function experiments. To this end, we analyzed the hepatocyte proliferation and liver-to-body weight ratio at different timepoints after two-thirds PHx.

In summary, the aim of the present study was to investigate the role of MYDGF on primary human hepatocytes and liver regeneration after two-thirds PHx in mice.

4. Material and Methods

Parts of the described materials and methods have already been published in Große-Segerath and Follert et al. 2024.

4.1 *In vitro* studies

4.1.1 Human hepatic endothelial cells (hepatic ECs)

Human liver sinusoidal microvascular endothelial cells (hepatic ECs, PELOBiotech, PB-CH-153-5511) from a female, 59-year-old, Caucasian, body mass index (BMI, kg/m^2): 18; Cause of death (COD): Anoxia second to cardiovascular (QC29B15F09) were cultured in microvascular endothelial cell growth medium kit enhanced (PELOBiotech, PB-MH-100-4099). Cryopreserved human hepatic ECs were thawed for 2 minutes (min) in a 37°C water bath, transferred into microvascular endothelial cell growth medium kit enhanced and seeded in a T-75 flask (Sarstedt, 83.3911), pre-coated with speed coating solution (PELOBiotech, PB-LU-000-0002-00) for 10 min at room temperature (RT). Cells were cultured at 37°C and 5% CO_2.

4.1.2 Human hepatocytes

Human hepatocytes from different donors were purchased from Thermo Fisher Scientific (HU4248, HU8296, HU8373, HU8300, HU8339-A, HU8284) and KaLy-Cell (S1426T, B1148T). Donors: Female, 12-year-old, White, BMI: 20.2, COD: Intracerebral hemorrhage-stroke (Lot: HU4248); Donors: Male, 23-year-old, Caucasian, BMI: 24.6, COD: Head trauma (Lot: HU8296); Female, 26-year-old, Caucasian, BMI: 18.6, COD: Asphyxiation (Lot: HU8373); Male, 31-year-old, Caucasian, BMI: 21, COD: Intracerebral hemorrhage (Lot: HU8300); Female, 31-year-old, African American, BMI: 18.9, COD: Asphyxiation (Lot: HU8339-A); Female, 46-year-old, Caucasian, BMI: 30.2, COD: Self-inflicted gunshot wound (Lot: HU8284); Female, 34-year-old, Caucasian, BMI: 27.6, COD: Cholangiocarcinoma (Lot: S1426T); Female, 27-year-old, Caucasian, COD: Focal nodular hyperplasia, Budd-Chiari Syndrome (Lot: B1148T). Cells were seeded on Nuc™ Lab-Tek™ Chamber Slides™ (Lab-Tek, 177445), or 24-well plates (Sarstedt, 83.3922) coated with 50 µg/ml collagen I rat tail (Gibco by Thermo Fisher Scientific, A10483-01) diluted in speed coating solution (PELOBiotech, PB-LU-000-0002-00). Cryopreserved hepatocytes were thawed for 2 min in a 37°C water bath and transferred to cryopreserved hepatocyte recovery medium (CHRM) (Thermo Fisher Scientific, CM7000) under sterile conditions. Cells were centrifuged at 100 x *g* for 10 min at RT, the supernatant was aspirated and the pellet was

resuspended by flicking in plating medium (Thermo Fisher Scientific, CM3000) (**Table 1**). 150,000-180,000 cells per chamber and 250,000 cells per 24-well plate were seeded and incubated for 6 hours (h) in plating medium at 37°C and 5% CO_2. Subsequently, incubation medium (Thermo Fisher Scientific, CM4000) (**Table 2**) was applied and cells were cultivated at 37°C and 5% CO_2.

To analyze the effect of MYDGF on primary human hepatocyte proliferation or survival, human hepatocytes (Lot: HU8296, HU8373, HU8300, HU8339-A) were incubated in incubation medium (**Table 2**) without (control) or with 1 ng/ml MYDGF (Novoprotein, CG64) for 6 h. After treatment, hepatocytes were fixed with 4% paraformaldehyde (PFA, Thermo Fisher Scientific, J19943) overnight at 4°C.

To analyze MYDGF signaling pathway in human hepatocytes, hepatocytes (Lot: HU8373) were starved for 4 h in William's E medium (Thermo Fisher Scientific, A1217601) and incubated afterwards without or with 1 ng/ml MYDGF (Novoprotein, CG64) for 0, 5, 15 and 30 min, or hepatocytes were starved for 3 h in William's E medium (Thermo Fisher Scientific, A1217601) and pretreated with 20 µM PD98059 (Sigma-Aldrich, P215) or/and 20 µM Stattic (Sigma-Aldrich, S7947) for 1 h. After the pretreatment, cells were treated without or with 1 ng/ml MYDGF plus 20 µM PD98059 or/and 20 µM Stattic for 0, 5 and 15 min, and then protein lysis buffer containing 50 mM HEPES (Sigma-Aldrich), 150 mM NaCl (Sigma-Aldrich), 10% Glycerol (Sigma-Aldrich), 1% Triton X-100 (Sigma-Aldrich), PhosSTOP™ phosphatase inhibitor (Sigma-Aldrich, 4906845001), cOmplete™ protease inhibitor cocktail (Roche, 11697498001), and H_2O was applied to the cells and incubated for 20 min on ice.

Hepatocytes (Lot: HU4248, HU8373, HU8300, B1148T) were pretreated for 1 h with 20 µM PD98059 and/or 20 µM Stattic or incubation medium (**Table 2**) to analyze the number of proliferating hepatocytes after MYDGF treatment without or with PD98059 and/or Stattic. After the pretreatment, medium only (control) (for Lot: HU4248), 1 ng/ml MYDGF alone or 1 ng/ml MYDGF plus 20 µM PD98059 or/and 20 µM Stattic was added for 6 h. In addition, 1 mg/ml 5-ethynyl-2'-deoxyuridine (EdU) (Invitrogen, C10337) was added simultaneously to all treatment conditions to be able to analyze cell proliferation. After treatment, hepatocytes were fixed with 4% PFA (Thermo Fisher Scientific, J19943) overnight at 4°C.

For all experiments, the respective amount of distilled water (dH_2O) instead of MYDGF was added to the control condition.

Table 1: Components of plating medium.

Volume	Components
25 ml	William's Medium E (Thermo Fisher Scientific, A1217601)
0.9 ml	Cocktail A (Thermo Fisher Scientific, CM3000)
1.25 ml	FBS (Thermo Fisher Scientific, CM3000)
2.5 µl	Dexamethasone (Thermo Fisher Scientific, CM3000)

Table 2: Components of incubation medium.

Volume	Components
25 ml	William's Medium E (Thermo Fisher Scientific, A1217601)
0.9 ml	Cocktail B (Thermo Fisher Scientific, CM4000)
0.25 µl	Dexamethasone (Thermo Fisher Scientific, CM4000)

4.1.3 Human hepatocyte organoids

To generate 3D human hepatocyte organoids, 250,000 human hepatocytes of a 23-year-old Caucasian male (BMI: 24.6, COD: Head trauma (HU8296)), or a 26-year-old Caucasian female (BMI: 18.6; COD: Asphyxiation (HU8373)) (Thermo Fisher Scientific, HMCPIS) were seeded in 3D medium (**Table 3**) in a well of a 24-well plate with low attachment surface (Corning, CLS3473). The composition of the medium is based on the protocol of previous publications (Hu et al., 2018, Garnier et al., 2018). Cells were incubated for three days at 37°C and 5% CO_2. Afterwards, organoids were picked under the stereomicroscope (Nikon, SMZ1500) and transferred into a new 24-well plate with low attachment surface, containing 3D medium without Noggin, Wnt-3a, and Y-27632. Human hepatocyte organoids were cultivated in 3D medium without or with 10 ng/ml MYDGF (Novoprotein, CG64) for seven days at 37°C und 5% CO_2. In addition, 1 mg/ml EdU (Invitrogen, C10337) was added to both treatment conditions to be able to analyze cell proliferation. Medium only (control) or MYDGF (10 ng/ml) was added daily and medium was changed every third day. EdU was added during the medium change. In the control condition, the respective amount of dH_2O instead of MYDGF was added. After seven days, organoids were picked and transferred into a black 96-well µ-clear-plate (Greiner, 655090) and fixed with 4% PFA (Thermo Fisher Scientific, J19943) overnight at 4°C. Next day, PFA was aspirated and whole mount staining was performed to determine the proliferation rate.

Table 3: Components of 3D medium.

Volume	Components	Company
10 ml	AdDMEM/F12	Gibco by Thermo Fisher Scientific, 12634010
100 µl	Penicillin-Streptomycin-Glutamine (100 x)	Thermo Fisher Scientific, 10378016
10 µl	10 mM HEPES [1 M]	Gibco by Thermo Fisher Scientific, 15630106
200 µl	1% B-27 Supplement (50 x)	Thermo Fisher Scientific, 17504044
50 µl	500 ng/ml R-spodin-1 (100 µg/ml)	PeproTech, 120-38
60 µl	3 µM CHIR 99021 [500 µM]	Tocris, 4423
25 µl	1.25 mM N-acetyl-L-cysteine [500 mM]	Sigma-Aldrich, A9165-5G
100 µl	10 mM Nicotinamide [1000 nM]	Sigma-Aldrich, N0636-100G
0.1 µl	10 nM Gastrin [1 mM]	Tocris, 3006
2.5 µl	50 ng/ml EGF [200 µg/ml]	R&D Systems, 236-EG-200
2 µl	20 ng/ml TGF-α (100 µg/ml)	PeproTech, 100-16A
5 µl	50 ng/ml FGF-7 (100 µg/ml)	PeproTech, 100-19
5 µl	50 ng/ml FGF-10 (100 µg/ml)	Miltenyi Biotec, 130-093-850
2.5 µl	25 ng/ml HGF (100 µg/ml)	Miltenyi Biotec, 130-093-872
40 µl	2 µM A 83-01 [500 µM]	Tocris, 2939
1 ml	10% Matrigel®	Corning, 356231
During the first 3 days after plating		
2.5 µl	25 ng/ml Noggin (100 µg/ml)	PeproTech, 120-10C
2.5 µl	50 ng/ml Wnt-3a (200 µg/ml)	R&D Systems, 5036-WN
32 µl	10 µM Y-27632 (3.125 mM)	Stem Cell Technologies, 72302

4.1.4 HepG2 cells

HepG2 cells from ATCC (ATCC® HB-8065™) were thawed and cultivated in ATCC-formulated Eagle's Minimum Essential Medium (ATCC, 30-2003) and 10% fetal bovine serum (FBS, Gibco, 10270-106) as provided by ATCC. To analyze the effect of MYDGF on HepG2 cell proliferation, 50,000 HepG2 cells were seeded on glass coverslips in 24-well plates (Sarstedt, 83.3922) and starved in ATCC-formulated Eagle's Minimum Essential Medium (ATCC, 30-2003) for 24 h. Afterwards HepG2 cells were treated without or with 1 ng/ml recombinant MYDGF (Novoprotein, CG64) for 6 h and fixed with 4% PFA (Thermo Fisher Scientific, J19943) overnight at 4°C. In the control condition, the respective amount of dH_2O instead of MYDGF was added.

4.2 *In vivo* and *ex vivo* studies

4.2.1 Human blood samples

To measure MYDGF level in human blood serum pre/post stage 1 in-situ split liver surgery (Alexander et al., 2023), blood serum from a 79-year-old man with a sigmoid carcinoma metastatic to the liver was analyzed at different timepoints pre/post stage1 in-situ split liver surgery (trisegmentectomy, i.e., segments 1 and 4–8). Human serum samples were provided from Department of General, Visceral, Thorax and Pediatric Surgery, Medical Faculty and University Hospital Düsseldorf. This study was approved by the local institutional review board (Heinrich Heine University, Duesseldorf, Germany; 2018–258-KFogU). Furthermore, MYDGF level in human blood plasma was analyzed in different patients with hepatocellular carcinoma pre and post liver resection (Heinrich and Lang, 2017). This study was approved by the Ethics Committee of the Landesärztekammer Rheinland-Pfalz (2020-15149). Human plasma samples were provided from Department of General, Visceral and Transplantation Surgery, University Hospital Center Mainz. Donors: Male, 54-year-old, BMI: 23.8, Resection: Laparoscopic left lateral resection (Segment (Seg) 2/3); Male, 59-year-old, BMI: 23.6, Resection: Hemihepatectomy right (Seg 5-8); Male, 61-year-old, BMI: 23, Resection: Hemihepatectomy left (Seg 2-4); Male, 68-year-old, BMI: 28.7, Resection: Open anterolateral sectorectomy (Seg 5/8); Male, 84-year-old, BMI: 28.1; Resection: Open atypical resection segment 8; Male, 89-year-old, BMI: 22.8, Resection: Open atypical resection (Seg 7/8). Donors with an BMI > 30 kg/m^2, were excluded from the analysis, since a correlation between systolic blood pressure (that stretches hepatic ECs) and liver size could be demonstrated only in metabolically healthy individuals without obesity (Lorenz et al., 2018).

4.2.2 Mouse models

Male C57BL/6J mice between 10-15 weeks-old from Janvier Labs were used for *in vivo* analysis of MYDGF expression kinetics and influence of MYDGF overexpression on liver regeneration post PHx. MYDGF was overexpressed using adeno-associated virus serotype 8 (AAV8) with a hepatocyte specific thyroxine binding globulin promotor (TBG). AAV8-TBG-Green fluorescent protein (GFP) was used as control. Furthermore, male C57BL/6N mice from Charles River and B6N.C-Mydgf^{tm1Kcw} (MYDGF KO) mice bred by Korf-Klingebiel et al. 2015 at 10-15 weeks of age, were used to study the influence of a MYDGF KO on liver regeneration post PHx. Mice were kept in rooms with controlled temperature at 22°C, humidity of 55% and lighting from 6 a.m. to 6 p.m., and fed with the standard laboratory chow and water *ad libitum*. All animal experiments were performed

according to the German animal protection laws (Animal Ethics Committee of the Landesamt für Natur, Umwelt und Verbraucherschutz, Nordrhein-Westfalen).

4.2.3 Tail vein injection

To overexpress MYDGF in the mouse liver a AAV8-TBG mediated overexpression was performed. Therefore, male C57BL/6J mice received $1x10^{12}$ genome copies (GC) AAV8-TBG-MYDGF or AAV8-TBG-GFP via tail vein injection. For the injection, C57BL/6J mice were placed in a restrainer and the tail was immersed in warm water to dilate the blood vessels. Tail was disinfected and 100 µl of AAV8-TBG-GFP (Vigene Biosciences) or AAV8-TBG-MYDGF (Vigene Biosciences) suspension ($1x10^{12}$ GC) was slowly injected into the tail vein. PHx was performed seven days after injection.

4.2.4 Two-thirds partial hepatectomy (PHx)

Two-thirds PHx was performed according to the protocol from Mitchell and Willenbring (Mitchell and Willenbring, 2008). Mice received 5 mg/kg Rimadyl (Carprofen, Zoetis) intraperitoneally as an analgesic and were anesthetized with 1.5–2% isoflurane. Then the median and left liver lobes were surgically resected and the mice were kept warm to avoid hypothermia. After 3, 6, 12, 24, 30 or 96 h the mice were sacrificed via cervical dislocation and the right and caudate liver lobes were isolated. Mice with improperly perfused (light brown) livers and hemorrhages in the livers were excluded from further analysis. Half of the right liver lobe was used for protein and RNA isolation and was directly placed in liquid nitrogen and stored at -80°C. The other half of the right liver lobe, caudate liver lobe and reference organs (spleen, kidney, heart) were placed in 4% PFA (Thermo Fisher Scientific, J19943) for immunohistochemical analysis. To analyze the expression kinetics of MYDGF post PHx in hepatic ECs, the right liver lobe from C57BL/6J mice was used. 20 mg of the right liver lobe was dissected for isolation of protein and the remaining right liver lobe was used for isolation of hepatic ECs via magnetic activated cell sorting (MACS).

4.2.5 Magnetic activated cell sorting (MACS) of mouse hepatic ECs

The MACS method was used to isolate hepatic ECs ($CD146^+$ cells) from the right liver lobe of C57BL/6J mice. The customer protocols "Liver Dissociation Kit mouse" (Miltenyi Biotec, 130105807) and "CD146 (LSEC) MicroBeads" (Miltenyi Biotec, 130092007) served as a basis for the isolation experiment. Only the application of the cell suspension on the MS columns (Miltenyi Biotec, 130042201) was changed. First, a liver cell suspension was prepared, using the liver dissociation kit (Miltenyi Biotec, 130105807), gentleMACS™ C Tubes (Miltenyi Biotec, 130093237) and the gentleMACS™ Octo Dissociator with heaters (Miltenyi Biotec, 130096427). Afterwards, mouse hepatic ECs were labeled with $CD146^+$ magnetic beads (Miltenyi Biotec, 130092007), and the cell suspension with the $CD146^+$ magnetically labeled cells was applied twice on two different MS columns, which were placed in a QuadroMACS™ separator (Miltenyi Biotec, 130090976) on a MACS® MultiStand (Miltenyi Biotec, 130042303), to increase the purity of the isolated cells. To isolate the magnetically labeled cells, which retained in the columns, columns were removed from the magnetic field and flushed with PEB buffer (MACS® bovine serum albumin stock solution (Miltenyi Biotec, 130091376) diluted 1/20 in autoMACS® rinsing solutions (Miltenyi Biotec, 130091222)). Cells were centrifuged for 5 min at 9,000 x *g* and resuspended in 100 µl protein lysis buffer containing 50 mM HEPES (Carl Roth), 150 mM NaCl (Carl Roth), 10% Glycerol (Carl Roth), 1% Triton X-100 (AppliChem), PhosSTOP™ phosphatase inhibitor (Sigma-Aldrich, 4906845001) and cOmplete™ protease inhibitor cocktail (Roche, 11697498001). Lysates were stored at -80°C.

4.3 Mechanical stretching of human hepatic ECs

Stretching experiment was performed with 200,000 human hepatic ECs in passage 4 seeded on STREX stretch chambers (STREX, STB-CH-04), pre-coated with speed coating solution (PELOBiotech, PB-LU-000-0002-00) overnight at RT. Cells were allowed to attach for up to one day. For stretching, microvascular endothelial cell growth medium without supplements (PELOBiotech, PB-MH-100-4099 - basal medium) was added and cells were unidirectionally stretched with an automated cell stretching system (STREX, STB-1400-10). Cells were stretched 20% static for 30 min plus 20% cyclic (30 cycles/min) for 1 h at 37°C and 5% CO_2. Cells seeded on stretch chambers, without stretching, were used as control.

4.4 Flow cytometry analysis of mechanically stretched human hepatic ECs

To analyze the number of living and dead cells from unstretched and mechanically stretched human hepatic ECs, flow cytometry analysis was performed. Stretching of hepatic ECs was performed as described above. Medium, containing possible detached dead cells, was aspirated and filled into a round-bottom polystyrene tube (Falcon, 352052). Afterwards, adherent ECs were detached by trypsinization (Gibco, 25300-054) and transferred to the corresponding tube. Tubes were centrifuged for 5 min at 400 x *g* and washed with PBS (Gibco, 10010-015). Centrifugation step was repeated and BD Horizon™ Fixable Viability Stain 660 (FVS660, 1/1000) (BD Biosciences, 564405), diluted in 1x PBS was added for 15 min at RT in the dark. Cells were washed with PBS and centrifuged for 3 min at 400 x *g*. The cell pellet was resuspended in PBS and FVS660 positive ($FVS660^+$, dead cells) and FVS660 negative ($FVS660^-$, living cells) cells were determined using a CytoFlex S (Beckman Coulter) flow cytometer. For quantification FlowJo software version 10 (BD Biosciences, RRID:SCR_008520) was used.

4.5 Quantitative polymerase chain reaction

Before the quantitative polymerase chain reaction (qPCR) was started, ribonucleic acid (RNA) was isolated using the high pure RNA isolation kit (Roche, 11828665001), according to the manufacturer's instructions (Roche, 11828665001). To transcribe RNA into complementary deoxyribonucleotide acids (cDNA), oligo(dT) 18 bases primers (Eurogentec, UN-PR100-005), deoxynucleotide mix (dNTP mix) (Sigma-Aldrich, D7295), 5 x First-Standard-Buffer, 0.1 M DTT, and Super-Script™ II Reverse Transcriptase (Thermo Fisher Scientific, 18064014) were used according to the manufacturer´s protocol (Thermo Fisher Scientific, 18064014).

A qPCR was performed to determine the *AFP* expression in HepG2 cells and human hepatocytes (HU8296, HU8284, HU8373, S1426T). For qPCR, QuantStudio™ 1 Real-Time PCR Instrument (Applied Biosystems, A40425) with the QuantStudio™ Design & Analysis Software v1.5.1 (Thermo Fisher Scientific) and FastStart Essential DNA Green Master (Roche, 06402712001) were used. cDNA samples were diluted 1/5 with H_2O, run in duplicates, and were normalized to the housekeeping genes: *ribosomal protein lateral stalk subunit P0* (*RPLP0*), *beta-2-microglobulin* (*B2M*), and *hypoxanthine-phosphoribosyltransferase* (*HPRT*). Gene expression, measured by qPCR, was calculated according to the protocol “Analyzing real-time PCR data by the comparative CT method” (Schmittgen and Livak, 2008).

Following qPCR thermal profiles (**Table 4**) and primer sequences (**Table 5**) were used:

Table 4: Thermal profile used in qPCR.

Step	Pre-incubation	3-step amplification			Melting	
Temperature	95°C	95°C	60°C	72°C	60°C	95°C
Time	2 min	20 s	20 s	20 s	20 s	1 s
Cycle	1	40			1	

Table 5: Human primer sequences used in qPCR.

Primer	Sequence
AFP	forward 5´–ACA TCC TCA GCT TGC TGT CT–3´
	reverse 5´–AAT GCT TGG CTC TCC TGG AT–3´
RPLP0	forward 5'–GAA GAC AGG GCG ACC TGG AA–3'
	reverse 5'–CCA CAT TGT CTG CTC CCA CA–3'
B2M	forward 5'–TTT CAT CCA TCC GAC ATT GA–3'
	reverse 5'–CCT CCA TGA TGC TGC TTA CA–3'
HPRT	forward 5'–GCA GAC TTT GCT TTC CTT GG–3'
	reverse 5'–AAC ACT TCG TGG GGT CCT TT–3'

4.6 Histochemical methods

4.6.1 Staining of human hepatocytes and HepG2 cells

Human hepatocytes, seeded on Nunc® Lab-Tek® Chamber Slides™ (Lab-Tek, 177445) were used for phospho-Histone H3 (PH3), caspase-3 or EdU staining. To determine HepG2 cell proliferation PH3 staining was performed. Human hepatocytes and HepG2 cells were fixed with 4% PFA (Thermo Fisher Scientific, J19943) overnight at 4°C under agitation.

For PH3 and caspase-3 staining cells were washed thrice in in 1 x phosphate-buffered saline with calcium and magnesium (1x $PBS^{Ca2+Mg2+}$: 5.4 mM KCl, 0.27 M NaCl, 3 mM KH_2PO_4, 1.3 mM Na_2HPO_4, 5 mM $MgCl_2$, 9 mM $CaCl_2$ in H_2O) for 5 min and blocked in 0.3% Triton X-100 (AppliChem) and 5% normal donkey serum (NDS, Jackson ImmunoResearch) diluted in 1 x $PBS^{Ca2+Mg2+}$ for 1 h at RT. Afterwards primary antibodies: rabbit anti-phospho-Histone H3 (Ser10) (Sigma-Aldrich, 06-570, 1/50) or rabbit anti-caspase-3 (Sigma-Aldrich, C8487, 1/200) diluted in antibody dilution buffer (0.3% Triton X-100 (AppliChem), 1% bovine serum albumin (BSA, AppliChem) in 1 x $PBS^{Ca2+Mg2+}$) were incubated for 1 h at RT. Slides were washed three times with 1 x $PBS^{Ca2+Mg2+}$ and secondary antibodies: donkey anti-rabbit Alexa Fluor 488™ (Invitrogen, A-21206, 1/500) and 4′,6-diamidino-2-phenylindole (DAPI) (Sigma-Aldrich, D9542, 1/1000) diluted in antibody dilution buffer were added for 1 h at RT. The slides were washed thrice in 1 x $PBS^{Ca2+Mg2+}$ for 5 min and coverslips were mounted with Fluoroshield™ (Sigma-Aldrich, F6182). All washing steps were performed under agitation.

EdU Click-iT® reaction (Thermo Fisher Scientific, C10337) was performed as described in manufacturer's instructions and cells were co-stained for rabbit anti-hepatocyte nuclear factor 4α (HNF4α, Cell Signaling, C11F12, 3113, 1/500) and DAPI (Sigma-Aldrich, D9542, 1/1000). Slides were washed three times with 1 x $PBS^{Ca2+Mg2+}$ and secondary antibodies: donkey anti-rabbit Alexa Fluor™ 555 (Invitrogen, A-31572, 1/500) and DAPI (Sigma-Aldrich, D9542, 1/1000) diluted in antibody dilution buffer were added for 1 h at RT. The slides were washed thrice in 1 x $PBS^{Ca2+Mg2+}$ for 5 min and coverslips were mounted with Fluoroshield™ (Sigma-Aldrich, F6182).

To analyze the number of proliferating human hepatocytes a tile scan image consisting of 7x7 tiles were acquired at 10x magnification using the laser scanning microscope 710 (LSM 710, Zeiss). To analyze the number of apoptotic hepatocytes and proliferating HepG2 cells, five images per well were acquired at 20x magnification using the LSM 710 (Zeiss). Proliferating cells were counted manually in Fiji (open-source software focused on biological-image analysis) (Schindelin et al., 2012) in a blinded manner. The same threshold was used to determine the caspase-3^+ area and the $DAPI^+$ area in each image. For quantification, caspase-3^+ area was divided by the $DAPI^+$ area.

4.6.2 Whole mount staining of human hepatocyte organoids

Human hepatocyte organoids (Donor: HU8296, HU8373), previously fixed with 4% PFA (Thermo Fisher Scientific, J19943) (incubated overnight at 4°C) and stored in 1 x $PBS^{Ca2+Mg2+}$, were washed three times with wash buffer (0.1% Triton X-100 (AppliChem) in 1 x $PBS^{Ca2+Mg2+}$) for 5 min at RT. Blocking solution (0.1% Triton-X-100 (AppliChem) + 10% NDS (Jackson ImmunoResearch, 017000121) + 1% BSA (AppliChem) in 1 x $PBS^{Ca2+Mg2+}$) was added to each well and incubated for 30 min at RT. Afterwards, EdU Click-iT® reaction reagent (Invitrogen, C10337) was applied and incubated in the dark for 30 min at RT. Subsequently, organoids were washed three times with wash buffer for 5 min at RT and incubated overnight at 4°C with rabbit anti-HNF4α (Cell Signaling, C11F12, 3113, 1/250) diluted in blocking solution. The following day, organoids were washed three times for 5 min at RT with wash buffer and secondary antibody, donkey anti-rabbit Alexa Fluor™ 555 (Invitrogen, A-31572, 1/500) plus DAPI (Sigma-Aldrich, D9542, 1/1000) diluted in blocking solution, were incubated for 2 h at RT. Then organoids were washed three times with wash buffer for 5 min at RT, and stored in 1 x $PBS^{Ca2+Mg2+}$. All washing and antibody incubation steps were performed under agitation. Z-stack images were acquired at 20x magnification using the LSM 710 (Zeiss) and analyzed using Fiji (Schindelin et al., 2012). Organoid area was measured with the free hand selection tool and EdU^+ cells were counted manually in a blinded manner.

4.6.3 Immunohistochemical staining

For immunohistochemical staining the PFA fixed liver lobes of AAV8-TBG-GFP and AAV8-TBG-MYDGF mice, and C57BL/6N and MYDGF KO mice, and reference organs (heart, kidney, spleen) of AAV8-TBG-GFP mice were first equilibrated by placing them in 15% and 30% sucrose (Carl Roth, 4621.1). Second, the liver lobes and organs were placed in Peel-A-Way® embedding molds (Polysciences, 18986-1) filled with Tissue-Tek® O.C.T™ embedding medium (Sakura, 4583) and stored at -80°C. Afterwards, 12 µm cryo-sections were prepared using a cryostat microtome HM 560 (Thermo Fisher Scientific). Sections were placed on SuperFrost Plus™ slides (Thermo Fisher Scientific, J1800AMNZ) and stored at -20°C until staining.

For the immunohistochemical staining the tissue sections were first washed twice in 1 x $PBS^{Ca2+Mg2+}$ and once in 1 x $PBS^{Ca2+Mg2+}$ containing 0.2% Triton X-100 (AppliChem) for 5 min at RT. Then the slides were blocked for 1 h at RT in $PBS^{Ca2+Mg2+}$ containing 0.2% Triton X-100 (AppliChem) and 1% BSA (AppliChem), and the primary antibodies: goat anti-GFP (Sicgen, AB0020-200, 1/500), goat anti-ICAM-1/CD54 (R&D, AF796, 1/100), rabbit anti-phospho-Histone H3 (Ser10) (Sigma, 06-570, 1/50), rat anti-Ki-67 (SolA15) (Invitrogen, 14-5698-82, 1/100), or rabbit anti-HNF4α (Abcam, ab181604, 1/100) were incubated at 4°C overnight. The following day, slides were washed twice in 1 x $PBS^{Ca2+Mg2+}$ and once in 1 x $PBS^{Ca2+Mg2+}$ containing 0.2% Triton X-100 for 10 min. Secondary antibodies: donkey anti-goat Alexa Fluor™ 555 (Invitrogen, A-21432, 1/500), donkey anti-rabbit Alexa Fluor™ 555 (Invitrogen, A-31572, 1/500), donkey anti-rabbit Alexa Fluor™ 488 (Invitrogen, A-21206, 1/500), donkey anti-rat Alexa Fluor™ 488 (Invitrogen, A-21208, 1/500), donkey anti-goat Alexa Fluor™ 488 (Invitrogen, A-11055, 1/500), and DAPI (Sigma-Aldrich, D9542, 1/1000) were added and incubated for 45 min at RT. Slides were washed thrice for 10 min in 1 x $PBS^{Ca2+Mg2+}$ and mounted with Fluoroshield™ (Sigma-Aldrich, F6182). All washing steps were performed under agitation.

To analyze the proliferation rate, five images of up to four sections were acquired at 20x magnification using the LSM 710 (LSM 710, Zeiss). Proliferating cells were counted manually with Fiji (Schindelin et al., 2012) or QuPath (Bankhead et al., 2017), and $DAPI^{+}$ cells were analyzed automatically by setting an individual threshold which was applied uniformly to each image using Fiji. All images were analyzed in a blinded fashion.

4.7 Biochemical methods

4.7.1 Protein isolation, BCA assay, and Western blot

For protein isolation, protein lysis buffer containing 50 mM HEPES (Sigma-Aldrich), 150 mM NaCl (Sigma-Aldrich), 10% Glycerol (Sigma-Aldrich), 1% Triton X-100 (Sigma-Aldrich), PhosSTOP™ phosphatase inhibitor (Sigma-Aldrich, 4906845001), cOmplete™ protease inhibitor cocktail (Roche, 11697498001), and H_2O was applied to the cells and incubated for 20 min on ice. By using a cell scratcher and pipetting up and down, cells were lysed and subsequently transferred into 1.5 ml plastic tubes. For protein isolation from mouse liver tissue, 20 mg liver tissue was added in gentleMACS™ M Tubes (Miltenyi Biotec, 130093236) containing protein lysis buffer. M-tubes were placed on the gentleMACS™ Octo Dissociator with heaters (Miltenyi Biotec, 130096427) running program 'protein_01_01'. All protein lysates were centrifuged at 13,000 x rpm for 10 min at 4°C, and supernatant was transferred into a new tube. Subsequently, a bicinchoninic acid assay (BCA assay) was performed to determine protein concentration in each sample. The standard of the Pierce™ BCA™ Protein Assay (Thermo Fisher Scientific, 23225) was pipetted in duplicates into a 96-well plate (Sarstedt, 7022611). In addition to the standard, samples were diluted 1/10 (cell lysates) or 1/40 (liver lysates). 200 µl working reagent, consisting 50 parts A and 1 part B from Pierce™ BCA protein assay kit (Thermo Fisher Scientific, 23225) was added to the standard and samples, and incubated for 30 min at 37°C (200 rpm) in the dark on a thermoshaker (HLC BioTech, MKR 23). The protein concentration was detected with a plate reader (GloMax® Discover Version 3.2.3 (Promega GmbH)) at 560 nm. The samples were diluted with H_2O so that 20 µg protein could be filled in the pockets for a sodium dodecyl sulfate polyacrylamide gel electrophoresis (SDS-PAGE). Besides, 4x Laemmli sample buffer (Bio-Rad, 1610747) diluted 1/10 with β-mercaptoethanol (CarlRoth), was added to the samples and heated at 95°C for 5 min. Samples and Precision plus protein dual color standards (BioRad, 1610374) were loaded on Mini-protean™ TGX stain-free protein gels (Bio-Rad, 4568086 and 4568085) and gels were run for 40 min at 180 V. All steps were followed by manufacturer's instructions from BioRad. Afterwards, proteins were transferred onto a membrane by using trans-blot turbo mini 0.2 µm PVDF transfer packs (Bio-Rad, 1704156), and trans-blot® turbo™ transfer system (Bio-Rad, 1704150) with the mixed molecular weight program (1.3 A, 25 V, 7 min). After blotting, membranes were blocked with blocking buffer, containing 5% BSA (AppliChem), and 0.5% Tween-20 (Sigma-Aldrich) in $PBS^{Ca2+Mg2+}$ for 1 h at RT. Primary antibodies: rabbit anti-phospho-p44/42 MAPK (ERK1/2) (Thr202/Tyr204) (Cell Signaling, 4376, 1/750 or 1/500), rabbit anti-p44/42 MAPK (ERK1/2) (137F5) (Cell Signaling, 4695, 1/750 or 1/500), rabbit anti-phospho-Stat3 (Ser727) (Cell Signaling, 9134, 1/500), rabbit anti-Stat3 (D3Z2G) (Cell Signaling, 12640, 1/750), rabbit

anti-phospho-AKT (Ser473) (D9E) (Cell Signaling, 4060, 1/750), rabbit anti-AKT (pan) (C67E7) (Cell Signaling, 4691, 1/750), rabbit anti-MYDGF (Proteintech, 11353-1-AP, 1/1000), rabbit anti-GAPDH (Abcam, Ab9485, 1/5000 or 1/2000) and rabbit anti-β tubulin antibody – Loading Control (Abcam, ab6046, 1/2000) were added and incubated overnight at 4°C under agitation. On the next day, membranes were washed ($PBS^{Ca2+Mg2+}$ and 0.5% Tween-20) and secondary antibody goat anti-rabbit IgG, horseradish peroxidase (HRP)-linked (Cell Signaling, 7074, 1/2000) was incubated for 1 h at RT. For detection, Clarity Western ECL Substrate (Bio-Rad, 170-5061) or WesternBright™ Peroxide Chemiluminescent Detection Reagent (Advansta, R-03025-D10) were added and visualized with ChemiDoc MP Imaging System (Bio-Rad). Densitometrical analysis was performed using Image Laboratory Software Versions 6.1 (Bio-Rad).

4.7.2 Enzyme-linked Immunosorbent Assay (ELISA)

To analyze the MYDGF and HGF concentrations in human blood serum and blood plasma, the blood samples were tested in duplicates using the MYDGF/SF20 quant ELISA (LSBio, LS-F13143) or human HGF quantikine ELISA (R&D Systems, DHG00B). ELISAs were performed according to the manufacturer's instructions (LSBio, LS-F13143 and R&D Systems, DHG00B). To analyze MYDGF and HGF concentrations in the isolated hepatic ECs from the right liver lobe of C57BL/6J mice at different timepoints post PHx, the mouse MYDGF ELISA (AVIVA Systems Biology, OKEI00375) or mouse/rat Quantikine® ELISA (R&D Systems MHG00) were performed according to the manufacturer's instructions (AVIVA Systems Biology, OKEI00375 and R&D Systems MHG00). Protein lysates from the isolated mouse hepatic ECs were added in duplicates at the ELISA plates. ELISA results were detected with a plate reader (GloMax® Discover Version 3.2.3 (Promega GmbH)).

4.8 Statistical analysis

P values were calculated using two-tailed paired or unpaired Student's *t*-test with Welch's correction, multiple unpaired *t*-test with Welch's correction, one-way ANOVA with Dunnett's post-hoc test and two-way ANOVA with Tukey's or Šidák´s post-hoc test. Statistical significance was calculated using Excel (Microsoft) or Prism 9 (GraphPad). Furthermore, all data are expressed as mean ± standard error of the mean (± SEM). Results were determined as significant with a *P*-value < 0.05 and exact *P*-values are stated in each figure. Outliers were determined using GraphPad Prism Grubb's outlier method and excluded from further analysis.

4.9 Personal contributions

Most of the experiments were performed by Paula Follert, supervised by Prof. Dr. Eckhard Lammert and funded by the "Intra- and interorgan communication of the cardiovascular system (IRTG 1902)".

Experiments in which Paula Follert received assistance from others are listed below:

For the flow cytometry analysis experiment (**Figure 5**) Paula Follert performed the stretch experiments and stained the cells, while Philip Kirschner helped Paula Follert with the analysis of cell viability via flow cytometry.

3D organoid culture was established by Linda Große-Segerath. Analysis of organoid area and proliferating hepatocytes in **Figure 8a-d**, was performed by Linda Große-Segerath and Paula Follert. The graphs show the average of both analyses.

Tail vein injections of the mice were performed by Linda Große-Segerath and Paula Follert (**Figure 17-22**). Tobias Buschmann performed partial hepatectomy of AAV8-TBG-GFP and AAV8-TBG-MYDGF transfected mice isolated 30 hours after PHx, while all other partial hepatectomies were performed by Kristina Behnke and Julia Ettich. Cryosections of liver lobes and reference organs were performed by Linda Große-Segerath and Paula Follert. For **Figure 17** Paula Follert stained and imaged the median liver lobes of AAV8-TBG-GFP transfected mice, while Linda Große-Segerath performed the analysis of GFP-infected hepatocytes. Staining, imaging and analysis of the number of $PH3^+$ and $ICAM\text{-}1^-$ cells in the right liver lobe of AAV8-TBG-GFP and AAV8-TBG-MYDGF transfected mice was performed by Linda Große-Segerath (**Figure 19a-c**).

5. Results

The liver is characterized by its considerable regenerative capacity, whereby angiocrine signals play a crucial role (Ding et al., 2010, Ding et al., 2014, Rafii et al., 2016, Zhang et al., 2020). After PHx, sinusoidal hepatic ECs get mechanically stretched and release angiocrine signals, such as HGF, to enhance proliferation of hepatocytes and to restore the liver mass (Lorenz et al., 2018). In previous experiments, we were able to identify increased levels of the paracrine-acting protein MYDGF in the supernatant of mechanically stretched primary human hepatic ECs by liquid chromatography-tandem mass spectrometry (LC-MS/MS) (Große-Segerath, 2020, Große-Segerath and Follert et al., 2024). Additionally, we demonstrated that MYDGF enhances proliferation and survival of primary human hepatocytes (Große-Segerath, 2020, Große-Segerath and Follert et al., 2024).

In this thesis, we further examined the effect of the angiocrine signal MYDGF on cultured primary human hepatocytes and liver regeneration. First, we analyzed whether our stretching conditions, which have been shown to induce the release of MYDGF from primary human hepatic ECs (Große-Segerath, 2020, Große-Segerath and Follert et al., 2024), lead to increased cell death. Second, we examined whether the proliferation- and survival-enhancing effect of MYDGF on primary human hepatocytes in a 2D culture system can be verified, using an additional proliferation and apoptosis marker. Third, we analyzed whether daily MYDGF treatment has a growth- and proliferation-enhancing effect on primary human hepatocyte organoids. Next, we identified the signaling pathway that is involved in MYDGF-induced hepatocyte proliferation. In the last part of this thesis, we determined the relevance of MYDGF in *in vivo* systems. For this, we first examined the expression kinetic of MYDGF after liver resection in humans and after two-thirds PHx in mice and compared it with the expression kinetic of HGF. Second, we analyzed the influence of MYDGF on liver regeneration using gain- and loss-of-function experiments. We studied the impact of MYDGF overexpression, mediated by AAV8-TBG transfection, on hepatocyte proliferation and associated liver regeneration, as well as the effect of a MYDGF knockout on hepatocyte proliferation after PHx.

5.1 Mechanical stretching of human hepatic ECs does not lead to enhanced cell death

After demonstrating that increased MYDGF levels can be measured in the supernatant of mechanically stretched primary human hepatic ECs (Große-Segerath, 2020, Große-Segerath and Follert et al., 2024), we aimed to confirm that MYDGF levels were not elevated due to increased cell death. Therefore, we investigated cell viability in unstretched and mechanically stretched primary human hepatic ECs. The latter were seeded on silicone stretch chambers and were allowed to attach for up to one day. The next day, the silicone stretch chambers were placed in an automated cell stretching system and unidirectionally stretched for 30 minutes statically and for one hour cyclically (20% stretch each). Primary human hepatic ECs seeded on stretch chambers, without stretching, were used as control. Cell viability was then measured by flow cytometry analysis (**Figure 5a, b**). The results of the flow cytometry analysis show that in the unstretched condition, an average of 5.5% of the cells are dead, while in the stretched condition, an average of 3.6% are dead (**Figure 5c**). Thus, the percentage of dead cells is significantly decreased in mechanically stretched primary human hepatic ECs.

To sum up, mechanical stretching of primary human hepatic ECs does not lead to an increase in cell death compared to the unstretched primary human hepatic ECs and even slightly decreases cell death.

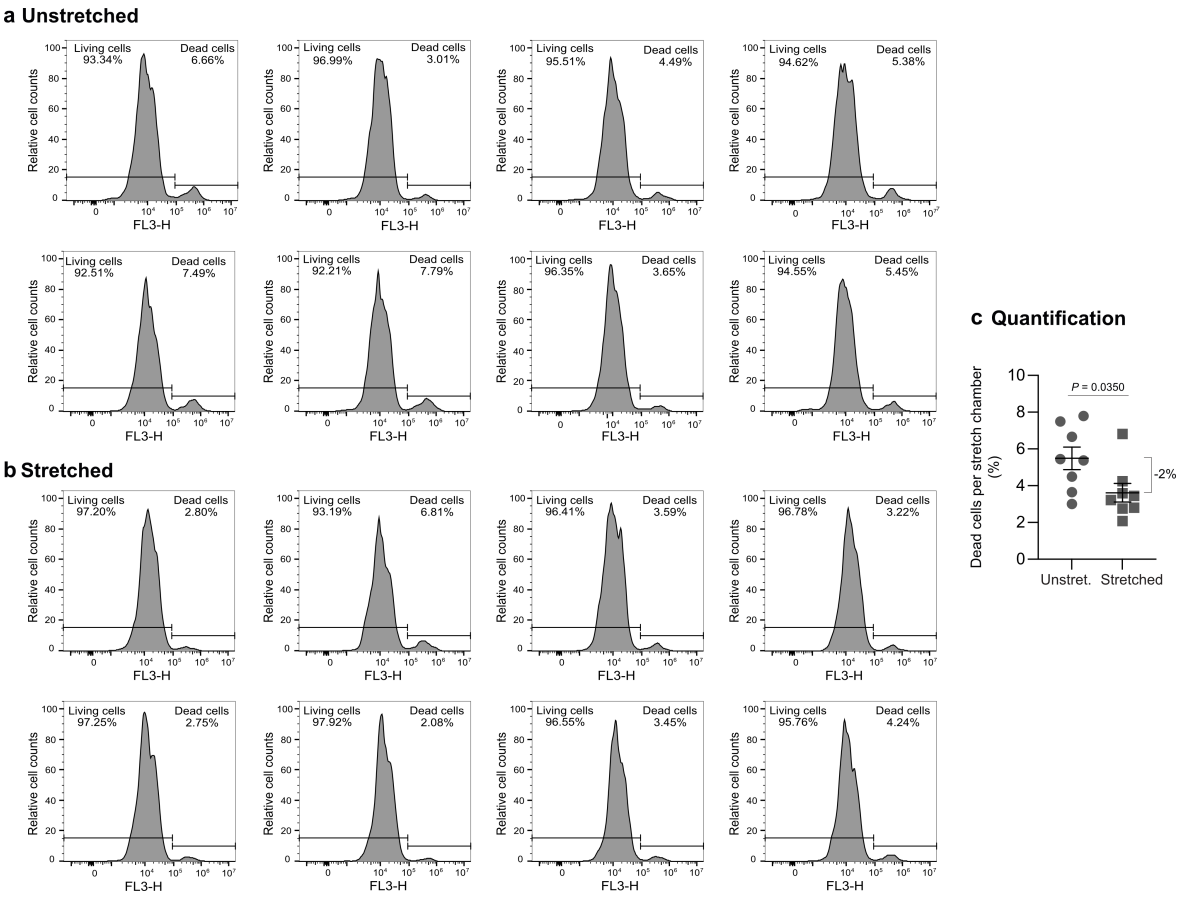

Figure 5: Mechanical stretching of primary human hepatic ECs does not lead to increased cell death.
Flow cytometric analysis of cell viability using Fixable Viability Stain 660 (FVS660). Histograms show primary human hepatic endothelial cells (ECs) that were either unstretched (**a**) or mechanically stretched (**b**). (**c**) Quantification of precent of dead cells per stretch chamber in unstretched and stretched condition. n = 8 stretch chambers for each condition. Data are presented as mean ± SEM. *P* value was calculated using two-tailed unpaired Student´s *t*-test with Welch's correction.

5.2 MYDGF improves proliferation and survival of human hepatocytes

Since we were able to show that the elevated levels of MYDGF in the supernatant of stretched primary human hepatic ECs were not caused by an increase in cell death, we next analyzed whether MYDGF treatment has a proliferation- and survival-enhancing effect on primary human hepatocytes. Previous experiments in our laboratory have already shown that MYDGF promotes proliferation and survival of primary human (Große-Segerath, 2020, Große-Segerath and Follert et al., 2024). This was demonstrated by comparing primary human hepatocytes, treated without (control) or with 1 ng/ml recombinant MYDGF for six hours, and stained for 5-ethynyl-2'-deoxyuridine (EdU, proliferation marker) or TUNEL (apoptosis marker). To reproduce these results, we repeated the experiments and stained primary human hepatocytes with an additional proliferation and apoptosis marker. PH3 is a proliferation marker that stains cells in the late G_2 phase of the cell cycle (Elmaci et al.,

2018) and caspase-3 is a cell death protease and thus represents an apoptosis marker (Porter and Janicke, 1999).

To analyze whether MYDGF leads to increased number of $PH3^+$ cells, primary human hepatocyte from three different donors (female, 26 years; male, 23 years; and female, 31 years) were treated without (control) or with 1 ng/ml recombinant MYDGF for six hours. Hepatocytes were then fixed and stained for the proliferation marker PH3 (**Figure 6a, b**). To determine the number of proliferating cells, $PH3^+$ hepatocytes per well were counted manually. Our results show that primary human hepatocytes treated with recombinant MYDGF display an increased number of proliferating hepatocytes per well (**Figure 6c-e**). Human hepatocytes from the 26-year-old female donor show a 74% increase in $PH3^+$ hepatocytes per well in the MYDGF-treated condition (**Figure 6c**). In the 23-year-old male donor, MYDGF treatment increases hepatocyte proliferation by 42% (**Figure 6d**). The slightly older female donor (31 years) shows a tendential increase (44%) in the number of $PH3^+$ hepatocytes in the MYDGF-treated compared to the control condition (**Figure 6e**).

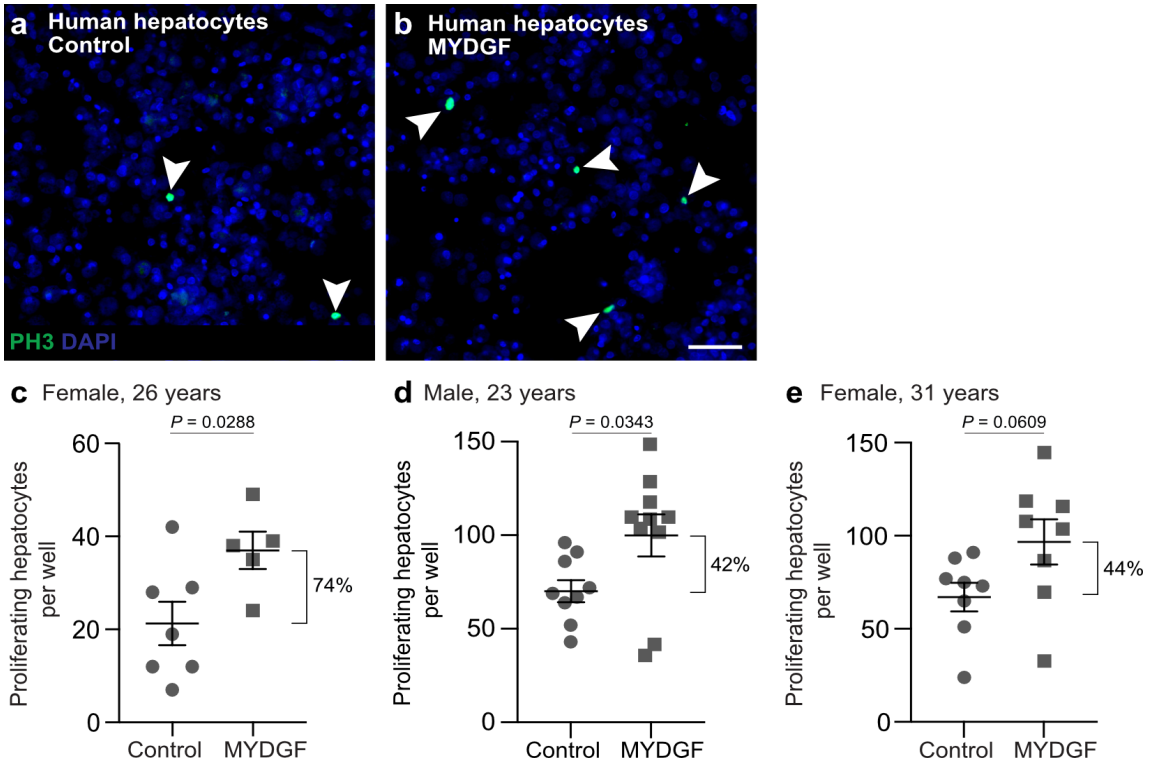

Figure 6: Increased proliferation rate of primary human hepatocytes after MYDGF treatment. (**a, b**) Laser scanning microscope (LSM) images of primary human hepatocytes treated without (control) (a) or with MYDGF (b), stained for the proliferation marker PH3 (green) in a female, 26-year-old donor. Cell nuclei were counterstained for DAPI. White arrowheads point to the proliferating cells. (**c-e**) Quantification of the number of proliferating hepatocytes per well in a female, 26-year-old donor, n = 7 control versus n = 5 MYDGF treated wells (c); male, 23-year-old donor, n = 9 control versus n = 10 MYDGF treated wells (d); female, 31-year-old, n = 8 wells each (e). Scale bar: 50 µm. Data are presented as mean ± SEM. *P* values were calculated using a two-tailed unpaired Student´s *t*-test with Welch's correction.

After we were able to verify the proliferation promoting effect of recombinant MYDGF on primary human hepatocytes using an additional proliferation marker, we analyzed the effect of recombinant MYDGF treatment on primary human hepatocyte survival. To analyze whether MYDGF leads to a reduced caspase-3 area, primary human hepatocytes from three different donors (female, 26 years; male, 31 years; and male, 23 years) were treated without (control) or with 1 ng/ml recombinant MYDGF for six hours. The cells were then fixed and stained for caspase-3 (**Figure 7a, b**). To determine the apoptosis rate, caspase-3$^+$ area was normalized to DAPI$^+$ area, whereas the control was set to 100%. In all three donors a significant reduction of caspase-3$^+$ hepatocytes is visible. MYDGF treatment results in an approximately 40% reduction in caspase-3$^+$ area in primary human hepatocytes from the 26-year-old female and 31-year-old male donors and an 18% reduction in caspase-3$^+$ area in hepatocytes from the 23-year-old male donor compared to control **(Figure 7c-e**).

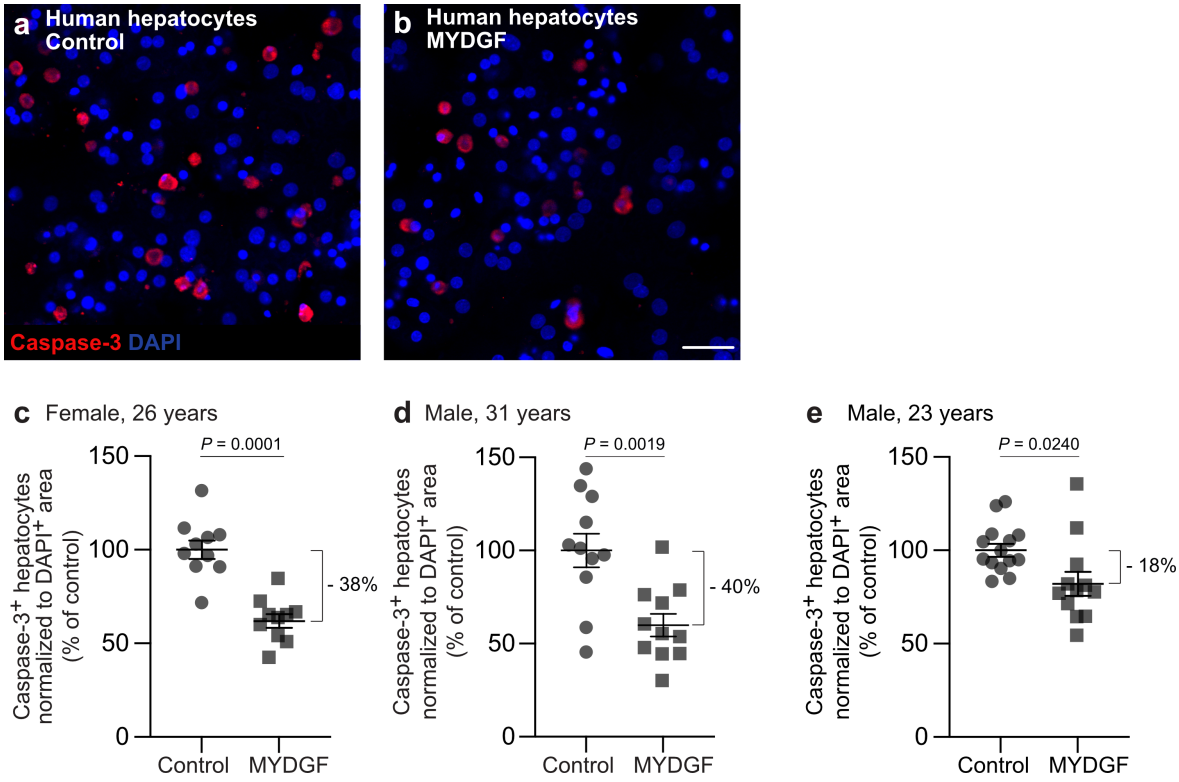

Figure 7: Reduced caspase-3 area in MYDGF treated primary human hepatocytes.
(**a, b**) LSM images of primary human hepatocytes treated without (control) (a) or with MYDGF (b), stained for the apoptosis marker caspase-3 (red) in a female, 26-year-old donor. Cell nuclei were counterstained for DAPI. (**c-e**) Quantification of caspase-3$^+$ hepatocytes normalized to DAPI$^+$ area in percent of control in a female, 26-year-old donor, n = 10 wells each (c); male, 31-year-old donor, n = 11 wells each (d); and male, 23-year-old donor, n = 14 control versus n = 12 MYDGF treated wells (e). Scale bar: 50 µm. Data are presented as mean ± SEM. *P* values were calculated using a two-tailed unpaired Student´s *t*-test with Welch's correction.

In summary, our results confirm the outcomes of our previously performed experiments and show that treatment with recombinant MYDGF leads to an increase in cell proliferation and survival rate of cultured primary human hepatocytes.

5.3 MYDGF treatment increases organoid size and proliferation rate in human hepatocyte organoids

Further, we want to elucidate the effect of MYDGF on primary human hepatocytes cultured in a 3D system. 3D culture systems have become increasingly important in recent years as they provide the ability to culture cells under conditions that more closely resemble the *in vivo* situation (Edmondson et al., 2014, Duval et al., 2017, Kapalczynska et al., 2018). However, it should be noted that the organoids due to their “grape-like” structure (Hu et al., 2018), have a nutrient-access-gradient. Cells located further inside the organoid receive a lower concentration of the treatment compared to cells located further outside (Edmondson et al., 2014, Duval et al., 2017). To overcome this problem, we used a 10-fold higher concentration of MYDGF in 3D compared to the 2D culture system.

To generate human hepatocyte organoids, primary human hepatocytes were cultured in 3D medium. Three days after seeding, organoids with previously described “grape-like” structures had formed (Hu et al., 2018), which were then treated with 10 ng/ml recombinant MYDGF. Earlier experiments showed that treatment of human hepatocyte organoids with a single dose of 10 ng/ml recombinant MYDGF leads to a tendentially enlarged organoid area and increased hepatocyte proliferation (Große-Segerath, 2020, Große-Segerath and Follert et al., 2024). Therefore, we decided to treat the human hepatocyte organoids with 10 ng/ml recombinant MYDGF daily in the presence of the proliferation marker EdU for a longer period of time (seven days). Human hepatocyte organoids treated without MYDGF in the presence of EdU served as a control. To investigate the effect of MYDGF on human hepatocyte organoid area and proliferation, a whole mount staining was performed (**Figure 8a, b**). Daily treatment of human hepatocyte organoids for seven days was performed with human hepatocytes from two different donors (Male, 23 years; Female, 26 years). After seven days, both donors show a significant increase in organoid area of up to 25% after daily MYDGF treatment compared to control (**Figure 8c, g**). Also, the number of EdU^+ human hepatocytes per organoid in each well was two to three times higher in MYDGF treated human hepatocyte organoids (**Figure 8d, h**).

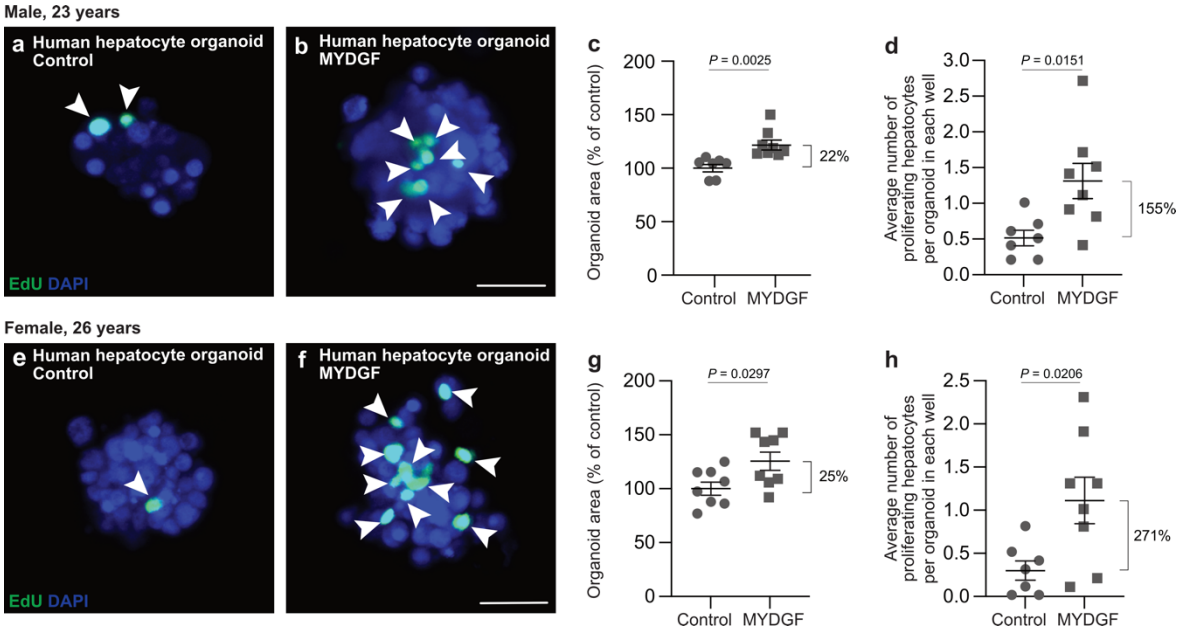

Figure 8: Daily MYDGF treatment increases organoid area and proliferation rate in human hepatocyte organoids.
(**a, b**) LSM images (maximum intensity projections) of human hepatocyte organoids treated for seven days daily without (control) (a) or with MYDGF (b), stained for the proliferation marker EdU (green). Cell nuclei were counterstained for DAPI. White arrowheads point to the proliferating cells. (**c, d**) Quantification of organoid area (c) and average number of proliferating hepatocytes per organoid in each well (d) in control (n = 7 wells with 5 organoids each) versus MYDGF (n = 8 wells 5 organoids each) treated human hepatocyte organoids of a male, 23-year-old donor. (**e, f**) LSM images (maximum intensity projections) of human hepatocyte organoids treated for seven days daily without (control) (e) or with MYDGF (f), stained for the proliferation marker EdU (green). Cell nuclei were counterstained for DAPI. White arrowheads point to the proliferating cells. (**g, h**) Quantification of organoid area (g) and average number of proliferating hepatocytes per organoid in each well (h) in control (n = 7-8 wells with 5 organoids each) versus MYDGF (n = 8 wells with 5 organoids each) treated human hepatocyte organoids of a female, 26-year-old donor. Scale bar: 50 µm. Data are presented as mean ± SEM. *P* values were calculated using a two-tailed unpaired Student´s *t*-test with Welch's correction.

Taken together, the results show that daily MYDGF treatment of human hepatocyte organoids promotes organoid area and proliferation rate.

5.4 *AFP*-positive HepG2 cell line does not respond to MYDGF

Since previous publications have shown that MYDGF also has a proliferation-promoting effect on hepatocellular carcinoma (Sunagozaka et al., 2011, Wang et al., 2021), we wanted to exclude the possibility that treatment with 1 ng/ml recombinant MYDGF has a cancer-promoting effect. Sunagozaka et al. showed that a knockout of *C19orf10* (*MYDGF*) in *alpha-fetoprotein* (*AFP*)-positive cell lines (such as Hep3B and HuH7 cells) results in reduced cell proliferation (Sunagozaka et al., 2011). AFP, produced in the fetal liver, is the fetal equivalent of albumin (Galle et al., 2019). In adults, AFP is replaced by albumin, and

only low levels of AFP can be measured throughout life (Bergstrand and Czar, 1956). However, an elevated AFP level can be measured in people with HCC and liver disease, making AFP a widely used hepatocellular tumor marker (Galle et al., 2019, Hu et al., 2022b). To exclude that treatment with MYDGF has a proliferation-promoting effect on an *AFP*-positive cell line, we treated HepG2 cells, an epithelial cell line isolated from hepatocellular carcinoma of a 15-year-old male, with MYDGF. Before we analyzed the number of proliferating HepG2 cells, we measured *AFP* expression in HepG2 cells and primary human hepatocytes from four different donors (male, 23 years; females, 46, 26, and 34 years) using quantitative PCR and normalized *AFP* expression to three different housekeeping genes (*B2M*, *HPRT*, and *RPLP0*). *AFP* was found to be expressed exclusively in HepG2 cells, but not in primary human hepatocytes from the four donors of different sex and age (**Figure 9**).

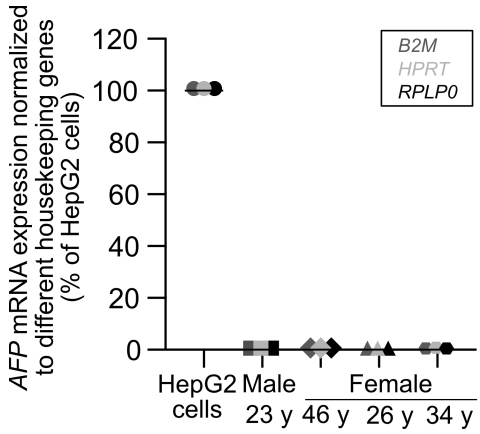

Figure 9: HepG2 cells and primary human hepatocytes display different *AFP* expression levels.
AFP expression in lysates from HepG2 cells and primary human hepatocytes from four different donors (23-year-old, male; 46-year-old, 26-year-old, 34-year-old female) normalized to the three different housekeeping genes *B2M*, *HPRT*, *RPLP0*. n = 1 cell lysate.

We then investigated whether MYDGF promotes proliferation in *AFP*-positive HepG2 cells. Therefore, we treated HepG2 cells without (control) or with recombinant MYDGF, using the same treatment concentration and duration as for primary human hepatocytes (1 ng/ml recombinant MYDGF and six hours of treatment). To determine the number of proliferating HepG2 cells, PH3 (proliferation marker) staining was performed and cell nuclei were counterstained with DAPI (**Figure 10a, b**). For the quantification $PH3^+$ cells were counted and normalized to the $DAPI^+$ cells as a percentage of the control. Treatment with 1 ng/ml recombinant MYDGF does not increase HepG2 cell proliferation after six hours (**Figure 10c**).

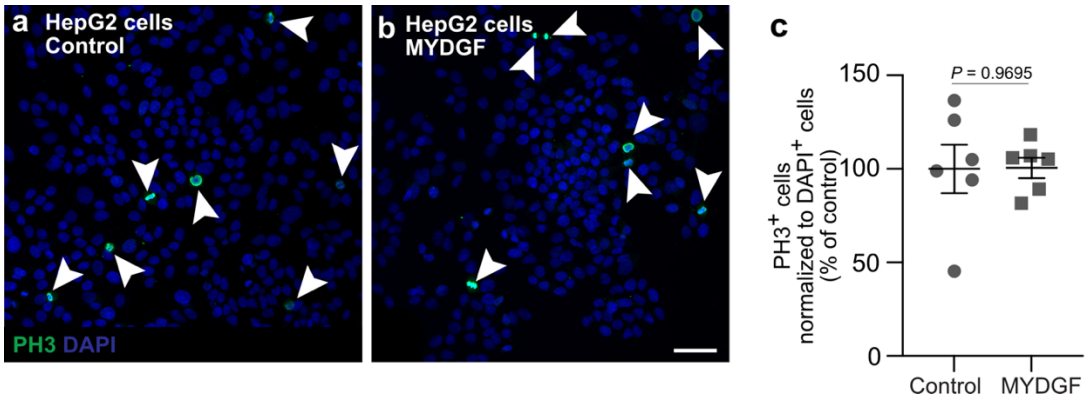

Figure 10: MYDGF treatment does not promote cell proliferation in the *AFP*-positive HepG2 cancer cell line.
(**a, b**) LSM images of HepG2 cells treated without (control) (a) or with MYDGF (b), stained for the proliferation marker PH3 (green). Cell nuclei were counterstained for DAPI. White arrowheads point to the proliferating cells. (**c**) Quantification of proliferating HepG2 cells per well as a percentage of control; n = 6 wells each. Scale bar: 50 µm. Data are presented as mean ± SEM. *P* value was calculated using two-tailed unpaired Student´s *t*-test with Welch's correction.

Hence, it can be concluded that 1 ng/ml recombinant MYDGF treatment for six hours does not promote the proliferation of the *AFP*-positive HepG2 cell line.

5.5 MYDGF leads to phosphorylation of MAPK, STAT3 and AKT in human hepatocytes

After demonstrating that MYDGF promotes cell survival and proliferation of human hepatocytes but not HepG2 cells, we were interested in identifying the signaling pathway that mediates this proliferation-enhancing effect of MYDGF on primary human hepatocytes. Korf-Klingebiel et al. 2015 have shown that MYDGF activates the PI3K/AKT signaling pathway in cardiac myocytes to protect them from cell death, while in HCAECs MYDGF promotes cell proliferation via the activation of the MAPK/STAT3 pathway.

Thus, we were interested whether MYDGF also leads to increased phosphorylation of the above-mentioned signaling molecules in human hepatocytes. To investigate this, human hepatocytes were starved in William's E medium for four hours before treatment without or with 1 ng/ml recombinant MYDGF for 0, 5, 15 and 30 minutes. Protein lysates were subsequently prepared and phosphorylation of MAPK on T202/Y204 (ERK1/2), STAT3 on S727, and AKT on S473 was assessed by Western blot (**Figure 11**). Additionally, we examined the pan-protein levels of the corresponding signaling molecules to determine if they were already altered by treatment with recombinant MYDGF. The ratio of phospho-protein level to pan-protein level, as well as to the housekeeping protein (GAPDH or β-tubulin) was calculated. Treatment of human hepatocytes with recombinant MYDGF

results in rapid phosphorylation of MAPK on T202/Y204 (ERK1/2) within the first 5 minutes. Thereafter, the phospho-MAPK (T202/Y204) level decreases almost to baseline. No increased phosphorylation of MAPK on T202/Y204 (ERK1/2) is seen in the control treatment (**Figure 11a, b**). The phospho-STAT3 (S727) level peaks at 5 and 15 minutes after treatment with recombinant MYDGF compared to the control. Specifically, 5 minutes after MYDGF treatment, the amount of phospho-STAT3 (S727) is numerically increased between control and MYDGF treatment. After 15 minutes of treatment, phospho-STAT3 (S727) is significantly increased about two-fold compared to control. In the control condition the phosphorylation level of STAT3 on S727 remains unaltered (**Figure 11c, d**). Furthermore, recombinant MYDGF also leads to increased phosphorylation of AKT on S473 in human hepatocytes within the first 15 minutes after treatment (**Figure 11e, f**). At 30 minutes after treatment, the relative phospho-AKT (S473) level returns to the basal level, whereas an increased level is observed in the control.

In conclusion, primary human hepatocytes treated with recombinant MYDGF show a rapid increase in phosphorylation of MAPK on T202/Y204 (ERK1/2), as well as phosphorylation of STAT3 on S727, and AKT on S473. However, we next asked if these signaling molecules are crucial for the increased cell proliferation of human hepatocytes after MYDGF treatment.

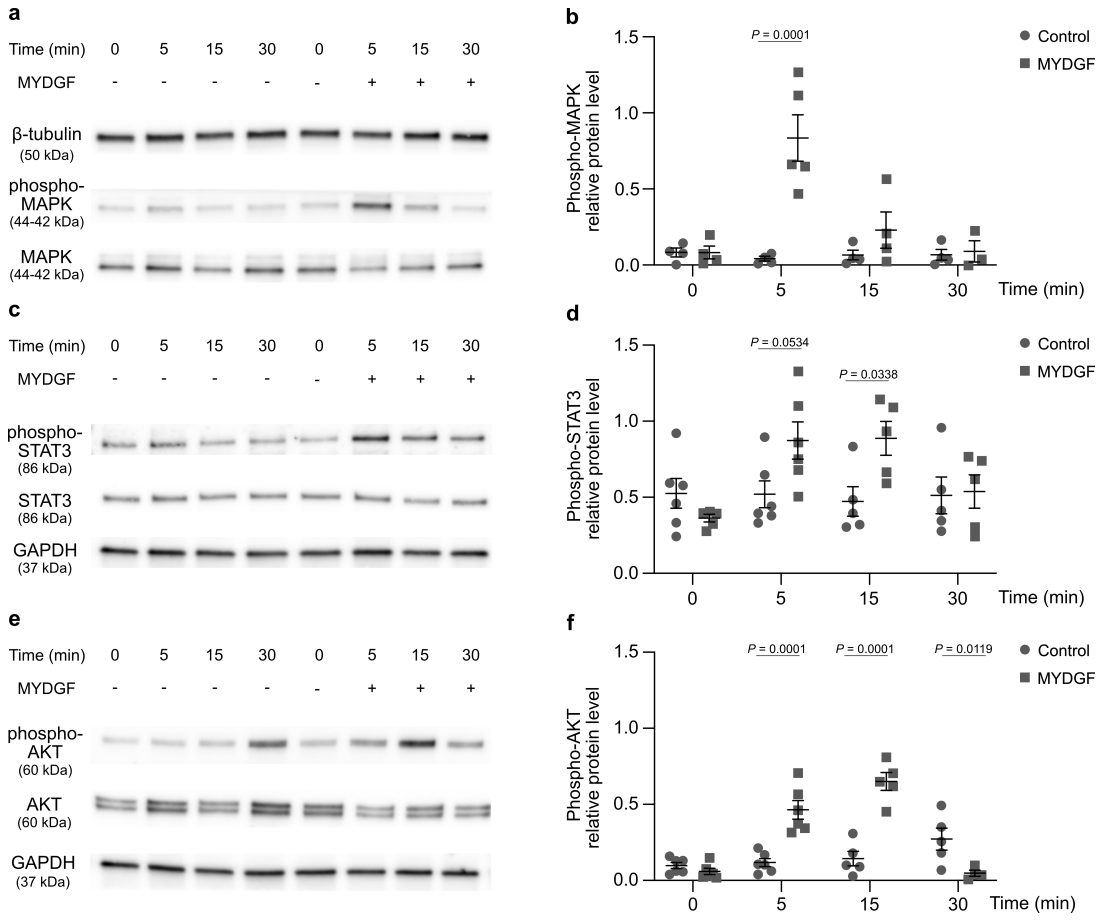

Figure 11: MYDGF treatment induces phosphorylation of MAPK (T202/Y204), STAT3 (S727) and AKT (S473) in primary human hepatocytes.
(**a**) Western blots showing β-tubulin (50 kDa), phospho-MAPK (T202/Y204; 44-42 kDa) and MAPK (44-42 kDa) in lysates from primary human hepatocytes treated without and with MYDGF for 0, 5, 15, 30 min. (**b**) Quantification of relative phospho-MAPK (T202/Y204) protein levels normalized to MAPK and β-tubulin in lysates from primary human hepatocytes; n = 4 (0, 5, 15 and 30 min) control- versus n = 4 (0 and 15 min), n = 5 (5 min) and n = 3 (30 min) MYDGF-treated human hepatocytes. (**c**) Western blots showing phospho-STAT3 (S727; 86 kDa), STAT3 (86 kDa) and GAPDH (37 kDa) in lysates from primary human hepatocytes treated without and with MYDGF for 0, 5, 15, 30 min. (**d**) Quantification of relative phospho-STAT3 (S727) protein levels normalized to STAT3 and GAPDH in lysates from primary human hepatocytes; n = 6 (0 and 5 min) and n = 5 (15 and 30 min) control- versus n = 5 (0, 15 and 30 min) and n = 6 (5 min) MYDGF-treated human hepatocytes. (**e**) Western blots showing phospho-AKT (S473; 60 kDa), AKT (60 kDa) and GAPDH (37 kDa) in lysates from primary human hepatocytes treated without and with MYDGF for 0, 5, 15, 30 min. (**f**) Quantification of relative phospho-AKT (S473) protein levels normalized to AKT and GAPDH in lysates from primary human hepatocytes; n = 6 (0 and 5 min) and n = 5 (15 and 30 min) control- versus n = 6 (0 and 5 min), n = 5 (15 min) and n = 4 (30 min) MYDGF-treated human hepatocytes. Data are presented as mean ± SEM. *P* values were calculated using two-way ANOVA followed by Šidák´s post hoc test.

5.6 MYDGF initiates human hepatocyte proliferation through phosphorylation of MAPK and STAT3

Since activation of the MAPK/STAT3 signaling pathway is essential in HCAECs to promote cell proliferation after MYDGF treatment (Korf-Klingebiel et al., 2015), we investigated whether this pathway is also required for MYDGF-induced hepatocyte proliferation. To answer this question, we inhibited the phosphorylation of MAPK on T202/Y204 (ERK1/2) and STAT3 on S727 in human hepatocytes and examined the effect of this inhibition by (i) Western blot and (ii) on hepatocyte proliferation.

To inhibit the phosphorylation of MAPK, the MEK-specific inhibitor PD98059 was used (Alessi et al., 1995), while the phosphorylation of STAT3 was inhibited by Stattic (McMurray, 2006). Human hepatocytes were starved in William's E medium for three hours, pretreated with PD98059 or Stattic for one hour, followed by stimulation with 1 ng/ml recombinant MYDGF plus PD98059 or Stattic for 0, 5, and 15 minutes. As a control, human hepatocytes were starved in William's E medium for four hours followed by treatment with 1 ng/ml recombinant MYDGF for 0, 5, and 15 minutes. Protein lysates were prepared and phosphorylation of MAPK on T202/Y204 (ERK1/2) and STAT3 on S727 was analyzed by Western blot (**Figure 12**). For the quantification, the ratio of phospho-protein level to pan-protein level, as well as to the housekeeping protein (β-tubulin) was calculated. Quantification of relative protein levels of phospho-MAPK (T202/Y204) in human hepatocytes treated with MYDGF, shows a significant increase 5 minutes after MYDGF treatment (**Figure 12a, b**). This effect is abolished by the treatment with PD98059. Hepatocytes, treated with recombinant MYDGF plus PD98059 show significantly reduced relative protein levels of phospho-MAPK (T202/Y204) 5 minutes after MYDGF treatment. Stattic does not significantly reduce the relative phospho-MAPK (T202/Y204) levels 5 minutes after MYDGF treatment. However, Stattic treatment results in increased basal phospho-MAPK (T202/Y204) levels in three out of six hepatocyte lysates.

Quantification of relative protein levels of phospho-STAT3 (S727) in human hepatocytes treated with MYDGF only, shows a significant increase 15 minutes after MYDGF treatment (**Figure 12c, d**). Human hepatocytes treated with recombinant MYDGF plus PD98059 or MYDGF plus Stattic show no increase in phospho-STAT3 (S727) at 5 and 15 minutes after treatment. More specifically, significantly reduced phospho-STAT3 (S727) levels can be measured 15 minutes after treatment with MYDGF plus PD98059 or Stattic compared to MYDGF treatment only.

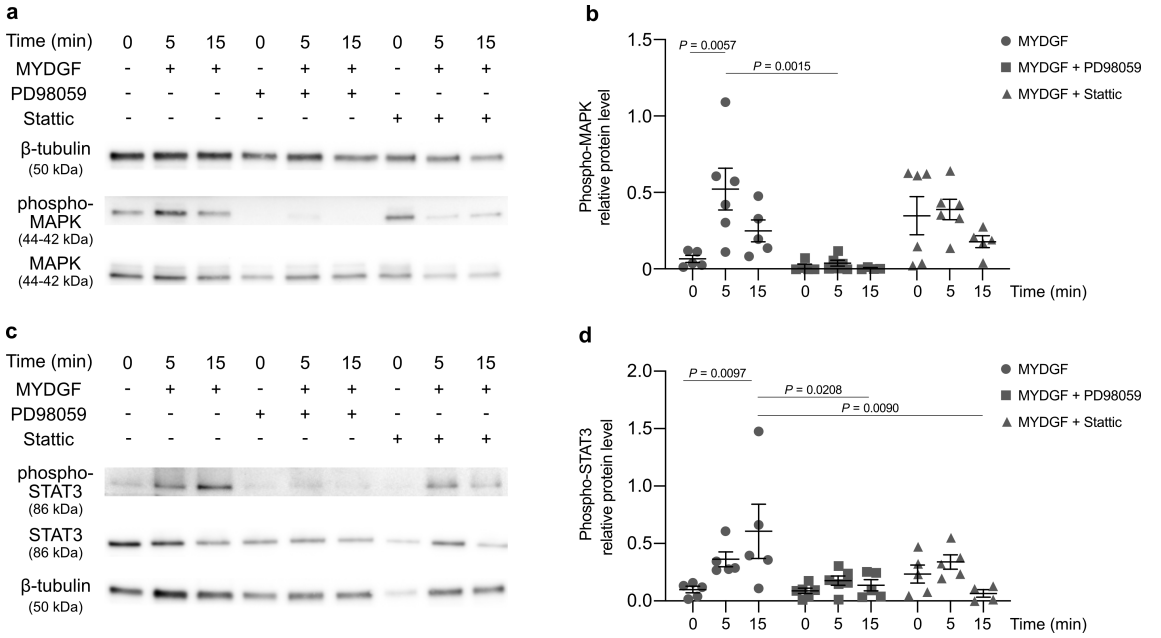

Figure 12: PD98059 and Stattic inhibit MYDGF-induced phosphorylation of MAPK and STAT3 in primary human hepatocytes.
(**a**) Western blots showing β-tubulin (50 kDa), phospho-MAPK (T202/Y204; 44-42 kDa) and MAPK (44-42 kDa) in lysates from primary human hepatocytes treated without or with MYDGF only, and MYDGF plus PD98059 or Stattic for 0, 5, 15 min. (**b**) Quantification of relative phospho-MAPK (T202/Y204) protein levels normalized to MAPK and β-tubulin in lysates from primary human hepatocytes; n = 5 (0, 15 min) and n = 6 (5 min) MYDGF; n = 5 (0 min), n = 6 (5 min) and n = 4 (15 min) MYDGF + PD98059; n = 6 (0, 5 min) and n = 5 (15 min) MYDGF + Stattic. (**c**) Western blots showing phospho-STAT3 (S727; 86 kDa), STAT3 (86 kDa) and β-tubulin (50 kDa) in lysates from primary human hepatocytes treated without or with MYDGF only, and MYDGF plus PD98059 or Stattic for 0, 5, 15 min. (**d**) Quantification of relative phospho-STAT3 (S727) protein levels normalized to STAT3 and β-tubulin in lysates from primary human hepatocytes; n = 5 (0, 5, 15 min) MYDGF; n = 6 (0, 5 min) and n = 5 (15 min) MYDGF + PD98059; n = 5 (0, 5 min) and n = 4 (15 min) MYDGF + Stattic. Donor: female, 26-year-old. Data are presented as mean ± SEM. *P* values were calculated using two-way ANOVA followed by Tukey´s post hoc test.

After demonstrating that treatment with PD98059 or Stattic leads to an inhibition of phospho-MAPK (T202/Y204) and/or phospho-STAT3 (S727), we investigated whether activation of either or both signaling molecules is important for MYDGF-induced proliferation of human hepatocytes. To assess the effect, we pretreated human hepatocytes obtained from a 12-year-old female donor with PD98059 and/or Stattic for one hour. Subsequently, hepatocytes were treated without recombinant MYDGF (control), with 1 ng/ml recombinant MYDGF, or with 1 ng/ml recombinant MYDGF plus PD98059 or/and Stattic for six hours in the presence of EdU. Next, the proliferating hepatocytes were stained for EdU. Additionally, we checked if the proliferating hepatocytes express hepatocyte nuclear factor 4 alpha (HNF4α) (**Figure 13 a-e**). To determine the number of proliferating hepatocytes, EdU^+ cells per chamber were counted manually. Treatment with recombinant MYDGF results in an approximately 40% increase in proliferating human hepatocytes compared to control (**Figure 13f**). The proliferation enhancing effect of MYDGF is reduced by 78% compared to

the control group when hepatocytes were treated with PD98059 plus MYDGF. Treatment with Stattic plus MYDGF, as well as the combined inhibition of MAPK and STAT3 by Stattic plus PD98059, completely abrogated MYDGF stimulatory effects on human hepatocyte proliferation.

We repeated this experiment in three additional donors (female, 27 years; female, 26 years; male, 31 years) (**Figure 13g-i**). Due to the limited number of cells in the purchased vials, no control condition (without MYDGF) was performed for these donors. Therefore, the treatment of hepatocytes with MYDGF only was used as a control. In all three donors, hepatocyte proliferation is reduced in hepatocytes treated with PD98059 plus MYDGF, while treatment with Stattic plus MYDGF, and Stattic plus PD98059 and MYDGF results in the strongest inhibition of hepatocyte proliferation.

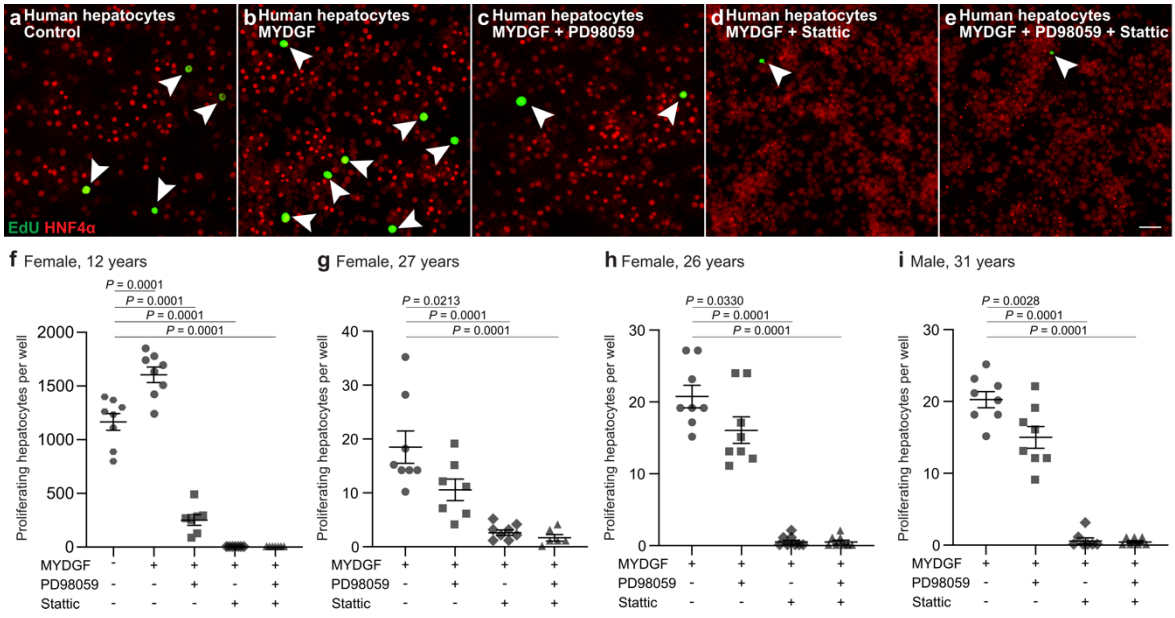

Figure 13: Proliferation-enhancing effect of MYDGF in primary human hepatocytes depends on the activation of MAPK and STAT3 signaling.
(**a-e**) LSM images of primary human hepatocytes treated without (control) (a), with MYDGF (b), MYDGF plus PD98059 (c), MYDGF plus Stattic (d), MYDGF plus PD98059 and Stattic (e) in a female, 12-year-old donor. White arrowheads point to proliferating hepatocytes stained for EdU (green) and HNF4α (red). (**f**) Quantification of proliferating hepatocytes per well. n = 8 (control), n = 8 (MYDGF), n = 7 (MYDGF + PD98059), n = 7 (MYDGF + Stattic), n = 5 (MYDGF + PD98059 + Stattic) wells of hepatocytes from a female, 12-year-old donor. (**g-i**) Quantification of proliferating human hepatocytes per well. n = 8 (MYDGF), n = 7 (MYDGF + PD98059), n = 8 (MYDGF + Stattic), n = 6 (MYDGF + PD98059 + Stattic) wells of hepatocytes from a female, 27-year-old donor (g); n = 8 wells of hepatocytes each from a female, 26-year-old donor (h); n = 8 (MYDGF), n = 8 (MYDGF + PD98059), n = 7 (MYDGF + Stattic), n = 7 (MYDGF + PD98059 + Stattic) wells of hepatocytes from a male, 31-year-old donor (i). Scale bar: 50 µm (e). Data are presented as mean ± SEM. *P* values were calculated using one-way ANOVA followed by Dunnett´s post hoc test.

In conclusion, these results indicate that treatment with PD98059 inhibits MYDGF-induced phosphorylation of MAPK on T202/Y204 (ERK1/2) and STAT3 on S727, whereas treatment with Stattic only inhibits MYDGF-induced phosphorylation of STAT3 on S727. When phosphorylation of MAPK on T202/Y204 (ERK1/2) and/or of STAT3 on S727 is inhibited, the proliferation promoting effect of MYDGF is diminished.

5.7 MYDGF levels increase earlier than HGF levels in human blood serum and plasma after liver surgery

Previous studies have already shown that MYDGF plasma levels are increased in human patients after MI (Korf-Klingebiel et al., 2015), whereas human patients with T2D (Wang et al., 2020a), DKD (He et al., 2020), osteoporosis (Xu et al., 2022), atherosclerosis (Meng et al., 2021, Xu et al., 2023a), and NAFLD (Ding et al., 2023) display reduced MYDGF serum or plasma levels. To determine whether MYDGF expression is also altered in human blood after liver surgery, we analyzed blood serum and blood plasma from patients who underwent in-situ split or liver resection. We also examined HGF levels in these blood samples to compare the expression kinetics of MYDGF and HGF. In the literature, HGF is described as a well-studied growth factor that increases its levels at postoperative day 1 (POD1) after stage 1 in-situ split liver surgery (Sparrelid et al., 2018) as well as after liver resection (Tomiya et al., 1992, Justinger et al., 2008, Murtha-Lemekhova et al., 2021).

First, we examined the time course of MYDGF and HGF levels in human blood serum after stage 1 in-situ split liver surgery to identify the timepoint at which MYDGF and HGF levels peaked. Blood was drawn from a 79-year-old male patient before and immediately after stage 1 in-situ split as well as at 1, 6, 12, 24 and 48 hours after surgery (**Figure 14a**). Serum MYDGF and HGF levels were measured using ELISA. Our results show that the basal MYDGF level (55 pg/ml) increases rapidly to 135 pg/ml in the first hour after surgery, representing an almost three-fold increase. 24 hours post-surgery, the MYDGF level returns to nearly basal levels (65 pg/ml) and drops slightly below basal levels (44 pg/ml) 48 hours after stage 1 in-situ split (**Figure 14b**). HGF, on the other hand, has a higher basal level (3,704 pg/ml), which increases to 4,615 pg/ml post stage 1 in-situ split, but then decreases to 2,400 pg/ml within the first 6 hours after surgery (**Figure 14c**). 24 hours after surgery HGF level starts to increase (5,918 pg/ml) and reaches its peak (8,826 pg/ml) 48 hours after surgery.

We also analyzed MYDGF and HGF levels in the blood plasma of six male patients before and after liver resection. In this case, the remaining part of the liver in the patients was large enough to avoid an in-situ split liver surgery. Analysis of HGF and MYDGF in blood plasma shows a higher basal concentration of HGF than MYDGF, but only the MYDGF concentration increases significantly by 40% after surgery (**Figure 14d**). Even in 4 out of 6 patients, HGF levels are slightly decreased at this timepoint after surgery (**Figure 14e**).

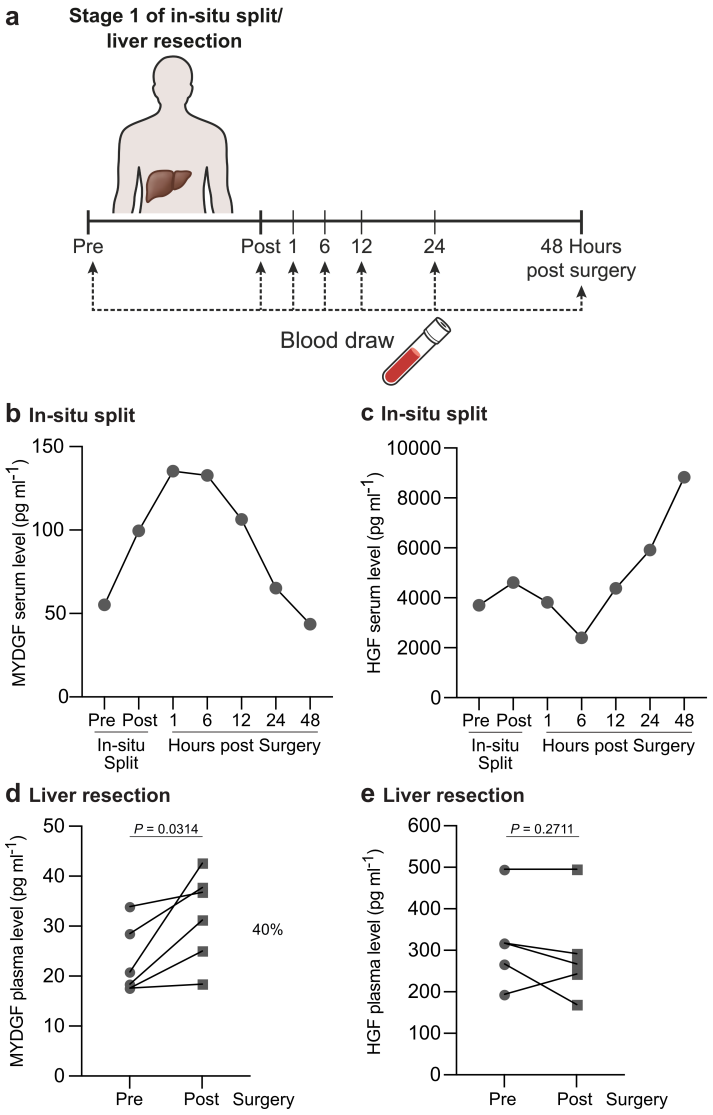

Figure 14: MYDGF levels increase at an earlier timepoint compared to HGF levels in human blood plasma and serum post liver surgery.
(**a**) Schematic illustration of blood drawn from human patients post stage 1 of in-situ split or liver resection. (**b, c**) MYDGF levels (pg ml^{-1}) (b) and HGF levels (pg ml^{-1}) (c) in blood serum of a male 79-year-old patient pre and at different timepoints post stage 1 in-situ split liver surgery. (**d, e**) MYDGF plasma levels (pg ml^{-1}) (d) and HGF levels (pg ml^{-1}) (e) in human patients pre and post liver resection; n = 6 male patients (two data points are overlaid, so only n = 5 is visible in panel e), 54-89-year-old, BMI < 30 kg m^{-2}. *P* values were calculated using a two-tailed paired Student´s *t*-test (d, e). Experimental setup (a) was illustrated by Yousun Koh.

In conclusion, unlike HGF, MYDGF levels in human blood serum increase rapidly within the first six hours after stage 1 in-situ split liver surgery. Even in human blood plasma, only MYDGF levels show a significant increase after liver resection, while HGF levels do not significantly increase at this timepoint.

5.8 MYDGF levels increase earlier than HGF levels in the remaining mouse liver and hepatic ECs after PHx

Based on our results on the expression of MYDGF in humans after liver surgery, we investigated whether this observation could be transferred to mice. For this purpose, we performed a two-thirds PHx in mice, whereby the median and left liver lobe (corresponding to two-thirds of the liver volume) were surgically dissected (Mitchell and Willenbring, 2008). The right and caudate liver lobe remained in the mice and were isolated 3, 6, 12 and 24 hours after PHx (**Figure 15a**). Isolation of the liver lobes at timepoint zero served to determine the basal MYDGF level. First, we analyzed the MYDGF level in the right liver lobe (isolated after PHx) normalized to GAPDH compared to the left liver lobe (resected during PHx) normalized to GAPDH by Western blot. This allowed us to compare MYDGF levels in the liver lobes before and after PHx in the same mouse (**Figure 15b**). Quantification of MYDGF levels in the right liver lobe as a percentage of the left liver lobe shows an increase in MYDGF level 3 hours after PHx, which then decreases to basal level (0 hours without PHx) 24 hours after PHx. We then analyzed MYDGF and HGF levels in isolated hepatic ECs from the right liver lobe by ELISA, to determine whether both factors are simultaneously elevated in hepatic ECs after PHx (**Figure 15c, d**). Also, in the isolated mouse hepatic ECs a rapid increase in MYDGF levels (11 pg/ml) is observed 3 hours after PHx compared to the basal level (0 hours without PHx) (5 pg/ml). MYDGF levels fell below the basal level 12 and 24 hours after PHx (**Figure 15c**). In contrast, HGF exhibits a different expression pattern in isolated mouse hepatic ECs after PHx. HGF levels increase 9 hours later than MYDGF after a PHx, but then show a three-fold increase, whereas MYDGF levels increase two-fold after 3 hours (**Figure 15d**).

Taken together, these results are consistent with our human data (**Figure 14**) showing that MYDGF is secreted at an earlier timepoint but with a lower concentration than HGF after liver surgery. Next, we asked whether MYDGF also has a proliferation-promoting effect on hepatocytes in mice and thus could promote liver regeneration.

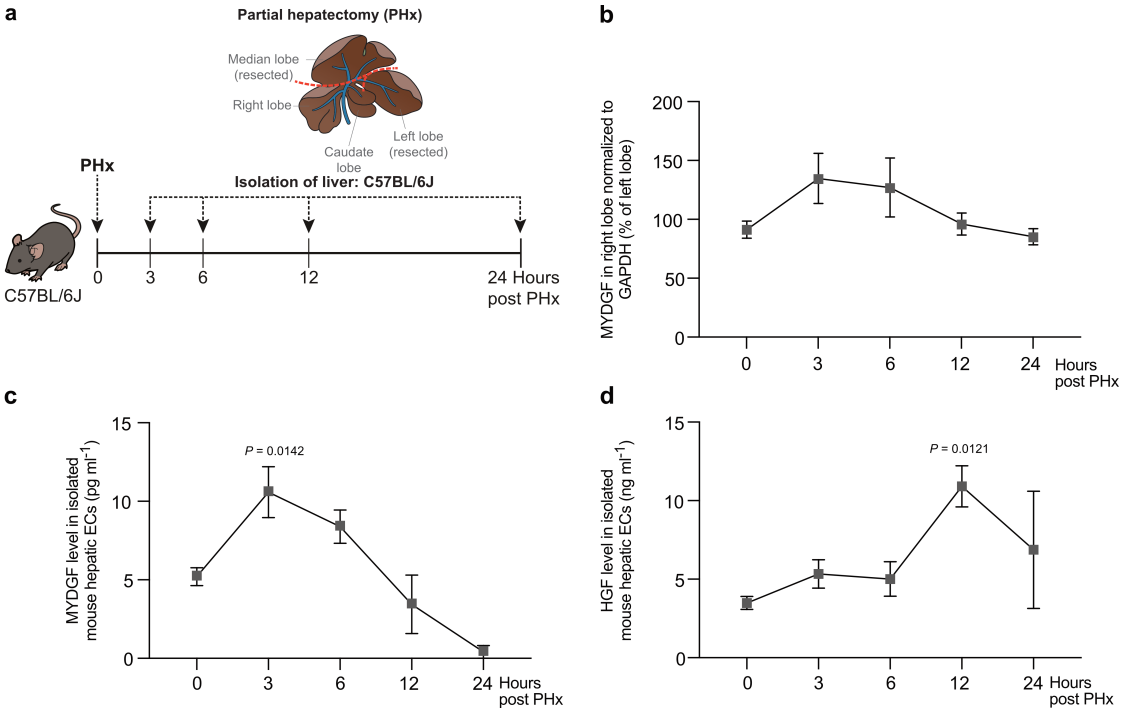

Figure 15: MYDGF levels increase at an earlier timepoint compared to HGF levels in the right liver lobe of mice post PHx.
(**a**) Schematic illustration of a mouse liver, showing the liver lobes resected during partial hepatectomy (PHx) (median + left lobe) and isolated post PHx (right + caudate lobe). Timeline for the kinetic study of MYDGF expression. (**b**) MYDGF protein levels in right liver lobe normalized to GAPDH in percent of left liver lobe (resected during PHx), at different timepoints post PHx. (**c**) MYDGF levels (pg ml^{-1}) in mouse hepatic ECs, isolated from the right liver lobe, at different timepoints post PHx. (**d**) HGF levels (ng ml^{-1}) in mouse hepatic ECs, isolated from the right liver lobe, at different timepoints post PHx. n = 5 (0 and 3 h), n = 4 (6 and 12 h) and n = 3 mice (24 h) (b, c, d). Data are presented as mean ± SEM. *P* values were calculated using one-way ANOVA followed by Dunnett's post hoc test (b, c, d). Illustration of experimental setup (a) was illustrated by Yousun Koh.

5.9 Effect of AAV8-TBG-mediated overexpression of MYDGF on liver regeneration in mice

To answer the question if MYDGF has a beneficial effect on liver regeneration in mice, we performed a gain-of-function experiment. Therefore, we used adeno-associated viruses serotype 8 (AAV8) with a *thyroxine-binding-globulin* (TBG) promoter, to induce a hepatocyte specific overexpression of MYDGF in the mouse liver (Nakai et al., 2005, Kiourtis et al., 2021). Overexpression of MYDGF in the hepatic ECs was not possible due to the lack of an endothelial cell-specific promoter. As a control AAV8-TBG-GFP was used, which will lead to an expression of GFP in the mouse liver.

Mice received AAV8-TBG-GFP or AAV8-TBG-MYDGF via tail vein injection at day zero (**Figure 16**). Seven days post injection a two-thirds PHx was performed and 30 hours later the remaining liver lobes were isolated.

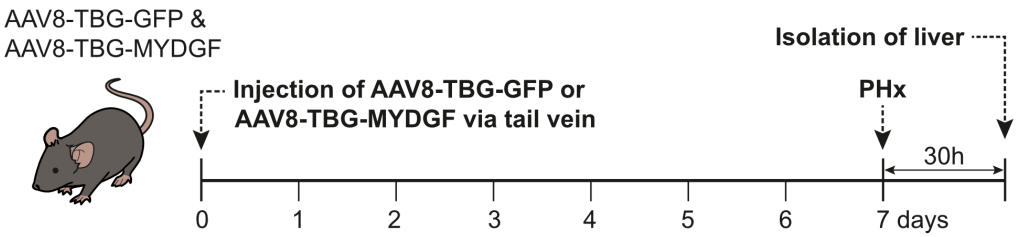

Figure 16: Experimental setup for AAV8-TBG injection followed by PHx in mice.
AAV8-TBG-GFP or AAV8-TBG-MYDGF were injected into the tail vein of C57BL/6J mice on day zero. Seven days after injection, a two-thirds PHx (resection of the median + left liver lobe) was performed, and the remaining liver lobes (caudate + right liver lobe) were isolated 30 hours post PHx. Illustration of experimental setup was illustrated by Yousun Koh.

5.9.1 Overexpression of GFP or MYDGF in mouse liver using AAV8-TBG-GFP or AAV8-TBG-MYDGF

Before we analyzed the effects of MYDGF overexpression on liver regeneration in mice, we determine if the TBG promotor of the AAV's acts in a liver-specific manner. Therefore, we analyzed the GFP expression via GFP staining in the right and caudate liver lobes, as well as in the reference organs (heart, kidney, and spleen) (**Figure 17a**). The right and caudate liver lobes show a GFP signal, whereas it was not detectable in the reference organs. We then examined the transfection rate of AAV8-TBG-GFP in the mouse liver by staining for GFP in liver sections from the median liver lobe seven days post AAV8-TBG-GFP injection. Additionally, we investigated the expression of HNF4α in the GFP^+ cells to confirm the hepatocyte specificity of the TBG promoter. To quantify how many cells in a 0.05 mm^2 stained section were infected by AAV8-TBG-GFP, we counted the HNF4α positive and HNF4α plus GFP double-positive hepatocytes (**Figure 17b, c**). Over 50% of the counted hepatocytes are HNF4α and GFP double positive.

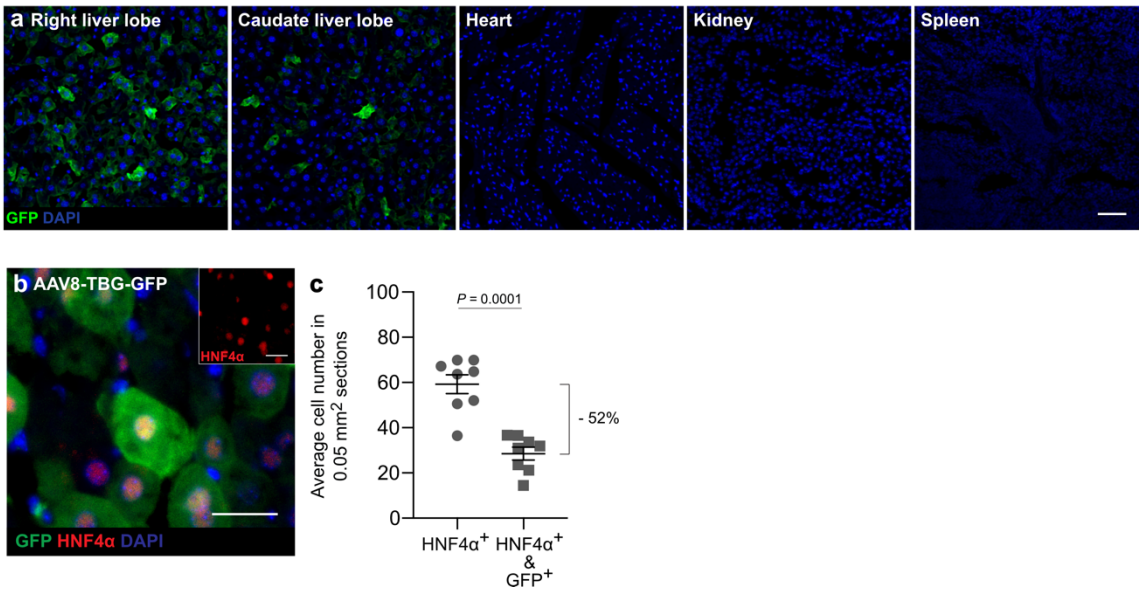

Figure 17: AAV8-TBG-GFP injection leads to a liver specific expression of GFP.
(**a**) LSM images of transversal sections of the right and caudate liver lobes, heart, kidney, and spleen seven days post AAV8-TBG-GFP injection, stained for GFP (green). Cell nuclei were counterstained for DAPI. (**b**) LSM image of a transversal section of the median mouse liver lobe of AAV8-TBG-GFP mouse, stained for GFP (green), and hepatocytes stained for HNF4α (red; shown in inset top right). Cell nuclei were counterstained for DAPI. (**c**) Quantification of average cell number of $HNF4\alpha^+$ and $HNF4\alpha^+$ + GFP^+ cells in 0.05 mm^2 sections. n = 8 AAV8-TBG-GFP transfected mice. Scale bars: 50 µm (a), 25 µm (b). Data are presented as mean ± SEM. *P* value was calculated using two-tailed unpaired Student's *t*-test with Welch's correction.

Next, we analyzed whether the injection of AAV8-TBG-MYDGF results in an overexpression of MYDGF in the mouse liver. Therefore, we generated protein lysates from the right liver lobe of AAV8-TBG-GFP or AAV8-TBG-MYDGF transfected mice and measured MYDGF levels using Western blot (**Figure 18a**). The quantification of MYDGF levels in the right liver lobe, normalized to GAPDH as a percentage of AAV8-TBG-GFP, shows an almost 90% overexpression of MYDGF in the AAV8-TBG-MYDGF mouse liver (**Figure 18b**).

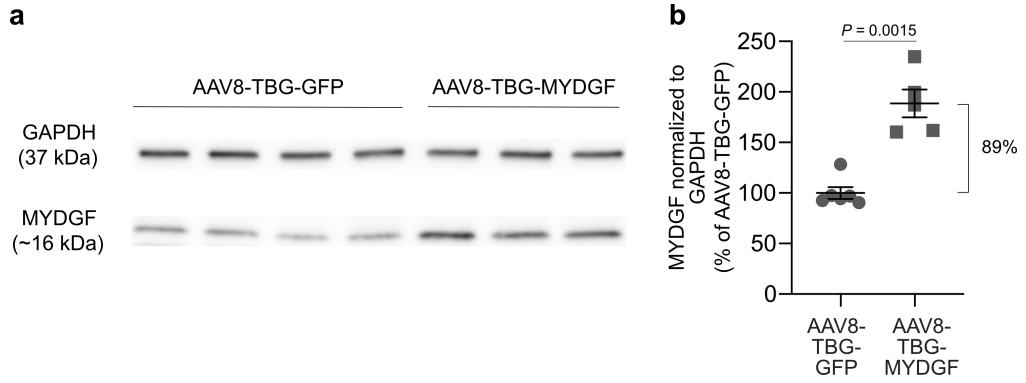

Figure 18: AAV8-TBG-MYDGF injection results in liver-specific overexpression of MYDGF. (**a**) Western blots showing GAPDH (37 kDa) and MYDGF (~16 kDa) in lysates of the right liver lobe of AAV8-TBG-GFP and AAV8-TBG-MYDGF transfected mice. (**b**) Quantification of MYDGF levels normalized to GAPDH levels in percent of AAV8-TBG-GFP mice; n = 6 AAV8-TBG-GFP versus n = 5 AAV8-TBG-MYDGF liver lysates. Data are presented as mean ± SEM. *P* value was calculated using two-tailed unpaired Student's *t*-test with Welch's correction.

In conclusion, our results show that AAV8-TBG-MYDGF tail vein injection results in significant liver-specific overexpression of MYDGF in the mouse liver in comparison to AAV8-TBG-GFP mice.

5.9.2 MYDGF overexpression promotes liver regeneration in mice after PHx

To determine whether AAV8-TBG-mediated MYDGF overexpression improves liver regeneration compared to AAV8-TBG-GFP mice, we isolated the right and caudate liver lobes 30 hours after PHx. Based on our expression data, showing a rapid secretion of MYDGF within the first hours after PHx (**Figure 15**), we hypothesized that MYDGF overexpression promotes hepatocyte proliferation at an earlier timepoint after PHx. Therefore, we decided to isolate the remaining liver lobes (right and caudate lobe) six hours before the proliferation peak (36-48 hours after PHx) normally occurs after two-thirds PHx in mice (Mitchell and Willenbring, 2008). To quantify the number of proliferating cells, liver sections from the right and caudate lobes were stained for the proliferation marker PH3 (**Figure 19**). Furthermore, the liver sections were counterstained for the intercellular adhesion molecule 1 (ICAM-1), which is a blood vessel marker expressed by hepatic ECs (Poisson et al., 2017, Shetty et al., 2018). To analyze whether MYDGF overexpression has a proliferation-promoting effect on hepatocytes after two-thirds PHx, $PH3^+$ but $ICAM\text{-}1^-$ cells were counted and normalized to $DAPI^+$ cells. A significantly higher percentage of proliferating hepatocytes can be observed in the right and caudate liver lobe from AAV8-TBG-MYDGF in comparison to AAV8-TBG-GFP mice 30 hours after PHx (**Figure 19c, f**).

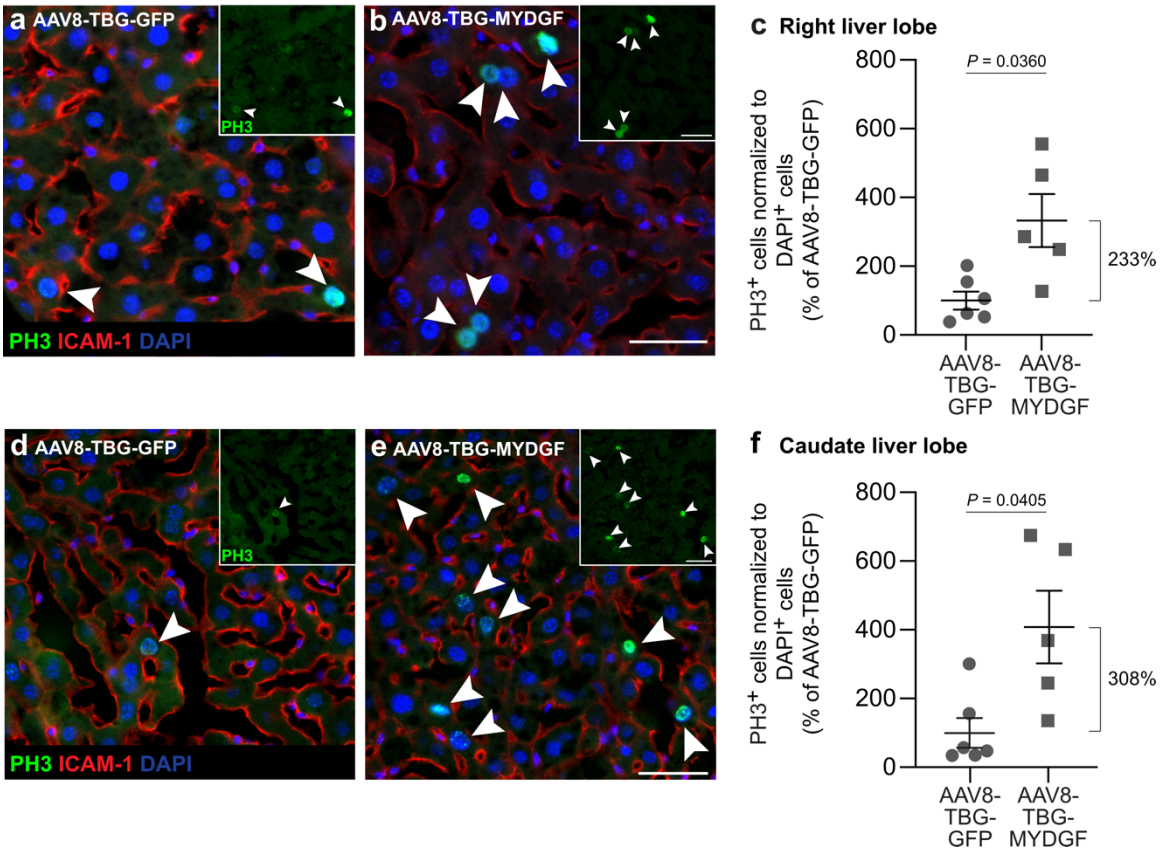

Figure 19: MYDGF overexpression leads to an increase of PH3⁺ hepatocytes in the remaining mouse liver lobes 30 hours after PHx.
(**a, b**) LSM images of transversal sections of the right liver lobe of AAV8-TBG-GFP (a) and AAV8-TBG-MYDGF (b) transfected mice stained for proliferation marker PH3 (green, shown in inset top right), and blood vessel marker ICAM-1 (red). Cell nuclei were counterstained for DAPI. White arrowheads point to proliferating cells. (**c**) Quantification of proliferating cells ($PH3^+$ and $ICAM\text{-}1^-$) normalized to $DAPI^+$ cells in AAV8-TBG-GFP versus AAV8-TBG-MYDGF mice, shown as percentage of AAV8-TBG-GFP. (**d, e**) LSM images of transversal sections of the caudate liver lobe of AAV8-TBG-GFP (d) and AAV8-TBG-MYDGF (e) transfected mice stained for PH3 (green, shown in inset top right), and ICAM-1 (red). Cell nuclei were counterstained for DAPI. White arrowheads point to proliferating cells. (**f**) Quantification of proliferating cells ($PH3^+$ and $ICAM\text{-}1^-$) normalized to $DAPI^+$ cells in AAV8-TBG-GFP versus AAV8-TBG-MYDGF mice, shown as percentage of AAV8-TBG-GFP. n = 6 AAV8-TBG-GFP versus n = 5 AAV8-TBG-MYDGF transversal sections of the right (c) and caudate (f) liver lobe. Scale bars: 50 µm (b, e). Data are presented as mean ± SEM. *P* values were calculated using two-tailed unpaired Student's *t*-test with Welch's correction.

To confirm our results that MYDGF overexpression leads to significantly increased hepatocyte proliferation 30 hours after PHx, we performed a staining with an additional proliferation marker, namely Ki67 (**Figure 20**). Ki67 stains cells in the S, G_2, and M phases of the cell cycle, but is absent in cells in the G_0 phase (Gerdes et al., 1984). The liver sections were further stained for the hepatocyte marker HNF4α. For analysis, only Ki67 and HNF4α double positive cells were counted and normalized to $DAPI^+$ cells. Quantification of the Ki67 staining also shows a greater percentage of proliferating hepatocytes in the right and caudate liver lobe of AAV8-TBG-MYDGF compared to AAV8-TBG-GFP mice 30 hours

after PHx (**Figure 20a-f**). Hepatocyte proliferation increases by approximately 90% in the right liver lobe and by around 110% in the caudate liver lobe (**Figure 20c, f**).

In addition, we isolated the right and caudate liver lobes from AAV8-TBG-GFP and AAV8-TBG-MYDGF mice at 24 and 96 hours after PHx to check whether 30 hours after PHx reflects the peak of hepatocyte proliferation. To investigate whether the injection of AAV8 alone or the overexpression of MYDGF has an effect on hepatocyte proliferation, we isolated the right and caudate liver lobes from AAV8-TBG-GFP and AAV8-TBG-MYDGF mice without performing a PHx (0 hours). Liver sections from both lobes isolated at these different timepoints were stained for Ki67 and HNF4α. For analysis, only Ki67 and HNF4α double positive cells were counted and normalized to $DAPI^+$ cells. Our results show that the basal hepatocyte proliferation does not differ in both the right and caudate liver lobes of the AAV8-TBG-GFP and AAV8-TBG-MYDGF mice isolated 0 hours after PHx (**Figure 20g, h**). 24 hours after PHx, hepatocyte proliferation slightly increases in the right and caudate liver lobe from AAV8-TBG-GFP and AAV8-TBG-MYDGF mice. Nevertheless, a greater increase in hepatocyte proliferation is visible in the right liver lobe of the AAV8-TBG-MYDGF mice. The number of $Ki67^+$ hepatocytes peaks at 30 hours after PHx in both the right and caudate liver lobes from AAV8-TBG-GFP and AAV8-TBG-MYDGF mice. However, a significantly increased hepatocyte proliferation is observed in the liver lobes of AAV8-TBG-MYDGF mice. 96 hours after PHx, almost no hepatocyte proliferation is visible in both liver lobes from AAV8-TBG-GFP and AAV8-TBG-MYDGF mice.

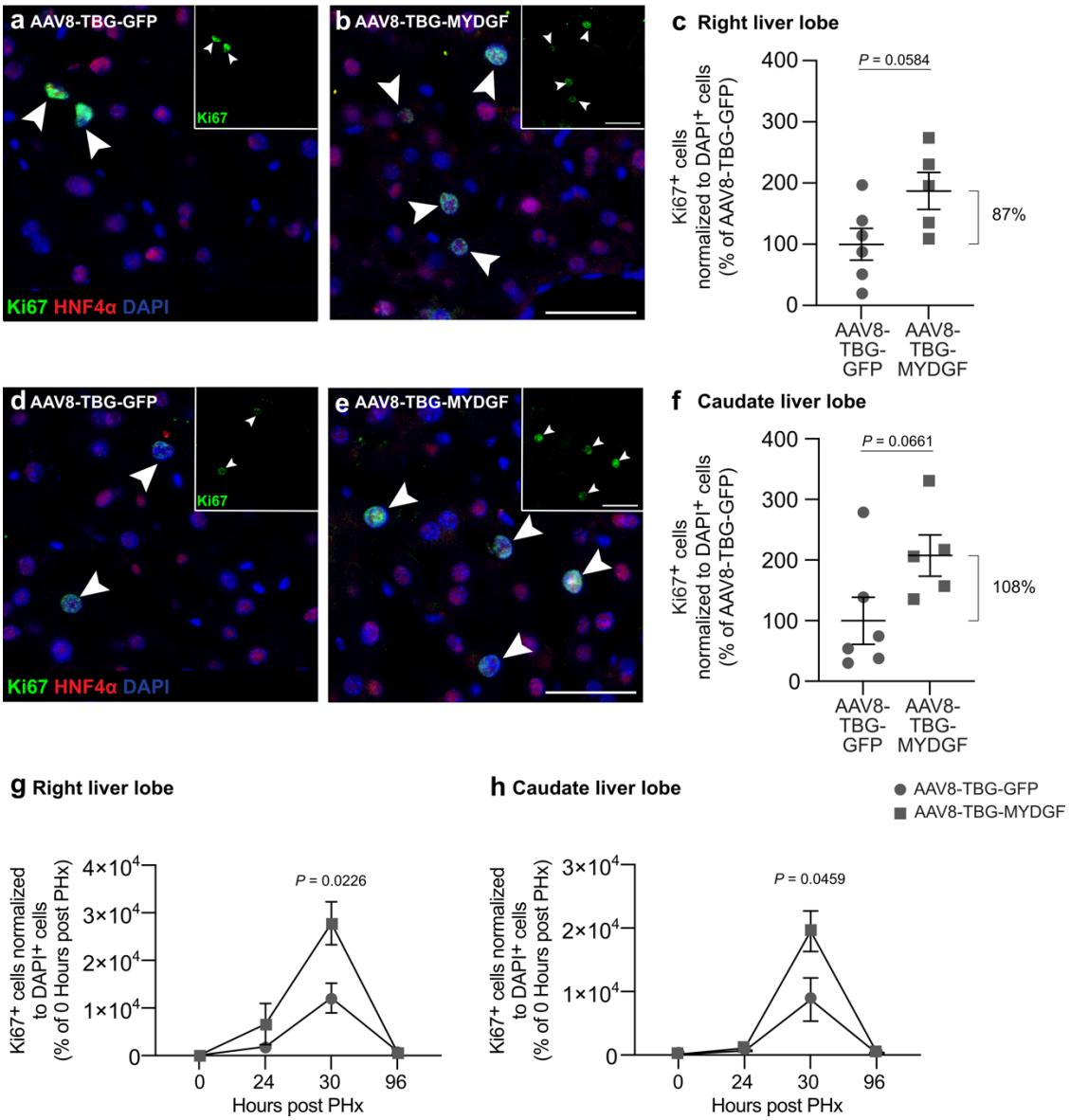

Figure 20: MYDGF overexpression increases hepatocyte proliferation in the remaining mouse liver lobes 30 hours after PHx.

(**a, b**) LSM images of transversal sections of the right liver lobe of AAV8-TBG-GFP (a) or AAV8-TBG-MYDGF (b) transfected mice, stained for proliferation marker Ki67 (green, shown in inset top right) and hepatocyte marker HNF4α (red). Cell nuclei were counterstained for DAPI. White arrowheads point to proliferating cells. (**c**) Quantification of proliferating cells (Ki67$^+$ and HNF4α$^+$) normalized to DAPI$^+$ cells in AAV8-TBG-GFP versus AAV8-TBG-MYDGF mice, shown as percentage of AAV8-TBG-GFP. (**d, e**) LSM images of transversal sections of the caudate liver lobe of AAV8-TBG-GFP (d) and AAV8-TBG-MYDGF (e) transfected mice, stained for Ki67 (green, shown in inset top right) and HNF4α (red). Cell nuclei were counterstained for DAPI. White arrowheads point to proliferating cells. (**f**) Quantification of proliferating cells (Ki67$^+$ and HNF4α$^+$) normalized to DAPI$^+$ cells in AAV8-TBG-GFP versus AAV8-TBG-MYDGF mice, shown as percentage of AAV8-TBG-GFP. n = 6 AAV8-TBG-GFP versus n = 5 AAV8-TBG-MYDGF transversal sections of the right (c) and caudate (f) liver lobe. Scale bars: 50 µm (b, e). (**g, h**) Time course of Ki67$^+$ cells normalized to DAPI$^+$ cells in right (g) and caudate (h) liver lobe of AAV8-TBG-GFP and AAV8-TBG-MYDGF transfected mice, shown as percentage of 0 hours post PHx; n = 4 (0 and 96 hours), n = 5 (24 hours), n = 6 (30 hours) AAV8-TBG-GFP versus n = 4 (0 and 24 hours), n = 5 (30 hours), n = 7 (96 hours) AAV8-TBG-MYDGF transversal sections of the right (g) and caudate (h) liver lobe each. Data are presented as mean ± SEM. *P* values were calculated using two-tailed unpaired Student's *t*-test with Welch's correction (c, f), or multiple unpaired *t*-test with Welch's correction (g, h).

Since overexpression of MYDGF leads to increased hepatocyte proliferation 30 hours after PHx (**Figure 19, 20**), we investigated whether this also results in improved liver regeneration. To test this, we determined the liver-to-body weight ratio in AAV8-TBG-GFP and AAV8-TBG-MYDGF mice 96 hours after PHx. This timepoint was chosen because the proliferation of hepatocytes is almost complete four days after PHx and only the proliferation of endothelial cells takes place (Michalopoulos and DeFrances, 1997). Our results show that four days after PHx a 10% higher liver-to-body weight ratio can be observed in AAV8-TBG-MYDGF compared to AAV8-TBG-GFP mice (**Figure 21a**). In addition, the increased liver-to-body weight ratio is reflected by a larger caudate liver lobe in AAV8-TBG-MYDGF mice (**Figure 21b**).

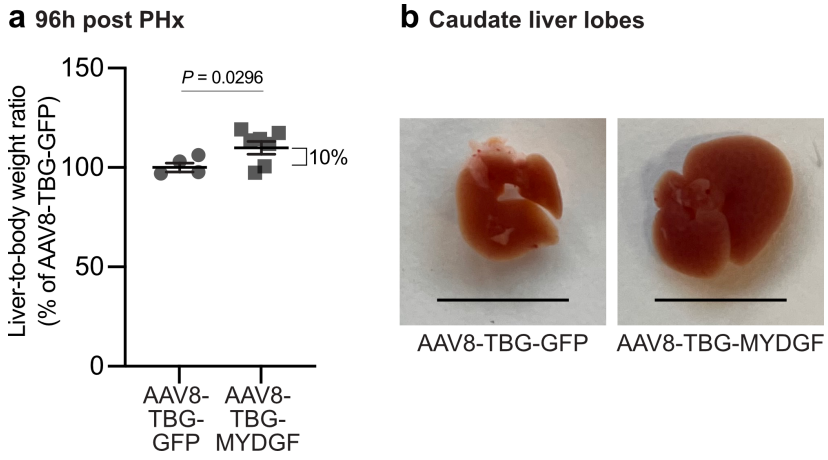

Figure 21: Increased liver-to-body weight ratio in AAV8-TBG-MYDGF mice 96 hours post PHx. (**a**) Quantification of liver-to-body weight ratio in AAV8-TBG-GFP and AAV8-TBG-MYDGF transfected mice 96 hours post PHx, shown as percentage of AAV8-TBG-GFP, n = 4 AAV8-TBG-GFP versus n = 7 AAV8-TBG-MYDGF. (**b**) Representative images of caudate liver lobes of AAV8-TBG-GFP and AAV8-TBG-MYDGF transfected mice 96 hours post PHx. Scale bar: 1 cm (b). Data are presented as mean ± SEM. *P* value was calculated using two-tailed unpaired Student's *t*-test with Welch's correction.

In summary, mice with a liver specific overexpression of MYDGF show increased hepatocyte proliferation 30 hours after PHx and a 10% higher liver-to-body weight ratio associated with a larger caudate liver lobe 96 hours after PHx.

5.9.3 MYDGF overexpression increases phosphorylation of MAPK and STAT3 in the remaining mouse liver after PHx

Our previous *in vitro* experiments demonstrated that treatment of human hepatocytes with recombinant MYDGF leads to increased hepatocyte proliferation via phosphorylation of MAPK on T202/Y204 (ERK1/2) and STAT3 on S727 (**Figure 11**). Since our *in vivo* data indicate that overexpression of MYDGF in the mouse liver results in increased hepatocyte proliferation and promotes liver regeneration after PHx, we investigated whether MYDGF overexpression alters phosphorylation levels of MAPK on T202/Y204 (ERK1/2), and of STAT3 on S727 after two-thirds PHx. Based on the literature (Chung et al., 1997, Korf-Klingebiel et al., 2015, Xu et al., 2022) that MAPK can activate STAT3, and our results that PD98059 inhibits MYDGF-induced phosphorylation of MAPK on T202/Y204 (ERK1/2) and STAT3 on S727, whereas Stattic only inhibits MYDGF-induced phosphorylation of STAT3 on S727 (**Figure 12**), we hypothesized that MYDGF activates MAPK upstream of STAT3. Therefore, we examined the phosphorylation of MAPK on T202/Y204 (ERK1/2) in liver lysates from the right liver lobe of AAV8-TBG-GFP and AAV8-TBG-MYDGF mice 24 hours after PHx, while we analyzed the phosphorylation of STAT3 on S727 24 and 30 hours after PHx. Thus, we expected an increased phospho-MAPK (T202/Y204) signal at an earlier timepoint after PHx (24 hours), whereas the phospho-STAT3 (S727) level should increase at a late timepoint after PHx (30 hours). For quantification, the ratio of phospho-protein levels to pan-protein level, as well as to the housekeeping proteins (β-tubulin or GAPDH), was calculated.

Significantly increased phosphorylation of MAPK on T202/Y204 (ERK1/2) but unchanged phospho-STAT3 (S727) levels in the right liver lobe of AAV8-TBG-MYDGF compared to AAV8-TBG-GFP mice are visible 24 hours after PHx (**Figure 22a, b**). Meanwhile, trend towards increased phospho-STAT3 (S727) levels in the right liver lobe of AAV8-TBG-MYDGF mice compared to AAV8-TBG-GFP mice can be observed 30 hours after PHx (**Figure 22c**).

Thus, it can be concluded that overexpression of MYDGF in the mouse liver first leads to an increased phosphorylation of MAPK on T202/Y204 (ERK1/2), followed by phosphorylation of STAT3 on S727 after PHx.

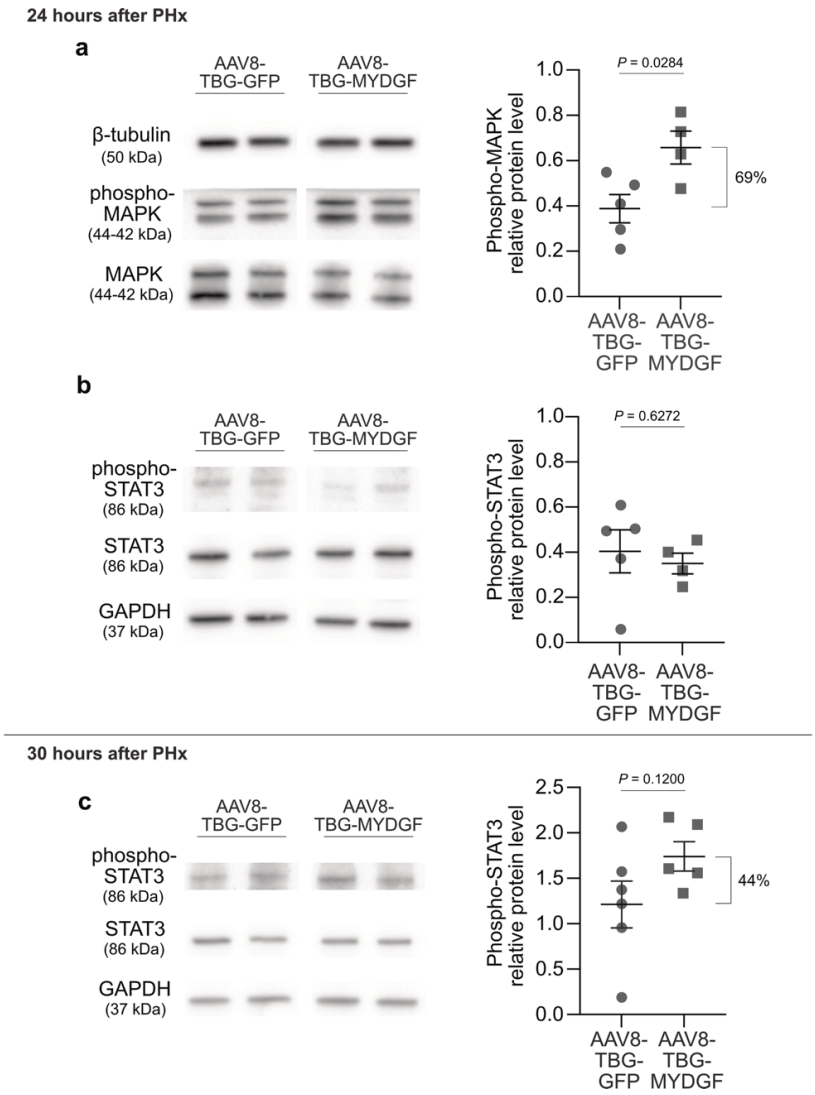

Figure 22: Increased levels of phospho-MAPK and phospho-STAT3 in AAV8-TBG-MYDGF mice within the first 30 hours post PHx.
(**a**) Western blots showing β-tubulin (50 kDa), phospho-MAPK (T202/Y204; 44-42 kDa) and MAPK (44-42 kDa) in right liver lobe lysates of AAV8-TBG-GFP or AAV8-TBG-MYDGF transfected mice 24 hours after PHx and quantification of relative phospho-MAPK (T202/Y204) protein levels normalized to MAPK and β-tubulin. (**b**) Western blots showing phospho-STAT3 (S727; 86 kDa), STAT3 (86 kDa) and GAPDH (37 kDa) in right liver lobe lysates of AAV8-TBG-GFP or AAV8-TBG-MYDGF transfected mice 24 hours post PHx and quantification of relative phospho-STAT3 (S727) protein levels normalized to STAT3 and GAPDH. (**c**) Western blots showing phospho-STAT3 (S727; 86 kDa), STAT3 (86 kDa) and GAPDH (37 kDa) in right liver lobe lysates of AAV8-TBG-GFP or AAV8-TBG-MYDGF transfected mice 30 hours after PHx and quantification of relative phospho-STAT3 (S727) protein levels normalized to STAT3 and GAPDH. n = 5 AAV8-TBG-GFP versus n = 4 AAV8-TBG-MYDGF liver lysates 24 hours after PHx (a, b) and n = 6 AAV8-TBG-GFP versus n = 5 AAV8-TBG-MYDGF liver lysates 30 hours after PHx (c). Data are presented as mean ± SEM. *P* values were calculated using two-tailed unpaired Student's *t*-test with Welch's correction.

5.10 Diminished liver regeneration in MYDGF knockout (KO) mice

After demonstrating that MYDGF levels increase after liver surgery in humans and mice (**Figure 14, 15**), and that overexpression of MYDGF increases hepatocyte proliferation and liver-to-body weight ratio in mice after two-thirds PHx (**Figure 19-21**), we wanted to further investigate the role of MYDGF in liver regeneration by performing a loss-of-function experiment. To this end, we performed a two-thirds PHx in MYDGF knockout (MYDGF KO) mice and examined the signaling pathway and hepatocyte proliferation 30 hours after PHx. The isolation timepoint of 30 hours after PHx was chosen because mice with liver-specific overexpression of MYDGF show a peak in hepatocyte proliferation at this timepoint (**Figure 20**).

First, we verified the knockout efficiency of MYDGF KO mice, generated by Korf-Klingebiel et al. (2015). Since the MYDGF KO mice were generated on a BALB/c background and back-crossed to a C57BL/6N background, C57BL/6N mice were used as control. To analyze the knockout efficiency, we prepared protein lysates from the left (isolated before PHx) and right liver lobes (isolated 30 hours after PHx) of control and MYDGF KO mice and determined the MYDGF levels by Western blot (**Figure 23a**). In both liver lobes from MYDGF KO mice, no MYDGF can be detected compared to the control mice (**Figure 23b, c**). This indicates that MYDGF is absent in the liver of MYDGF KO mice before and after PHx.

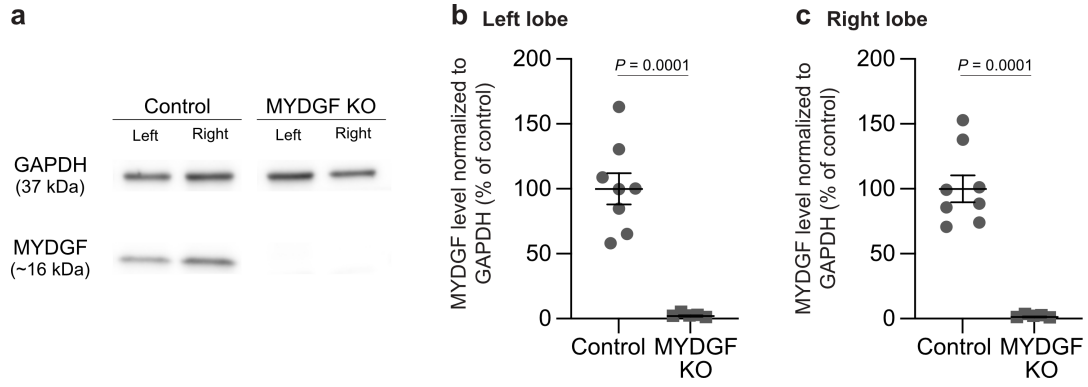

Figure 23: Absence of MYDGF in liver of MYDGF KO versus control mice.
(**a**) Western blots showing GAPDH (37 kDa) and MYDGF (~16 kDa) in left and right liver lobe lysates of control and MYDGF KO mice. (**b, c**) Quantification of MYDGF levels normalized to GAPDH levels in percent of control mice in lysates of the left liver lobe (resected during PHx) (b) and in lysates of the right liver lobe (isolated 30 hours post PHx) (c). n = 8 control versus n = 5 MYDGF KO left (b) and right (c) liver lysates. Data are presented as mean ± SEM. *P* values were calculated using two-tailed unpaired Student's *t*-test with Welch's correction.

5.10.1 MYDGF KO mice show abolished hepatocyte proliferation 30 hours after PHx

After verifying the knockout efficiency of the animals, we examined whether the proliferation rate in the right and caudate liver lobes of MYDGF KO mice was altered compared to control mice 30 hours after PHx. To analyze the proliferation rate, liver sections of the right and caudate liver lobe from control and MYDGF KO mice were first stained for the proliferation maker PH3. In addition, blood vessels were stained for ICAM-1. To analyze whether KO of MYDGF results in reduced hepatocyte proliferation, only $PH3^+$ but $ICAM\text{-}1^-$ cells were counted and normalized to $DAPI^+$ cells (**Figure 24**). Strikingly, the hepatocyte proliferation rate in both the right and caudate liver lobes from MYDGF KO mice is reduced by almost 90% compared to control mice 30 hours after two-thirds PHx (**Figure 24 c, f**).

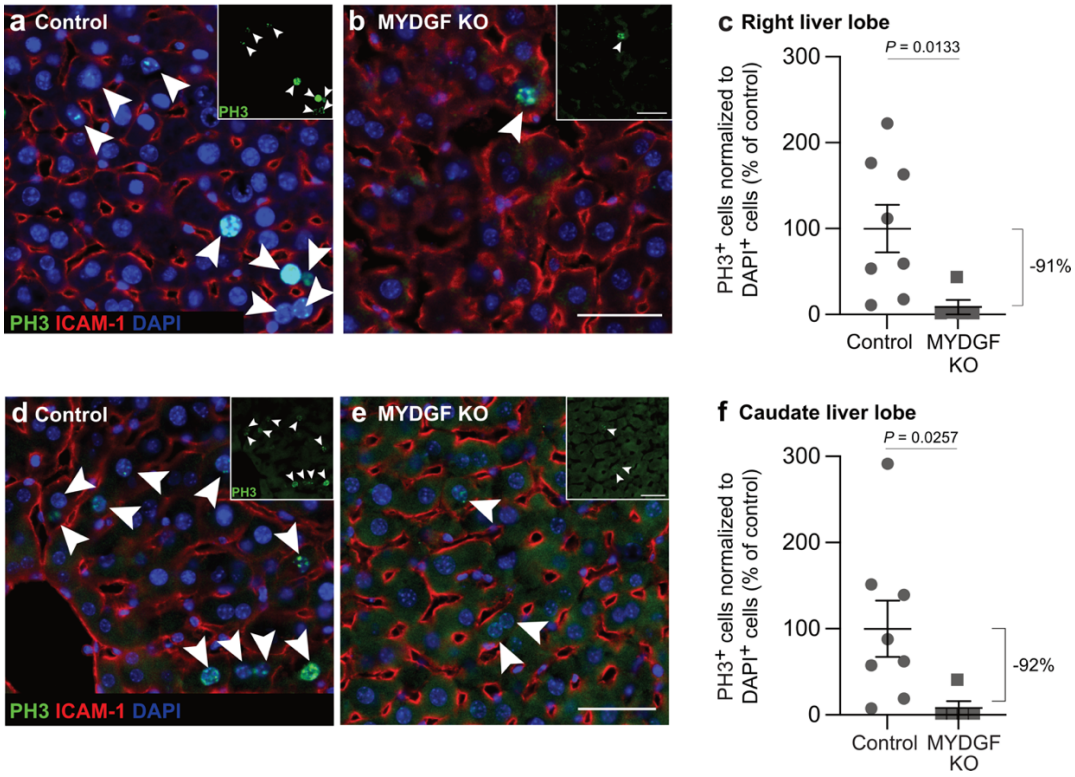

Figure 24: MYDGF KO almost abolishes the number of $PH3^+$ hepatocytes in the remaining mouse liver lobes 30 hours after PHx.
(**a, b**) LSM images of transversal sections of the right liver lobe of control (a) and MYDGF KO (b) mice stained for proliferation marker PH3 (green, shown in inset top right), and blood vessel marker ICAM-1 (red). Cell nuclei were counterstained for DAPI. White arrowheads point to proliferating cells. (**c**) Quantification of proliferating cells ($PH3^+$ and $ICAM\text{-}1^-$) normalized to $DAPI^+$ cells in control versus MYDGF KO mice, shown as percentage of control. (**d, e**) LSM images of transversal sections of the caudate liver lobe of control (d) and MYDGF KO (e) mice stained for PH3 (green, shown in inset top right), ICAM-1 (red). Cell nuclei were counterstained for DAPI. White arrowheads point to proliferating cells. (**f**) Quantification of proliferating cells ($PH3^+$ and $ICAM\text{-}1^-$) normalized to $DAPI^+$ cells in control versus MYDGF KO mice, shown as percentage of control. n = 8 control versus n = 5 MYDGF KO transversal sections of the right (c) and caudate (f) liver lobe. Scale bars: 50 µm (b, e). Data are presented as mean ± SEM. *P* values were calculated using two-tailed unpaired Student's *t*-test with Welch's correction.

To verify these proliferation data, liver sections were additionally stained for proliferation marker Ki67 (**Figure 25**). To validate if the proliferating cells are hepatocytes, the slides were also stained for the hepatocyte marker HNF4α. For analysis, only Ki67 and HNF4α double positive cells were counted and normalized to DAPI$^+$ cells. Quantification of the Ki67 staining shows almost completely abolished hepatocyte proliferation in the right and caudate liver lobes of MYDGF KO mice 30 hours after two-thirds PHx (**Figure 25c, f**).

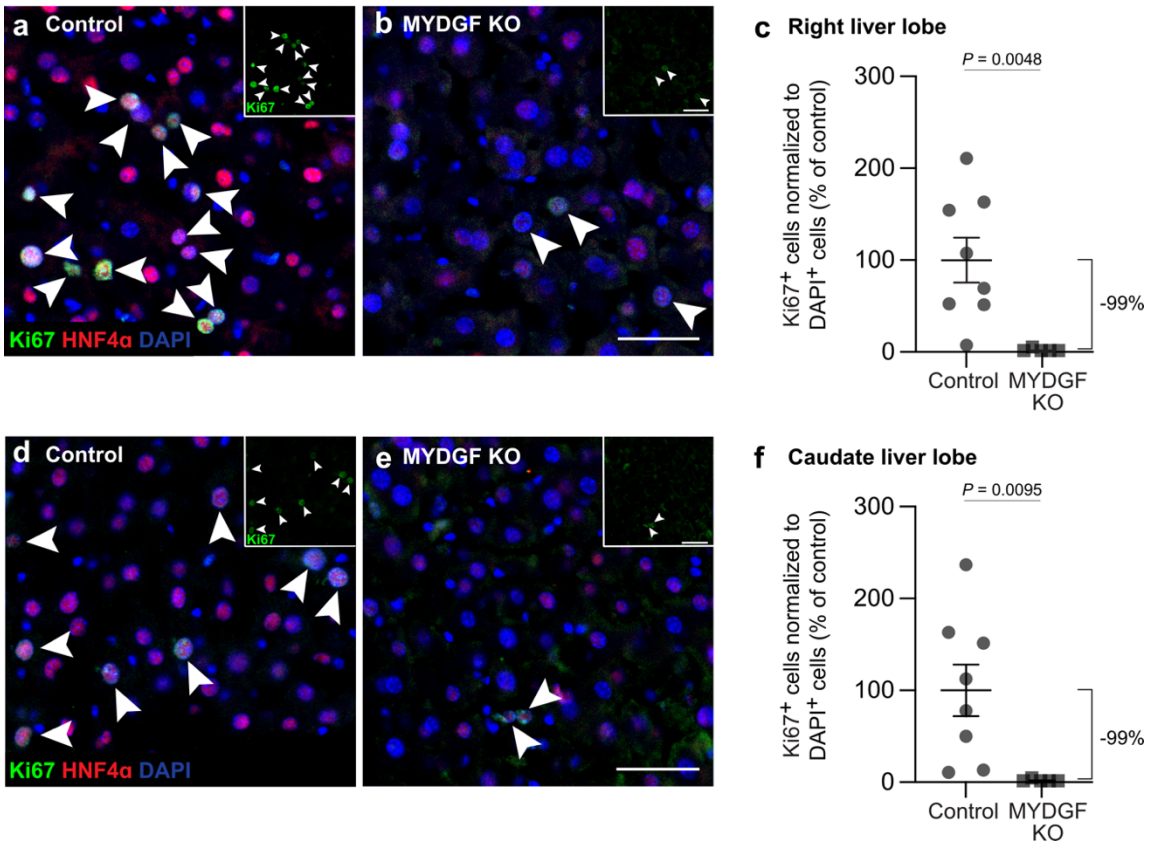

Figure 25: MYDGF KO almost abolishes the number of Ki67$^+$ hepatocytes in the remaining mouse liver lobes 30 hours after PHx.
(**a, b**) LSM images of transversal sections of the right liver lobe of control (a) or MYDGF KO (b) mice, stained for proliferation marker Ki67 (green, shown in inset top right) and hepatocyte marker HNF4α (red). Cell nuclei were counterstained for DAPI. White arrowheads point to proliferating cells. (**c**) Quantification of proliferating cells (Ki67$^+$ and HNF4α$^+$) normalized to DAPI$^+$ cells in control versus MYDGF KO mice, shown as percentage of control. (**d, e**) LSM images of transversal sections of the caudate liver lobe of control (d) and MYDGF KO (e) mice, stained for Ki67 (green, shown in inset top right) and HNF4α (red). Cell nuclei were counterstained for DAPI. White arrowheads point to proliferating cells. (**f**) Quantification of proliferating cells (Ki67$^+$ and HNF4α$^+$) normalized to DAPI$^+$ cells in control versus MYDGF KO mice, shown as percentage of control. n = 8 control versus n = 5 MYDGF KO transversal sections of the right (c) and caudate (f) liver lobe. Scale bars: 50 µm (b, e). Data are presented as mean ± SEM. *P* values were calculated using two-tailed unpaired Student's *t*-test with Welch's correction.

Taken together, these results show that MYDGF KO mice have significantly abolished hepatocyte proliferation compared to control mice 30 hours after two-thirds PHx.

5.10.2 MYDGF KO reduces phosphorylation of STAT3 in the remaining mouse liver 30 hours after PHx

We further wanted to determine if the MYDGF KO also has an effect on the STAT3 signaling 30 hours after PHx. Since overexpression of MYDGF in the mouse liver results in a trend toward increased phospho-STAT3 (S727) signaling compared to control mice 30 hours after PHx (**Figure 22c**), we hypothesized that phospho-STAT3 (S727) signaling is altered in MYDGF KO mice compared to the control mice. To verify this hypothesis, we analyzed the phospho-STAT3 (S727) levels in the right liver lobe from control and MYDGF KO mice 30 hours after PHx by Western blot. For the quantification phospho-STAT3 (S727) levels were normalized to STAT3 and GAPDH (**Figure 26a**). We observed a 30% reduction in relative phospho-STAT3 (S727) levels in right liver lobe lysates from MYDGF KO mice 30 hours after two-thirds PHx (**Figure 26b**).

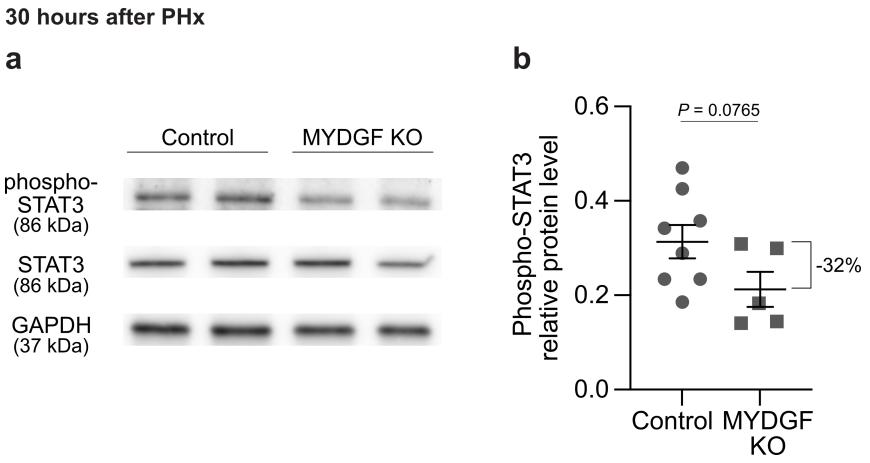

Figure 26: Reduced phosphorylation of STAT3 in the remaining liver of MYDGF KO mice 30 hours after PHx.
(**a**) Western blots showing phospho-STAT3 (S727) (86 kDa), STAT3 (86 kDa) and GAPDH (37 kDa) in right liver lobe lysates of control and MYDGF KO mice 30 hours after PHx. (**b**) Quantification of relative phospho-STAT3 (S727) protein levels normalized to STAT3 and GAPDH. n = 8 control versus n = 5 MYDGF KO liver lysates. Data are presented as mean ± SEM. *P* value was calculated using two-tailed unpaired Student's *t*-test with Welch's correction.

All in all, these results strongly indicate that a deletion of MYDGF leads to significantly abolished hepatocyte proliferation and reduced phosphorylation of STAT3 on S727 30 hours after two-thirds PHx.

6. Discussion

The aim of this study was to investigate the role of the angiocrine signal MYDGF on hepatocyte proliferation and liver regeneration. We demonstrated that the secretion of MYDGF by stretched primary human hepatic ECs (Große-Segerath, 2020, Große-Segerath and Follert et al., 2024) is not associated with an increase in cell death (**Figure 5**). Further we showed that MYDGF promotes proliferation (**Figure 6**) and survival (**Figure 7**) of 2D and proliferation of 3D (**Figure 8**) cultured primary human hepatocytes, but not of the *AFP*-positive HepG2 cell line (**Figure 9, 10**). Moreover, we identified that MAPK/STAT3 signaling is involved in MYDGF-induced hepatocyte proliferation (**Figure 11, 12, 13**). We also revealed that MYDGF is expressed at an earlier timepoint than HGF after liver surgery in humans (**Figure 14**) and mice (**Figure 15**). We further demonstrated that AAV8-TBG induced overexpression of MYDGF in the mouse liver (**Figure 18**) enhances hepatocyte proliferation (**Figure 19, 20**) and liver-to-body weight ratio (**Figure 21**) after two-thirds PHx. Furthermore, we observed and increased phosphorylation of MAPK (T202/Y204) 24 hours after PHx and a tendentially increased phosphorylation of STAT3 (S727) 30 hours after PHx (**Figure 22**). In contrast, deletion of MYDGF leads to impaired liver regeneration, as reflected by diminished hepatocyte proliferation 30 hours after two-thirds PHx (**Figure 23, 24, 25**). Also, a numerically reduced phosphorylation of STAT3 (S727) can be observed at this timepoint after two-thirds PHx (**Figure 26**). Hence, this study describes the positive effect of MYDGF on the proliferation and survival of human hepatocytes and its requirement for liver regeneration.

6.1 *In vitro* relevance of MYDGF as an angiocrine signal for human hepatocyte proliferation and survival

After two-thirds PHx, the same amount of blood flows to the remaining smaller part of the liver, resulting in hemodynamic changes (Michalopoulos, 2007, Eipel et al., 2010, Lorenz et al., 2018, Grosse-Segerath and Lammert, 2021). These hemodynamic changes can be mimicked *in vitro* by mechanically stretching primary human hepatic ECs, which triggers the release of angiocrine signals such as HGF (Lorenz et al., 2018). In a previous experiment we measured elevated levels of the paracrine-acting protein MYDGF in the supernatant of mechanically stretched primary human hepatic ECs (Große-Segerath, 2020, Große-Segerath and Follert et al., 2024). Since mechanical stretching of ECs is associated with morphological and structural changes (Jufri et al., 2015), we investigated whether our stretching conditions lead to enhanced cell death and thus to increased MYDGF levels in the supernatants of stretched primary human hepatic ECs. Here, we show that our

stretching conditions do not lead to increased cell death of human hepatic ECs (**Figure 5**) and therefore conclude that MYDGF is secreted as an angiocrine signal by stretched human hepatic ECs.

MYDGF was first described in the heart in 2015, and in recent years has been claimed as a potential therapeutic drug for diseases in several organs (Xu et al., 2023b). While in the heart, MYDGF treatment promotes angiogenesis and cardiac repair after MI, it reduces the inflammatory response and hepatic *de novo* lipid synthesis in mice with NAFLD (Korf-Klingebiel et al., 2015, Ding et al., 2023). Due to the close connection between the heart and the liver that occurs during embryonic development (Lammert et al., 2001, Møller and Bernardi, 2013, Zhang et al., 2016) and continues in the adult organism through the blood supply (Lammert et al., 2003), we first investigated whether MYDGF also has an effect on *in vitro* cultured primary human hepatocytes.

Studying the effect of angiocrine signals on primary human hepatocytes is challenging because these cells are demanding to culture. After seeding, hepatocytes undergo morphological changes, induce cell death, and have low proliferative potential (Guguen-Guillouzo and Guillouzo, 2010, Kaur et al., 2023, Zeilinger et al., 2016). Therefore, we investigated whether MYDGF treatment has a proliferation and survival enhancing effect on 2D cultured hepatocytes. We verified previous results from our laboratory (Große-Segerath, 2020, Große-Segerath and Follert et al., 2024) and showed that MYDGF treatment leads to an increased number of proliferating ($PH3^+$) human hepatocytes and a decreased caspase-3 area and thus to reduced programmed cell death (apoptosis) in primary human hepatocytes (**Figure 6, 7**). However, both the proliferation and survival data indicate that the youngest donor (23 years, male) shows the lowest response to MYDGF treatment. This contradicts the current state of research, which indicates that younger humans and mice show superior hepatocyte proliferation and liver regeneration than older ones (Fry et al., 1984, Iakova et al., 2003, Schmucker and Sanchez, 2011). The reduced response of the 23-year-old male donor to MYDGF treatment might be explained by his daily alcohol consumption and his higher BMI (BMI: 24.6) compared to the other donors (BMI: 18-21), as increased BMI and regular alcohol consumption are known to lead to liver damage (Fabbrini et al., 2010, Beier and McClain, 2010, Wang et al., 2016). Therefore, it is possible that the hepatocytes from this donor, although morphologically comparable to the hepatocytes from the other donors, were more severely damaged prior to culturing, resulting in a lower response to MYDGF treatment compared to the other donors.

As aforementioned cultivation of hepatocytes in 2D culture is challenging, we also investigated the effect of MYDGF treatment on human hepatocyte organoids. Our results show an increase in organ area and proliferation rate of human hepatocyte organoids after seven days of daily MYDGF treatment (**Figure 8**). 3D culture systems have the advantage

that human hepatocytes can be cultured for longer periods of time, which is particularly beneficial for hepatocytes that dedifferentiate rapidly in 2D culture (Bissell and Guzelian, 1980, Seirup et al., 2022). Furthermore, the culture conditions are closer to the *in vivo* situation, hence 3D culture systems are also widely used for drug testing, developmental studies, or disease modeling (Edmondson et al., 2014, Duval et al., 2017, Kapalczynska et al., 2018, Hora and Wuestefeld, 2023). In the pharmaceutical industry, several 3D systems are used to test the liver toxicity of various substances (Soldatow et al., 2013). However, 3D culture also has its limitations, such as the lack of complexity of the living organ or the limited vascularization (Hora and Wuestefeld, 2023). The formation of vascular networks can be partially achieved by co-culturing of mesodermal progenitor cells derived from induced pluripotent stem cells (iPSCs) with human organoids (Worsdorfer et al., 2019). Nevertheless, vascularization remains a challenging process in organoid culture. In addition to the challenging vascularization of the organoids, their "grape-like" structure (Hu et al., 2018) creates a nutrient-access-gradient within an organoid (Edmondson et al., 2014, Duval et al., 2017), consequently treatment needs to be adjusted accordingly. Our results show that MYDGF also has an effect on hepatocytes cultured more closely related to an *in vivo* situation. Thus, our results provide a basis for further investigation of the effect of MYDGF as a potential therapeutic drug. For example, it would be interesting to investigate whether continuous rather than daily administration over seven days would have an even more robust effect on hepatocyte proliferation, as MYDGF has a short half-life (15.3 minutes) (Korf-Klingebiel et al., 2015). In addition, the structure of MYDGF could be modified (e.g., via Fc-tag) to extend its half-life while maintaining its function. Furthermore, it would be interesting to test whether MYDGF also has a beneficial effect on a chronically damaged liver. A previous study has already shown that transplantation of *in vitro* cultured liver organoids into the liver via the portal vein of rats restores the regenerative capacity of a chronically damaged liver in rats (Tsuchida et al., 2019). Thus, it could be tested whether transplantation of MYDGF-treated hepatocyte organoids restores the regenerative capacity of a chronically damaged liver even faster.

However, in previous publications, C19orf10 (MYDGF) has also been described in association with the malignant stage of hepatocellular and gallbladder carcinoma (Sunagozaka et al., 2011, Wang et al., 2021, Li et al., 2021). In hepatocellular carcinoma *AFP* and *MYDGF* expression are correlated, and a depletion of *MYDGF* in *AFP*-positive cancer cells results in reduced cell proliferation (Sunagozaka et al., 2011). In this study we show that HepG2 cells compared to primary human hepatocytes are *AFP*-positive and do not respond to our MYDGF treatment conditions with an increase in proliferation (**Figure 9, 10**). This result can be explained by the fact that HepG2 cells do not reflect the adult human *in vivo* situation based on their *AFP* expression (Bergstrand and Czar, 1956). *AFP* is only

expressed in the embryo and takes over the function of albumin, while in the adult organism AFP is completely replaced by albumin (Galle et al., 2019). Therefore, the presence of AFP in the adult organism is atypical and is consequently used as a marker for HCC or liver diseases (Galle et al., 2019, Hu et al., 2022b). Accordingly, we can conclude that our *in vitro* treatment conditions do not promote proliferation of the *AFP*-positive HepG2 cell line.

In summary, we show that MYDGF has a proliferation- and survival-promoting effect on primary human hepatocytes *in vitro*. Thus, MYDGF represents a useful medium supplement to improve the cultivation of primary human hepatocytes. Consequently, it would be possible to culture primary human hepatocytes for a longer period of time and to investigate the influence of newly identified other angiocrine signals on the proliferation and survival of primary human hepatocytes. In addition, human hepatocyte organoids can be used to study the effect of MYDGF as a potential therapeutic drug for liver regeneration or chronic liver injury. Moreover, the identification of the yet unknown MYDGF receptor could open up further opportunities to study the function and treatment conditions of MYDGF.

6.1.1 Underlying signaling pathway of MYDGF on human hepatocyte proliferation

Hepatocyte proliferation and thus liver regeneration are associated with several signaling pathways (Talarmin et al., 1999, Wen et al., 2022, Yagi et al., 2020, Hong et al., 2000, Jackson et al., 2008). In this study, we identify that the MAPK/STAT3 signaling pathway is involved in MYDGF-induced hepatocyte proliferation (**Figure 11-13**). MYDGF induces phosphorylation of MAPK on T202/Y204 (ERK1/2), and the phosphorylation of STAT3 on S727 in primary human hepatocytes. This effect can be inhibited by pretreatment with PD98059 (MEK specific inhibitor), which results in significantly reduced phosphorylation of MAPK on T202/Y204 (ERK1/2) and STAT3 on S727 and decreased hepatocyte proliferation under MYDGF treatment. Several studies have shown that treatment of mouse and human hepatocytes with growth factors is associated with activation of the MAPK (ERK1/2) signaling pathway (Talarmin et al., 1999, Leu et al., 2003, Huh et al., 2004, Henklova et al., 2008, Factor et al., 2010, Chen et al., 2013). For example, treatment of human hepatocytes with the growth factor EGF and the treatment of mouse hepatocytes with HGF leads to activation of MAPK (ERK1/2) signaling and increased proliferation of mouse hepatocytes (Henklova et al., 2008, Huh et al., 2004). Mice with a silenced HGF receptor (*c-Met*) in hepatocytes exhibit reduced MAPK (ERK1/2) signaling after PHx (Factor et al., 2010). Primary cultured hepatocytes from these mice also exhibit reduced phospho-MAPK (ERK1/2) signaling, which can only be partially rescued by continuous administration of EGF (Factor et al., 2010). In addition, EGF plus insulin-induced

MAPK (ERK1/2) signaling and DNA synthesis in primary rat hepatocytes can be inhibited by PD98059 treatment. (Dixon et al., 1999).

In contrast, significantly increased phosphorylation of STAT3 on S727 occurs at a later timepoint after MYDGF treatment than phosphorylation of MAPK on T202/Y204 (ERK1/2) (**Figure 11**). However, MYDGF-induced phosphorylation of STAT3 on S727 can be prevented by pre-treatment with both the MEK-specific inhibitor (PD98059) and the STAT3-specific inhibitor (Stattic) (**Figure 12**). Therefore, we hypothesized that MYDGF treatment activates STAT3 downstream of MAPK in human hepatocytes. MAPK can activate STAT3 by phosphorylation on S727 residue without prior activation of JAK (Chung et al., 1997, Korf-Klingebiel et al., 2015, Xu et al., 2022), resulting in maximal transcriptional activity of STAT3 (Wen et al., 1995, Decker and Kovarik, 2000), as previously described in the literature. Furthermore, we showed that the activation of STAT3 is crucial for MYDGF-induced hepatocyte proliferation, as the proliferation-promoting effect of MYDGF on primary human hepatocytes is almost completely abolished when the phosphorylation of STAT3 is inhibited by Stattic (**Figure 13**). This indicates that the inhibition of STAT3 has a stronger impact on the proliferation-promoting effect of MYDGF on human hepatocytes than the inhibited phosphorylation of MAPK. This effect may occur because STAT3, as a transcription factor can directly activate cell proliferation (Tesoriere et al., 2021). However, when the phosphorylation of MAPK is inhibited, other signaling molecules may be activated to compensate for the inhibition of the MAPK pathway. The ability of other pathways to be activated to compensate for the inhibition of one signaling molecule can be seen in mice with liver-specific deletion of *Stat3*. In these mice, *Stat3* deletion results in increased activation of the PI3K/AKT pathway during liver regeneration after PHx (Haga et al., 2005). Furthermore, the inhibition of the proliferation-promoting effect of MYDGF on primary human hepatocytes by pretreatment with PD98059 or/and Stattic is comparable to that obtained by treating primary mouse hepatocytes with IL-6. The latter is a well-known cytokine that is essential for hepatocyte proliferation and survival during liver regeneration (Cressman et al., 1996, Sakamoto et al., 1999, Blindenbacher et al., 2003). Treatment of primary mouse hepatocytes *in vitro* with IL-6 results in the activation of MAPK (ERK1/2), STAT3 and YAP and an increased proliferation rate (Cheng et al., 2022). Inhibition of STAT3 leads to a nearly 46% reduction in hepatocyte proliferation, while inhibition of MAPK (ERK1/2) results in a 35% reduction in hepatocyte proliferation (Cheng et al., 2022). Inhibition of MAPK (ERK1/2), STAT3 and YAP completely abolished the proliferation-promoting effect of IL-6 on primary mouse hepatocytes. This indicates that these signaling molecules are critical for IL-6-mediated functions (Cheng et al., 2022). Another study shows that an induced albumin promoter-driven Cre-loxP-mediated *Stat3* deletion in adult mouse liver, leads to normal MAPK activation but one-third reduced DNA synthesis in hepatocytes

40 hours after PHx (Li et al., 2002). Comparing our results with previous publications, we conclude that MAPK and STAT3 are crucial for MYDGF-mediated functions, since depletion of one or both signaling molecules inhibited or almost abolished MYDGF-induced proliferation of human hepatocyte.

In addition, we observe increased phospho-AKT (S473) levels 5 and 15 minutes after MYDGF treatment, which returned to baseline levels 30 minutes after treatment (**Figure 11**). In this study, we did not investigate the influence of AKT inhibition on hepatocyte proliferation, as phosphorylation of AKT on S473, but also on residue T308, is mainly associated with a cell survival-promoting effect under MYDGF treatment (Korf-Klingebiel et al., 2015, He et al., 2020, Gao et al., 2023). In cardiac myocytes, MYDGF promotes the survival through the phosphorylation of AKT on residues S473 and T308, resulting in inhibition of the pro-apoptotic proteins Bcl-2-associated X protein (Bax) and Bcl-2 antagonist of cell death (Bad) (Korf-Klingebiel et al., 2015), whereas MYDGF-induced podocyte survival occurs in an AKT/Bad-dependent manner (He et al., 2020). High glucose-induced gingival fibroblasts, associated with increased apoptosis, can be prevented by overexpression of MYDGF, which leads to activation of AKT and inhibition of nuclear factor kappa-light-chain-enhancer of activated B cells (NF-κB) (Gao et al., 2023). In general, activation of AKT can lead to the phosphorylation and therefore inhibition of the pro-apoptotic proteins Bad and Bax (Datta et al., 1997, del Peso et al., 1997, Yamaguchi and Wang, 2001) and the pro-apoptotic proteases caspase-8/-9 (Liu et al., 2019, Cardone et al., 1998). AKT also has an anti-apoptotic effect during liver regeneration in mice by activating the Bad signaling (Hong et al., 2000). For example, AKT activation protects against TNF-α and Fas ligand mediated apoptosis in primary mouse hepatocytes (Hatano and Brenner, 2001). Suppression of AKT phosphorylation by various inhibitors leads to increased pro-caspase-8 activity and decreased survival of mice in liver injury models. This effect can be partially reversed by co-treatment with the AKT-specific activator SC79 (Liu et al., 2019). Thus, AKT plays a critical role in the survival of cells, including hepatocytes. In further experiments it would be of great interest to investigate the effect of AKT phosphorylation under MYDGF treatment on the survival but also on the proliferation of human hepatocytes. Western blots could be used to test whether MYDGF promotes the phosphorylation and thus inhibits pro-apoptotic markers (such as Bax, Bad) and pro-apoptotic caspase activity in human hepatocytes under AKT activation. In addition, the effect of AKT inhibition on hepatocyte survival and proliferation after MYDGF treatment needs to be investigated by immunostaining.

All in all, we identified that the MAPK/STAT3 signaling pathway is involved in MYDGF-induced primary human hepatocyte proliferation. Further experiments are required to

determine whether the phosphorylation of AKT after MYDGF treatment also has an effect on primary human hepatocyte proliferation and/or survival.

6.2 *In vivo* relevance of MYDGF on hepatocyte proliferation and liver regeneration

6.2.1 Expression kinetics of MYDGF and HGF after liver surgery in humans and mice

Since MYDGF is secreted by stretched primary human hepatic ECs (Große-Segerath, 2020, Große-Segerath and Follert et al., 2024), we investigated whether MYDGF levels are elevated after liver surgery in humans and mice. We hypothesized that MYDGF is secreted into the blood by hepatic ECs after liver surgery, due to vasodilation of blood vessels in the remaining liver. To analyze the expression kinetics of MYDGF after liver surgery, we measured MYDGF serum and plasma levels in humans at different timepoints after liver surgery and compared it to the well-studied expression kinetics of the angiocrine signal HGF. Our human data show that MYDGF is expressed in human blood serum within the first hour after stage 1 in-situ split liver surgery, whereas HGF begins to increase 24 hours after stage 1 in-situ split liver surgery (**Figure 14**). Consequently, we hypothesized that MYDGF, in contrast to HGF, is released at an earlier timepoint of liver regeneration. This hypothesis was confirmed by our plasma data. After liver resections, where different segments of the liver were removed from six male patients, a 40% increase in MYDGF levels is visible. In contrast, HGF does not show a significant increase at this timepoint. These data are consistent with the literature showing that basal blood serum and plasma HGF levels (range from 10-1,000 pg/ml) begin to increase (range from 100-10,000 pg/ml) 24 hours after stage 1 in-situ split liver surgery (Sparrelid et al., 2018) and liver resection (Tomiya et al., 1992, Justinger et al., 2008, Murtha-Lemekhova et al., 2021, Dehlke et al., 2022). In addition, our results confirm the fact that metabolite concentrations are generally higher in serum than in plasma (Yu et al., 2011). Nevertheless, HGF shows higher plasma and serum levels compared to MYDGF, suggesting that HGF levels are generally higher before and after liver surgery. This can be explained by the fact that HGF is not only secreted by hepatic ECs, but also by HSCs, Kupffer cells and mesenchymal cells, and is also stored in the ECM (Zhao et al., 2022). Furthermore, HGF mRNA levels also increase in distal organs such as the lung, kidney and spleen after liver surgery (Kono et al., 1992, Yanagita et al., 1992). In addition, HGF production is stimulated by pro-inflammatory cytokines such as IL-6 and TNF-α in distal organs and in the remaining liver (Nakamura and Mizuno, 2010). The possible storage of MYDGF in the ECM or an increase in MYDGF mRNA levels in distal organs after liver surgery is currently unknown. Therefore, further

experiments are needed to analyze the possible storage of MYDGF in the ECM and MYDGF mRNA levels in distal organs (e.g., spleen, kidney) after liver surgery.

Consistent with our human data, we measured a rapid increase of MYDGF in the remaining right liver lobe three hours after two-thirds PHx in mice (**Figure 15**). Since our previous experiments have shown that MYDGF is secreted as an angiocrine signal by stretched human hepatic ECs (Große-Segerath, 2020, Große-Segerath and Follert et al., 2024), we investigated whether isolated mouse hepatic ECs also display increased MYDGF levels after two-thirds PHx. In addition, we also measured the levels of HGF to compare the expression kinetics of both proteins. Our results show that in isolated mouse hepatic ECs, MYDGF levels increase at the same timepoint (3 hours after PHx) as measured in the whole liver lysates, whereas HGF levels increase at a later timepoint (12 hours after PHx). The increase of HGF 12 hours after PHx in mice has also been described in the literature (Zhang et al., 2020). In contrast, rats show a slightly earlier increase in HGF levels compared to mice. HGF mRNA and protein levels start to increase within the first 3 to 6 hours, peak 24 hours after PHx in rat liver, and gradually decline 72 to 96 hours after PHx (Zarnegar et al., 1991, Pediaditakis et al., 2001). This earlier increase may be related to the fact that in rats, hepatocyte proliferation peaks 12 hours earlier after PHx than in mice (Michalopoulos, 2007). Therefore, it would be interesting to examine the expression kinetics of MYDGF in rats after PHx to determine whether MYDGF is secreted at an earlier timepoint to promote the earlier hepatocyte proliferation. In addition, a higher level of HGF than MYDGF can be measured in the isolated hepatic ECs of the mice after PHx. Based on the already higher basal HGF levels (0 hours after PHx), it can be concluded that HGF is generally present in higher concentration than MYDGF in the mouse hepatic ECs.

In conclusion, our results indicate that MYDGF levels increase at an earlier timepoint after liver surgery in humans and mice, but at generally lower levels than HGF.

6.2.2 Effect of MYDGF overexpression on liver regeneration in mice

Since an increase in MYDGF is observed after liver surgery in humans and mice, we investigated whether overexpression of MYDGF in the mouse liver has an effect on liver regeneration after PHx. Our results reveal that AAV8-TBG-mediated overexpression of MYDGF in hepatocytes leads to significantly increased hepatocyte proliferation 30 hours after PHx via the activation of MAPK/STAT3 signaling and a 10% increased liver-to-body weight ratio 96 hours after PHx (**Figure 19-22**). In contrast, overexpression of MYDGF alone does not lead to excessive hepatocyte proliferation without the mechanical stimulus of two-thirds PHx (**Figure 20**). Recent studies have shown that overexpression of some liver specific genes have a negative effect on the healthy liver. For example, mice with

TGF-α overexpression driven by the metallothionein 1 (MT1) promoter exhibit formation of liver tumors (Jhappan et al., 1990). Or mice overexpressing HGF exhibit a liver-to-body weight ratio twice as high as control mice at four weeks of age and almost three times faster liver regeneration after PHx, but the *Hgf* transgenic animals develop benign and/or malignant liver tumors by 17 months of age (Sakata et al., 1996). This effect was observed even though HGF has been shown to have an inhibitory effect on the growth of hepatocellular cancer cell lines (Tajima et al., 1991, Shiota et al., 1992). Another study showed that transgenic mice overexpressing HGF under the control of an albumin regulatory sequence had increased liver weight at six months of age compared to controls, but did not develop liver tumors until nine months of age (Shiota et al., 1994). In addition, overexpression of HGF results in a 34% increase in liver-to-body weight one day after PHx and a doubled rate of liver regeneration compared to control mice (Shiota et al., 1994). In contrast, we did not observe the development of liver tumors in mice with hepatocyte-specific MYDGF overexpression four weeks after AAV8-injection (data not shown). Similarly, no phenotypic changes were described in other studies in which MYDGF was overexpressed by AAV injection (Wang et al., 2020a, He et al., 2020, Meng et al., 2021, Xu et al., 2022, Ding et al., 2023). On the other hand, the significantly increased proliferation of hepatocytes after two-thirds PHx indicates improved liver regeneration in AAV8-TBG-MYDGF transfected mice compared to AAV8-TBG-GFP transfected mice. Also, the significantly increased phosphorylation of MAPK on T202/Y204 (ERK1/2) (24 hours after PHx) and the numerically increased phosphorylation of STAT3 on S727 (30 hours after PHx) in the AAV8-TBG-MYDGF mice supports our aforementioned hypothesis that MYDGF activates MAPK upstream of STAT3 to promote hepatocyte proliferation (**Figure 22**). Based on this, it would be interesting to investigate whether treatment with recombinant MYDGF in wild-type and aged mice improves liver regeneration under activation of MAPK/STAT3 signaling after two-thirds PHx. Due to the relatively short half-life of MYDGF in plasma (15.3 minutes) (Korf-Klingebiel et al., 2015), daily and continuous treatment with MYDGF during the first days after PHx would be useful, as it has already been shown that proteins with a short half-life, e.g., HGF (half-life: 3-5 minutes), lead to undetectable or low levels of hepatic DNA synthesis after a single injection into intact animals (Webber et al., 1994, Ishii et al., 1995). However, continuous administration of HGF directly into the portal vein of intact mouse livers for five days resulted in a 140% increase in liver mass, returning to normal within four to five weeks (Patijn et al., 1998).

In addition, it would be interesting to investigate whether MYDGF promotes liver regeneration not only in mechanically but also in hepatoxically injured livers. To this end, liver tissue can be injured by treatment with hepatoxic chemicals such as CCl4, which triggers an inflammatory response (Michalopoulos, 2007). This model is more consistent

with the regenerative response in humans with liver disease because the regeneration process is preceded by an inflammatory response rather than a traumatic injury as in PHx (Ding et al., 2010, Huang et al., 2021). HGF gene therapy has been shown to improve liver function in cirrhotic (CCl4 treatment induced) mouse livers after PHx (Xue et al., 2003). On this basis, it would be interesting to investigate whether MYDGF also improves liver regeneration in chemically induced liver injury models, as recent studies have already shown that MYDGF alleviates the inflammatory response in high-fat diet-induced NAFLD mice (Ding et al., 2023).

In summary, we propose, for the first time that overexpression of MYDGF leads to significantly increased hepatocyte proliferation via activation of MAPK/STAT3 signaling and improved liver regeneration after two-thirds PHx. To emphasize the clinical relevance of MYDGF as a therapeutic drug, daily administration of MYDGF after two-thirds PHx or chemically induced liver regeneration needs to be investigated.

6.2.3 Effect of MYDGF knockout on liver regeneration in mice

To better understand the role of MYDGF in liver regeneration, we also performed a loss-of-function experiment. Loss-of-function experiments are widely used to study whether deletion of a specific gene results in impaired liver regeneration. In recent years, the relevance of known angiocrine signals and cytokines for liver regeneration have been investigated using various knockout mice (Huang et al., 2021, Hora and Wuestefeld, 2023). However, some knockout models are difficult to study, including homozygous deletion of *Hgf* and/or its receptor *c-Met*, which results in embryonic lethality and impaired liver development (Schmidt et al., 1995, Bladt et al., 1995, Uehara et al., 1995, Dietrich et al., 1999). Therefore, the influence of induced *Hgf* deletion in adult rodents on liver regeneration has been investigated in recent years. Endothelial cell-specific deletion of *Hgf* in mice was shown to result in significantly reduced hepatocyte proliferation 48 hours after PHx and a reduced liver-to-body weight ratio 72 hours after PHx compared to controls (Zhang et al., 2020). At 96 hours after PHx, no proliferation or weight-specific difference is observed, indicating a delay in liver regeneration (Zhang et al., 2020). In contrast, Cre-recombinase-induced deletion of *Hgf* in adult mice reduces the liver-to-body weight ratio by 20% and significantly inhibits hepatocyte proliferation two days after PHx combined with one month of CCl4 pre-treatment (Nejak-Bowen et al., 2013). Depletion of the HGF receptor *c-Met* in adult mice results in impaired liver regeneration with a 60% reduction in hepatocyte proliferation compared to controls 48 hours after PHx (Borowiak et al., 2004). Also, the activation of MAPK (ERK1/2), which is known to be activated in liver regeneration (Guegan et al., 2012), cannot be detected in *c-Met* mutant mice (Borowiak et al., 2004). Our results

show comparable and, in some cases, even stronger effects of MYDGF knockout on liver regeneration in mice. MYDGF KO mice do not exhibit embryonic lethality or impaired liver development indicating that MYDGF is not required for embryonic development (Korf-Klingebiel et al., 2015). However, the deletion of MYDGF leads to an almost abolished proliferation of hepatocytes and a numerically reduced phosphorylation of STAT3 (S727) 30 hours after PHx (**Figure 24-26**). To be able to make a more precise statement as to whether liver regeneration is only delayed (similar to the endothelial cell-specific deletion of *Hgf*) or completely abolished by the deletion of *Mydgf*, further timepoints after PHx (e.g., 24, 96 hours) need to be investigated. Thereby, it would be interesting to examine whether there is also a reduced phosphorylation of MAPK (ERK1/2) signaling 24 hours after PHx and an altered liver-to-body weight ratio 96 hours after PHx. Since a recent study has shown that MYDGF deficiency leads to increased liver dysfunction and inflammatory response in NAFLD mice (Ding et al., 2023), it would be interesting to analyze if the inflammatory response and the survival kinetics of MYDGF KO mice compared to controls after two-thirds PHx is altered. Therefore, further experiments need to be performed to investigate the apoptosis rate, necrotic area and also the expression of inflammatory markers in the MYDGF KO mice compared to the control mice after two-thirds PHx. In addition, the clinical relevance of MYDGF as a therapeutic drug in the KO animals could be tested by investigating whether administration of recombinant MYDGF to MYDGF KO mice reverses the impaired liver regeneration after PHx.

In general, our results show that a deletion of MYDGF abolishes hepatocyte proliferation 30 hours after two-thirds PHx. Further *in vivo* experiments are required to better characterize the phenotype of MYDGF deletion on liver regeneration and the associated MAPK/STAT3 signaling pathway. These experiments will allow a more precise statement as to whether deletion of MYDGF delays or prevents liver regeneration.

6.3 Clinical relevance of MYDGF

Liver diseases such as cirrhosis, viral hepatitis and liver cancer cause two million deaths worldwide each year, whereby alcohol consumption is the leading cause of cirrhosis. In addition, one quarter of the global adult population is affected by a fatty liver related to systemic metabolic dysregulation, which has been referred to metabolic dysfunction-associated fatty liver disease (MAFLD) since 2020 (Devarbhavi et al., 2023, Gofton et al., 2023). Since many liver dysfunctions, if undetected, progress to end-stage liver disease such as cirrhosis and/or HCC, liver surgery or transplantation are the only treatment options (Hora and Wuestefeld, 2023). Due to pre-existing liver diseases and the increasing age of our society, the number of available transplantable livers has decreased in recent years.

The liver is the second most commonly transplanted organ after the kidney, but less than 10% of the global demand for donor organs is currently covered (Devarbhavi et al., 2023). Hence, there is an urgent need to find new factors that not only treat liver diseases but also promote liver regeneration. MYDGF is a promising factor in this context, as in this study we show that MYDGF stimulates hepatocyte proliferation *in vitro* and *in vivo* and that its overexpression leads to improved liver regeneration. A previous study has shown that MYDGF treatment significantly reduces liver fibrosis and inflammatory response in mice with NAFLD (Ding et al., 2023). MYDGF treatment has also been described to have beneficial effects on cardiac repair after MI, atherosclerosis, and metabolic diseases such as T2D, glomerular diseases, and osteoporosis (Xu et al., 2023b). Therefore, MYDGF could be used as a therapeutic drug for patients with liver diseases such as hepatic fibrosis or MAFLD, and to improve liver regeneration after liver surgery or liver transplantation. Donor livers that are not fully suitable for donation due to prior diseases, could be treated *ex vivo* with MYDGF until the function of the liver is sufficient for transplantation. It is already possible to improve the function of human livers, which were declined for transplantation, in a liver perfusion machine. The liver perfusion machine allows *ex vivo* cultivation of the donor liver for up to seven days by mimicking liver function and blood and bile flow (Eshmuminov et al., 2020). The addition of MYDGF to the artificial blood stream of the externally cultured donor liver may result in improved organ survival and growth, and could improve the quality of livers that were originally insufficient for transplantation. In addition, it is already possible to split a donor liver and transplant it into two recipients using split liver transplantation (SLT) (Pichlmayr et al., 1988, Bismuth et al., 1989). This is particularly advantageous considering that only a small number of donor livers are currently available. However, one of the criteria for SLT is that the age of the donor is <50 years to avoid compromising liver regeneration with increasing age (Emre and Umman, 2011). Treatment with MYDGF might allow to use livers from older donors for SLT. In addition, the transplantable liver parts could be treated with MYDGF to stimulate liver growth to such an extent that the liver could even be divided between more than two recipients. Since MYDGF also contributes to a reduced rate of apoptosis in *in vitro* cultured hepatocytes, general treatment of donor livers could also improve the viability of the organ during transport to the recipient. In addition, therapeutic treatment with MYDGF within the first few days after liver surgery could stimulate liver growth and would therefore be particularly beneficial in elderly patients. Since MYDGF levels and the regenerative capacity of the liver decrease with age (Polten et al., 2019, Schmucker and Sanchez, 2011), additional administration of MYDGF could compensate this effect.

Overall, this study and previous studies suggest MYDGF as a promising therapeutic drug for liver diseases and liver regeneration.

6.4 Conclusion and Outlook

In this study, we characterized the role of MYDGF on primary human hepatocytes and liver regeneration after two-thirds PHx. Our results present MYDGF as a factor that initiates proliferation and facilitates survival of primary human hepatocytes. Thereby, the MYDGF-induced hepatocyte proliferation is mediated by the phosphorylation of MAPK on T202/Y204 (ERK1/2) and STAT3 on S727. In addition to its beneficial effects on human hepatocyte culture, MYDGF is rapidly expressed as an angiocrine signal after liver surgery in humans and mice. Using gain- and loss-of-function experiments, we were able to show that MYDGF is sufficient and required for liver regeneration in mice. MYDGF thus represents an angiocrine signal that holds great potential for future therapeutic applications, both *in vitro* and *in vivo*. To better elucidate the function of MYDGF as a therapeutic drug, further studies are needed.

In vitro, it would be interesting to investigate to what extent the activation of AKT affects the proliferation and survival of human hepatocytes treated with MYDGF. To this end, it should be investigated whether the inhibition of AKT phosphorylation leads to a reduced proliferation and survival rate in primary human hepatocytes. The proliferation rate could be examined by immunostaining (EdU or PH3 staining), while survival could be analyzed by immunostaining (caspase-3) or by Western blot (inhibition/activation of pro-apoptotic proteins and caspases). It would also be interesting to examine whether the activation of AKT is dependent or independent of MAPK/STAT3 signaling. Furthermore, it would be interesting to test whether Fc-tag-modified MYDGF has a stronger effect on the proliferation of 2D and 3D cultured hepatocytes due to its supposedly longer half-life. In addition, a pull-down assay could be used to identify interaction partners of MYDGF and possible receptor(s).

In vivo, it would be interesting to test whether the deletion of MYDGF reduces or completely inhibits liver regeneration. To this end, hepatocyte proliferation and liver-to-body weight ratio in MYDGF KO mice should be examined at further timepoints (e.g., 48 and 96 hours) after two-thirds PHx. In addition, survival kinetics could be used to investigate whether the survival of MYDGF KO mice after two-thirds PHx is reduced compared to control mice. In another cohort of MYDGF KO mice, the function of MYDGF as a therapeutic drug could be investigated. Thereby it could be test whether continuous treatment with recombinant MYDGF, administered via an osmotic pump within the first days after PHx, reverses the effect of MYDGF deletion on liver regeneration. If the Fc-tagged MYDGF shows an effect on primary human hepatocytes, the influence of a single administration of this protein on liver regeneration could also be tested.

To evaluate whether the release of MYDGF from LSECs alone is sufficient for liver regeneration, mice with an endothelial cell-specific knockout of MYDGF could be generated to study its influence on liver regeneration after two-thirds PHx.

Since MYDGF has already been described as an anti-inflammatory factor in atherosclerosis (Meng et al., 2021, Xu et al., 2023a), NAFLD (Ding et al., 2023), and wound healing response in zebrafish larvae (Houseright et al., 2021), it would be interesting to study whether MYDGF reduces the inflammatory response, while promoting liver regeneration, in CCl4-induced liver inflammation. This liver regeneration model mirrors the chronic liver inflammation caused by hepatitis viruses or MAFLD, which are common liver diseases nowadays (Devarbhavi et al., 2023). Therefore, it could be examined whether mice previously treated with CCl4 show a reduced inflammatory response and improved liver regeneration after additional MYDGF treatment compared to controls. This could further clarify the relevance of MYDGF as a therapeutic drug for liver diseases.

In summary, all these experiments would further emphasize the relevance of MYDGF *in vivo* and *in vitro* as well as clarify its use as a therapeutic drug.

7. Publications

Gross-Segerath, L.*, Follert, P.*, Behnke, K., Ettich, J., Buschmann, T., Kirschner, P., Hartwig, S., Lehr, S., Korf-Klingebiel, M., Eberhard, D., Lehwald-Tywuschik, N., Al-Hasani, H., Knoefel, W. T., Heinrich, S., Levkau, B., Wollert, K. C., Scheller, J. & Lammert, E. **Identification of myeloid-derived growth factor as a mechanically-induced, growth-promoting angiocrine signal for human hepatocytes**. Nature Communications, 2024.

(*equally contributed)

Henning, C., Branopolski, A., Follert, P., Lewandowska, O., Ayhan, A., Benkhoff, M., Flogel, U., Kelm, M., Heiss, C. & Lammert, E. 2021. **Endothelial beta1 Integrin-Mediated Adaptation to Myocardial Ischemia**. Thromb Haemost, 121, 741-754.

8. References

Abdel-Misih, S. R. & Bloomston, M. 2010. Liver anatomy. *Surg Clin North Am,* 90**,** 643-53.

Abu Rmilah, A., Zhou, W., Nelson, E., Lin, L., Amiot, B. & Nyberg, S. L. 2019. Understanding the marvels behind liver regeneration. *Wiley Interdiscip Rev Dev Biol,* 8**,** e340.

Ait Ahmed, Y., Fu, Y., Rodrigues, R. M., He, Y., Guan, Y., Guillot, A., Ren, R., Feng, D., Hidalgo, J., Ju, C., Lafdil, F. & Gao, B. 2021. Kupffer cell restoration after partial hepatectomy is mainly driven by local cell proliferation in IL-6-dependent autocrine and paracrine manners. *Cell Mol Immunol,* 18**,** 2165-2176.

Alamri, Z. Z. 2018. The role of liver in metabolism: an updated review with physiological emphasis. *International Journal of Basic & Clinical Pharmacology,* 7.

Alessi, D. R., Cuenda, A., Cohen, P., Dudley, D. T. & Saltiel, A. R. 1995. PD 098059 is a specific inhibitor of the activation of mitogen-activated protein kinase kinase in vitro and in vivo. *J Biol Chem,* 270**,** 27489-94.

Alexander, A., Lehwald-Tywuschik, N., Rehders, A., Dizdar, L., Fluegen, G., Safi, S. A. & Knoefel, W. T. 2023. Optimizing Growth of the Future Liver Remnant and Making In-Situ Liver Transsection Safe-A Standardized Approach to ISLT or ALPPS. *Current Oncology,* 30**,** 3277-3288.

Bailey, M. J., Lacey, D. C., De Kok, B. V., Veith, P. D., Reynolds, E. C. & Hamilton, J. A. 2011. Extracellular proteomes of M-CSF (CSF-1) and GM-CSF-dependent macrophages. *Immunol Cell Biol,* 89**,** 283-93.

Bankhead, P., Loughrey, M. B., Fernandez, J. A., Dombrowski, Y., Mcart, D. G., Dunne, P. D., Mcquaid, S., Gray, R. T., Murray, L. J., Coleman, H. G., James, J. A., Salto-Tellez, M. & Hamilton, P. W. 2017. QuPath: Open source software for digital pathology image analysis. *Sci Rep,* 7**,** 16878.

Bartlett, A., Vesco, K. K., Purnell, J. Q., Francisco, M., Goddard, E., Guan, X., Debarber, A., Leo, M. C., Baetscher, E., Rooney, W., Naugler, W., Guimaraes, A. R., Catalano, P., Xia, Z. & Schedin, P. 2021. Pregnancy and weaning regulate human maternal liver size and function. *Proc Natl Acad Sci U S A,* 118.

Beier, J. I. & Mcclain, C. J. 2010. Mechanisms and cell signaling in alcoholic liver disease. *Biol Chem,* 391**,** 1249-64.

Ben-Moshe, S., Shapira, Y., Moor, A. E., Manco, R., Veg, T., Bahar Halpern, K. & Itzkovitz, S. 2019. Spatial sorting enables comprehensive characterization of liver zonation. *Nat Metab,* 1**,** 899-911.

Bergstrand, C. G. & Czar, B. 1956. Demonstration of a new protein fraction in serum from the human fetus. *Scand J Clin Lab Invest,* 8**,** 174.

Bismuth, H., Morino, M., Castaing, D., Gillon, M. C., Descorps Declere, A., Saliba, F. & Samuel, D. 1989. Emergency orthotopic liver transplantation in two patients using one donor liver. *Br J Surg,* 76**,** 722-4.

Bissell, D. M. & Guzelian, P. S. 1980. Phenotypic stability of adult rat hepatocytes in primary monolayer culture. *Ann N Y Acad Sci,* 349**,** 85-98.

Bladt, F., Riethmacher, D., Isenmann, S., Aguzzi, A. & Birchmeier, C. 1995. Essential role for the c-met receptor in the migration of myogenic precursor cells into the limb bud. *Nature,* 376**,** 768-71.

Blindenbacher, A., Wang, X., Langer, I., Savino, R., Terracciano, L. & Heim, M. H. 2003. Interleukin 6 is important for survival after partial hepatectomy in mice. *Hepatology,* 38**,** 674-82.

Borowiak, M., Garratt, A. N., Wustefeld, T., Strehle, M., Trautwein, C. & Birchmeier, C. 2004. Met provides essential signals for liver regeneration. *Proc Natl Acad Sci U S A,* 101**,** 10608-13.

Bortnov, V., Annis, D. S., Fogerty, F. J., Barretto, K. T., Turton, K. B. & Mosher, D. F. 2018. Myeloid-derived growth factor is a resident endoplasmic reticulum protein. *J Biol Chem,* 293**,** 13166-13175.

Braun, L., Mead, J. E., Panzica, M., Mikumo, R., Bell, G. I. & Fausto, N. 1988. Transforming growth factor beta mRNA increases during liver regeneration: a possible paracrine mechanism of growth regulation. *Proc Natl Acad Sci U S A,* 85**,** 1539-43.

Broering, D. C., Schulte Am Esch, J., Fischer, L. & Rogiers, X. 2004. Split liver transplantation. *HPB (Oxford),* 6**,** 76-82.

Burke, Z. D., Reed, K. R., Phesse, T. J., Sansom, O. J., Clarke, A. R. & Tosh, D. 2009. Liver zonation occurs through a beta-catenin-dependent, c-Myc-independent mechanism. *Gastroenterology,* 136**,** 2316-2324 e1-3.

Cardone, M. H., Roy, N., Stennicke, H. R., Salvesen, G. S., Franke, T. F., Stanbridge, E., Frisch, S. & Reed, J. C. 1998. Regulation of cell death protease caspase-9 by phosphorylation. *Science,* 282**,** 1318-21.

Chen, X. G., Xu, C. S. & Liu, Y. M. 2013. Involvement of ERK1/2 signaling in proliferation of eight liver cell types during hepatic regeneration in rats. *Genet Mol Res,* 12**,** 665-77.

Cheng, N., Kim, K. H. & Lau, L. F. 2022. Senescent hepatic stellate cells promote liver regeneration through IL-6 and ligands of CXCR2. *JCI Insight,* 7.

Chung, J., Uchida, E., Grammer, T. C. & Blenis, J. 1997. STAT3 serine phosphorylation by ERK-dependent and -independent pathways negatively modulates its tyrosine phosphorylation. *Mol Cell Biol,* 17**,** 6508-16.

Corsini, A., Cercenelli, L., Zecchi, M., Marcelli, E. & Corazza, I. 2022. Basic Hemodynamic Parameters. *Advances in Cardiovascular Technology.*

Couinaud, C. 1954. [Liver lobes and segments: notes on the anatomical architecture and surgery of the liver]. *Presse Med (1893),* 62**,** 709-12.

Cressman, D. E., Greenbaum, L. E., Deangelis, R. A., Ciliberto, G., Furth, E. E., Poli, V. & Taub, R. 1996. Liver failure and defective hepatocyte regeneration in interleukin-6-deficient mice. *Science,* 274**,** 1379-83.

Datta, S. R., Dudek, H., Tao, X., Masters, S., Fu, H., Gotoh, Y. & Greenberg, M. E. 1997. Akt phosphorylation of BAD couples survival signals to the cell-intrinsic death machinery. *Cell,* 91**,** 231-41.

Decker, T. & Kovarik, P. 2000. Serine phosphorylation of STATs. *Oncogene,* 19**,** 2628-37.

Dehlke, K., Krause, L., Tyufekchieva, S., Murtha-Lemekhova, A., Mayer, P., Vlasov, A., Klingmuller, U., Mueller, N. S. & Hoffmann, K. 2022. Predicting liver regeneration following major resection. *Sci Rep,* 12**,** 13396.

Del Peso, L., González-García, M., Page, C., Herrera, R. & Nuñez, G. 1997. Interleukin-3-induced phosphorylation of BAD through the protein kinase Akt. *Science,* 278**,** 687-9.

Deleve, L. D. & Maretti-Mira, A. C. 2017. Liver Sinusoidal Endothelial Cell: An Update. *Semin Liver Dis,* 37**,** 377-387.

Demetriou, A. A., Reisner, A., Sanchez, J., Levenson, S. M., Moscioni, A. D. & Chowdhury, J. R. 1988. Transplantation of microcarrier-attached hepatocytes into 90% partially hepatectomized rats. *Hepatology,* 8**,** 1006-9.

Desbois-Mouthon, C., Wendum, D., Cadoret, A., Rey, C., Leneuve, P., Blaise, A., Housset, C., Tronche, F., Le Bouc, Y. & Holzenberger, M. 2006. Hepatocyte proliferation during liver regeneration is impaired in mice with liver-specific IGF-1R knockout. *Faseb j,* 20**,** 773-5.

Devarbhavi, H., Asrani, S. K., Arab, J. P., Nartey, Y. A., Pose, E. & Kamath, P. S. 2023. Global burden of liver disease: 2023 update. *J Hepatol,* 79**,** 516-537.

Dietrich, S., Abou-Rebyeh, F., Brohmann, H., Bladt, F., Sonnenberg-Riethmacher, E., Yamaai, T., Lumsden, A., Brand-Saberi, B. & Birchmeier, C. 1999. The role of SF/HGF and c-Met in the development of skeletal muscle. *Development,* 126**,** 1621-9.

Diez-Silva, M., Dao, M., Han, J., Lim, C. T. & Suresh, S. 2010. Shape and Biomechanical Characteristics of Human Red Blood Cells in Health and Disease. *MRS Bull,* 35**,** 382-388.

Ding, B. S., Cao, Z., Lis, R., Nolan, D. J., Guo, P., Simons, M., Penfold, M. E., Shido, K., Rabbany, S. Y. & Rafii, S. 2014. Divergent angiocrine signals from vascular niche balance liver regeneration and fibrosis. *Nature,* 505**,** 97-102.

Ding, B. S., Nolan, D. J., Butler, J. M., James, D., Babazadeh, A. O., Rosenwaks, Z., Mittal, V., Kobayashi, H., Shido, K., Lyden, D., Sato, T. N., Rabbany, S. Y. & Rafii, S. 2010. Inductive angiocrine signals from sinusoidal endothelium are required for liver regeneration. *Nature,* 468**,** 310-5.

Ding, Y., Xu, X., Meng, B., Wang, L., Zhu, B., Guo, B., Zhang, J., Xiang, L., Dong, J., Liu, M. & Xiang, G. 2023. Myeloid-derived growth factor alleviates non-alcoholic fatty liver disease alleviates in a manner involving IKKbeta/NF-kappaB signaling. *Cell Death Dis,* 14**,** 376.

Dixon, M., Agius, L., Yeaman, S. J. & Day, C. P. 1999. Inhibition of rat hepatocyte proliferation by transforming growth factor beta and glucagon is associated with inhibition of ERK2 and p70 S6 kinase. *Hepatology,* 29**,** 1418-24.

Duval, K., Grover, H., Han, L. H., Mou, Y., Pegoraro, A. F., Fredberg, J. & Chen, Z. 2017. Modeling Physiological Events in 2D vs. 3D Cell Culture. *Physiology (Bethesda),* 32**,** 266-277.

Ebenhoch, R., Akhdar, A., Reboll, M. R., Korf-Klingebiel, M., Gupta, P., Armstrong, J., Huang, Y., Frego, L., Rybina, I., Miglietta, J., Pekcec, A., Wollert, K. C. & Nar, H. 2019. Crystal structure and receptor-interacting residues of MYDGF - a protein mediating ischemic tissue repair. *Nat Commun,* 10**,** 5379.

Edmondson, R., Broglie, J. J., Adcock, A. F. & Yang, L. 2014. Three-dimensional cell culture systems and their applications in drug discovery and cell-based biosensors. *Assay Drug Dev Technol,* 12**,** 207-18.

Eipel, C., Abshagen, K. & Vollmar, B. 2010. Regulation of hepatic blood flow: the hepatic arterial buffer response revisited. *World J Gastroenterol,* 16**,** 6046-57.

Elmaci, I., Altinoz, M. A., Sari, R. & Bolukbasi, F. H. 2018. Phosphorylated Histone H3 (PHH3) as a Novel Cell Proliferation Marker and Prognosticator for Meningeal Tumors: A Short Review. *Appl Immunohistochem Mol Morphol,* 26**,** 627-631.

Emre, S. & Umman, V. 2011. Split liver transplantation: an overview. *Transplant Proc,* 43**,** 884-7.

Eshmuminov, D., Becker, D., Bautista Borrego, L., Hefti, M., Schuler, M. J., Hagedorn, C., Muller, X., Mueller, M., Onder, C., Graf, R., Weber, A., Dutkowski, P., Rudolf Von Rohr, P. & Clavien, P. A. 2020. An integrated perfusion machine preserves injured human livers for 1 week. *Nat Biotechnol,* 38**,** 189-198.

Fabbrini, E., Sullivan, S. & Klein, S. 2010. Obesity and nonalcoholic fatty liver disease: biochemical, metabolic, and clinical implications. *Hepatology,* 51**,** 679-89.

Factor, V. M., Seo, D., Ishikawa, T., Kaposi-Novak, P., Marquardt, J. U., Andersen, J. B., Conner, E. A. & Thorgeirsson, S. S. 2010. Loss of c-Met disrupts gene expression program required for G2/M progression during liver regeneration in mice. *PLoS One,* 5.

Fausto, N., Campbell, J. S. & Riehle, K. J. 2006. Liver regeneration. *Hepatology,* 43**,** S45-53.

Fausto, N., Mead, J. E., Braun, L., Thompson, N. L., Panzica, M., Goyette, M., Bell, G. I. & Shank, P. R. 1986. Proto-oncogene expression and growth factors during liver regeneration. *Symp Fundam Cancer Res,* 39**,** 69-86.

Fazel Modares, N., Polz, R., Haghighi, F., Lamertz, L., Behnke, K., Zhuang, Y., Kordes, C., Häussinger, D., Sorg, U. R., Pfeffer, K., Floss, D. M., Moll, J. M., Piekorz, R. P., Ahmadian, M. R., Lang, P. A. & Scheller, J. 2019. IL-6 Trans-signaling Controls Liver Regeneration After Partial Hepatectomy. *Hepatology,* 70**,** 2075-2091.

Fry, M., Silber, J., Loeb, L. A. & Martin, G. M. 1984. Delayed and reduced cell replication and diminishing levels of DNA polymerase-alpha in regenerating liver of aging mice. *J Cell Physiol,* 118**,** 225-32.

Galle, P. R., Foerster, F., Kudo, M., Chan, S. L., Llovet, J. M., Qin, S., Schelman, W. R., Chintharlapalli, S., Abada, P. B., Sherman, M. & Zhu, A. X. 2019. Biology and significance of alpha-fetoprotein in hepatocellular carcinoma. *Liver Int,* 39**,** 2214-2229.

Gao, L., Li, Z., Chang, W., Liu, Y. & Zhang, N. 2023. Myeloid-derived growth factor regulates high glucose-mediated apoptosis of gingival fibroblasts and induce AKT pathway activation and nuclear factor kappaB pathway inhibition. *J Dent Sci,* 18**,** 636-644.

Garnier, D., Li, R., Delbos, F., Fourrier, A., Collet, C., Guguen-Guillouzo, C., Chesne, C. & Nguyen, T. H. 2018. Expansion of human primary hepatocytes in vitro through their amplification as liver progenitors in a 3D organoid system. *Sci Rep,* 8**,** 8222.

Gerdes, J., Lemke, H., Baisch, H., Wacker, H. H., Schwab, U. & Stein, H. 1984. Cell cycle analysis of a cell proliferation-associated human nuclear antigen defined by the monoclonal antibody Ki-67. *The Journal of Immunology,* 133**,** 1710-1715.

Gilgenkrantz, H. & Collin De L'hortet, A. 2018. Understanding Liver Regeneration: From Mechanisms to Regenerative Medicine. *Am J Pathol,* 188**,** 1316-1327.

Gofton, C., Upendran, Y., Zheng, M. H. & George, J. 2023. MAFLD: How is it different from NAFLD? *Clin Mol Hepatol,* 29**,** S17-S31.

Gómez-Lechón, M. J., Castelli, J., Guillén, I., O'connor, E., Nakamura, T., Fabra, R. & Trullenque, R. 1995. Effects of hepatocyte growth factor on the growth and metabolism of human hepatocytes in primary culture. *Hepatology,* 21**,** 1248-54.

Gomez-Salinero, J. M., Izzo, F., Lin, Y., Houghton, S., Itkin, T., Geng, F., Bram, Y., Adelson, R. P., Lu, T. M., Inghirami, G., Xiang, J. Z., Lis, R., Redmond, D., Schreiner, R., Rabbany, S. Y., Landau, D. A., Schwartz, R. E. & Rafii, S. 2022. Specification of fetal liver endothelial progenitors to functional zonated adult sinusoids requires c-Maf induction. *Cell Stem Cell,* 29**,** 593-609 e7.

Große-Segerath, L. 2020. *Mechano-induced angiocrine signals from hepatic endothelial cells promote liver growth and regeneration.*

Große-Segerath, L., Follert, P., Behnke, K., Ettich, J., Buschmann, T., Kirschner, P., Hartwig, S., Lehr, S., Korf-Klingebiel, M., Eberhard, D., Lehwald-Tywuschik, N., Al-Hasani, H., Knoefel, W. T., Heinrich, S., Levkau, B., Wollert, K. C., Scheller, J. & Lammert, E. 2024. Identification of myeloid-derived growth factor as a mechanically-induced, growth-promoting angiocrine signal for human hepatocytes. *Nature Communications,* 15.

Grosse-Segerath, L. & Lammert, E. 2021. Role of vasodilation in liver regeneration and health. *Biol Chem,* 402**,** 1009-1019.

Guegan, J. P., Fremin, C. & Baffet, G. 2012. The MAPK MEK1/2-ERK1/2 Pathway and Its Implication in Hepatocyte Cell Cycle Control. *Int J Hepatol,* 2012**,** 328372.

Guguen-Guillouzo, C. & Guillouzo, A. 2010. General Review on In Vitro Hepatocyte Models and Their Applications. *In:* MAUREL, P. (ed.) *Hepatocytes: Methods and Protocols.* Totowa, NJ: Humana Press.

Guo, R., Jiang, M., Wang, G., Li, B., Jia, X., Ai, Y., Chen, S., Tang, P., Liu, A., Yuan, Q. & Xie, X. 2022. IL6 supports long-term expansion of hepatocytes in vitro. *Nat Commun,* 13**,** 7345.

Haga, S., Ogawa, W., Inoue, H., Terui, K., Ogino, T., Igarashi, R., Takeda, K., Akira, S., Enosawa, S., Furukawa, H., Todo, S. & Ozaki, M. 2005. Compensatory recovery of liver mass by Akt-mediated hepatocellular hypertrophy in liver-specific STAT3-deficient mice. *J Hepatol,* 43**,** 799-807.

Halpern, K. B., Shenhav, R., Matcovitch-Natan, O., Toth, B., Lemze, D., Golan, M., Massasa, E. E., Baydatch, S., Landen, S., Moor, A. E., Brandis, A., Giladi, A., Avihail, A. S., David, E., Amit, I. & Itzkovitz, S. 2017. Single-cell spatial reconstruction reveals global division of labour in the mammalian liver. *Nature,* 542**,** 352-356.

Hatano, E. & Brenner, D. A. 2001. Akt protects mouse hepatocytes from TNF-alpha- and Fas-mediated apoptosis through NK-kappa B activation. *Am J Physiol Gastrointest Liver Physiol,* 281**,** G1357-68.

Häussinger, D. 2014. Liver - Overview *In:* LAMMERT, E. & ZEEB, M. (eds.) *Metabolism of human diseases : organ physiology and pathophysiology.* Wien ; New York: Springer.

He, M., Li, Y., Wang, L., Guo, B., Mei, W., Zhu, B., Zhang, J., Ding, Y., Meng, B., Zhang, L., Xiang, L., Dong, J., Liu, M., Xiang, L. & Xiang, G. 2020. MYDGF attenuates

podocyte injury and proteinuria by activating Akt/BAD signal pathway in mice with diabetic kidney disease. *Diabetologia,* 63**,** 1916-1931.

Heinrich, S. & Lang, H. 2017. Hepatic resection for primary and secondary liver malignancies. *Innovative Surgical Sciences,* 2**,** 1-8.

Henklova, P., Vrzal, R., Papouskova, B., Bednar, P., Jancova, P., Anzenbacherova, E., Ulrichova, J., Maurel, P., Pavek, P. & Dvorak, Z. 2008. SB203580, a pharmacological inhibitor of p38 MAP kinase transduction pathway activates ERK and JNK MAP kinases in primary cultures of human hepatocytes. *European Journal of Pharmacology,* 593**,** 16-23.

Hildebrandt, F., Andersson, A., Saarenpaa, S., Larsson, L., Van Hul, N., Kanatani, S., Masek, J., Ellis, E., Barragan, A., Mollbrink, A., Andersson, E. R., Lundeberg, J. & Ankarklev, J. 2021. Spatial Transcriptomics to define transcriptional patterns of zonation and structural components in the mouse liver. *Nat Commun,* 12**,** 7046.

Hong, F., Nguyen, V. A., Shen, X., Kunos, G. & Gao, B. 2000. Rapid activation of protein kinase B/Akt has a key role in antiapoptotic signaling during liver regeneration. *Biochem Biophys Res Commun,* 279**,** 974-9.

Hora, S. & Wuestefeld, T. 2023. Liver Injury and Regeneration: Current Understanding, New Approaches, and Future Perspectives. *Cells,* 12.

Houseright, R. A., Miskolci, V., Mulvaney, O., Bortnov, V., Mosher, D. F., Rindy, J., Bennin, D. A. & Huttenlocher, A. 2021. Myeloid-derived growth factor regulates neutrophil motility in interstitial tissue damage. *J Cell Biol,* 220.

Hu, H., Gehart, H., Artegiani, B., C, L. O.-I., Dekkers, F., Basak, O., Van Es, J., Chuva De Sousa Lopes, S. M., Begthel, H., Korving, J., Van Den Born, M., Zou, C., Quirk, C., Chiriboga, L., Rice, C. M., Ma, S., Rios, A., Peters, P. J., De Jong, Y. P. & Clevers, H. 2018. Long-Term Expansion of Functional Mouse and Human Hepatocytes as 3D Organoids. *Cell,* 175**,** 1591-1606 e19.

Hu, J., Srivastava, K., Wieland, M., Runge, A., Mogler, C., Besemfelder, E., Terhardt, D., Vogel, M. J., Cao, L., Korn, C., Bartels, S., Thomas, M. & Augustin, H. G. 2014. Endothelial cell-derived angiopoietin-2 controls liver regeneration as a spatiotemporal rheostat. *Science,* 343**,** 416-9.

Hu, S., Liu, S., Bian, Y., Poddar, M., Singh, S., Cao, C., Mcgaughey, J., Bell, A., Blazer, L. L., Adams, J. J., Sidhu, S. S., Angers, S. & Monga, S. P. 2022a. Single-cell spatial transcriptomics reveals a dynamic control of metabolic zonation and liver regeneration by endothelial cell Wnt2 and Wnt9b. *Cell Rep Med,* 3**,** 100754.

Hu, X., Chen, R., Wei, Q. & Xu, X. 2022b. The Landscape Of Alpha Fetoprotein In Hepatocellular Carcinoma: Where Are We? *Int J Biol Sci,* 18**,** 536-551.

Huang, W., Han, N., Du, L., Wang, M., Chen, L. & Tang, H. 2021. A narrative review of liver regeneration-from models to molecular basis. *Ann Transl Med,* 9**,** 1705.

Huh, C. G., Factor, V. M., Sanchez, A., Uchida, K., Conner, E. A. & Thorgeirsson, S. S. 2004. Hepatocyte growth factor/c-met signaling pathway is required for efficient liver regeneration and repair. *Proc Natl Acad Sci U S A,* 101**,** 4477-82.

Iakova, P., Awad, S. S. & Timchenko, N. A. 2003. Aging reduces proliferative capacities of liver by switching pathways of C/EBPalpha growth arrest. *Cell,* 113**,** 495-506.

Inverso, D., Shi, J., Lee, K. H., Jakab, M., Ben-Moshe, S., Kulkarni, S. R., Schneider, M., Wang, G., Komeili, M., Velez, P. A., Riedel, M., Spegg, C., Ruppert, T., Schaeffer-Reiss, C., Helm, D., Singh, I., Boutros, M., Chintharlapalli, S., Heikenwalder, M., Itzkovitz, S. & Augustin, H. G. 2021. A spatial vascular transcriptomic, proteomic, and phosphoproteomic atlas unveils an angiocrine Tie-Wnt signaling axis in the liver. *Dev Cell,* 56**,** 1677-1693 e10.

Ishibashi, H., Nakamura, M., Komori, A., Migita, K. & Shimoda, S. 2009. Liver architecture, cell function, and disease. *Semin Immunopathol,* 31**,** 399-409.

Ishii, T., Sato, M., Sudo, K., Suzuki, M., Nakai, H., Hishida, T., Niwa, T., Umezu, K. & Yuasa, S. 1995. Hepatocyte growth factor stimulates liver regeneration and elevates blood protein level in normal and partially hepatectomized rats. *J Biochem,* 117**,** 1105-12.

Jackson, L. N., Larson, S. D., Silva, S. R., Rychahou, P. G., Chen, L. A., Qiu, S., Rajaraman, S. & Evers, B. M. 2008. PI3K/Akt activation is critical for early hepatic regeneration after partial hepatectomy. *Am J Physiol Gastrointest Liver Physiol,* 294**,** G1401-10.

Jhappan, C., Stahle, C., Harkins, R. N., Fausto, N., Smith, G. H. & Merlino, G. T. 1990. TGF alpha overexpression in transgenic mice induces liver neoplasia and abnormal development of the mammary gland and pancreas. *Cell,* 61**,** 1137-46.

Jufri, N. F., Mohamedali, A., Avolio, A. & Baker, M. S. 2015. Mechanical stretch: physiological and pathological implications for human vascular endothelial cells. *Vasc Cell,* 7**,** 8.

Justinger, C., Schluter, C., Oliviera-Frick, V., Kopp, B., Rubie, C. & Schilling, M. K. 2008. Increased growth factor expression after hepatic and pancreatic resection. *Oncol Rep,* 20**,** 1527-31.

Kapalczynska, M., Kolenda, T., Przybyla, W., Zajaczkowska, M., Teresiak, A., Filas, V., Ibbs, M., Blizniak, R., Luczewski, L. & Lamperska, K. 2018. 2D and 3D cell cultures - a comparison of different types of cancer cell cultures. *Arch Med Sci,* 14**,** 910-919.

Kaur, I., Vasudevan, A., Rawal, P., Tripathi, D. M., Ramakrishna, S., Kaur, S. & Sarin, S. K. 2023. Primary Hepatocyte Isolation and Cultures: Technical Aspects, Challenges and Advancements. *Bioengineering (Basel),* 10.

Kim, T. H., Mars, W. M., Stolz, D. B. & Michalopoulos, G. K. 2000. Expression and activation of pro-MMP-2 and pro-MMP-9 during rat liver regeneration. *Hepatology,* 31**,** 75-82.

Kiourtis, C., Wilczynska, A., Nixon, C., Clark, W., May, S. & Bird, T. G. 2021. Specificity and off-target effects of AAV8-TBG viral vectors for the manipulation of hepatocellular gene expression in mice. *Biol Open,* 10.

Knoefel, W. T., Gabor, I., Rehders, A., Alexander, A., Krausch, M., Schulte Am Esch, J., Furst, G. & Topp, S. A. 2013. In situ liver transection with portal vein ligation for rapid growth of the future liver remnant in two-stage liver resection. *Br J Surg,* 100**,** 388-94.

Koch, P. S., Lee, K. H., Goerdt, S. & Augustin, H. G. 2021. Angiodiversity and organotypic functions of sinusoidal endothelial cells. *Angiogenesis,* 24**,** 289-310.

Kojima, T., Yamamoto, T., Murata, M., Chiba, H., Kokai, Y. & Sawada, N. 2003. Regulation of the blood-biliary barrier: interaction between gap and tight junctions in hepatocytes. *Med Electron Microsc,* 36**,** 157-64.

Kono, S., Nagaike, M., Matsumoto, K. & Nakamura, T. 1992. Marked induction of hepatocyte growth factor mRNA in intact kidney and spleen in response to injury of distant organs. *Biochem Biophys Res Commun,* 186**,** 991-8.

Korf-Klingebiel, M., Reboll, M. R., Klede, S., Brod, T., Pich, A., Polten, F., Napp, L. C., Bauersachs, J., Ganser, A., Brinkmann, E., Reimann, I., Kempf, T., Niessen, H. W., Mizrahi, J., Schonfeld, H. J., Iglesias, A., Bobadilla, M., Wang, Y. & Wollert, K. C. 2015. Myeloid-derived growth factor (C19orf10) mediates cardiac repair following myocardial infarction. *Nat Med,* 21**,** 140-9.

Korf-Klingebiel, M., Reboll, M. R., Polten, F., Weber, N., Jackle, F., Wu, X., Kallikourdis, M., Kunderfranco, P., Condorelli, G., Giannitsis, E., Kustikova, O. S., Schambach, A., Pich, A., Widder, J. D., Bauersachs, J., Van Den Heuvel, J., Kraft, T., Wang, Y. & Wollert, K. C. 2021. Myeloid-Derived Growth Factor Protects Against Pressure Overload-Induced Heart Failure by Preserving Sarco/Endoplasmic Reticulum Ca(2+)-ATPase Expression in Cardiomyocytes. *Circulation*.

Kostallari, E. & Shah, V. H. 2016. Angiocrine signaling in the hepatic sinusoids in health and disease. *Am J Physiol Gastrointest Liver Physiol,* 311**,** G246-51.

Kruepunga, N., Hakvoort, T. B. M., Hikspoors, J., Kohler, S. E. & Lamers, W. H. 2019. Anatomy of rodent and human livers: What are the differences? *Biochim Biophys Acta Mol Basis Dis,* 1865**,** 869-878.

Lammert, E., Cleaver, O. & Melton, D. 2001. Induction of Pancreatic Differentiation by Signals from Blood Vessels. *Science,* 294**,** 564-567.

Lammert, E., Cleaver, O. & Melton, D. 2003. Role of endothelial cells in early pancreas and liver development. *Mech Dev,* 120**,** 59-64.

Lang, S. A., Loss, M. & Schlitt, H. J. 2014. ["In-situ split" (ISS) liver resection: new aspects of technique and indication]. *Zentralbl Chir,* 139**,** 212-9.

Lautt, W. W. & Greenway, C. V. 1987. Conceptual review of the hepatic vascular bed. *Hepatology,* 7**,** 952-63.

Lee, G. H., Merlino, G. & Fausto, N. 1992. Development of liver tumors in transforming growth factor alpha transgenic mice. *Cancer Res,* 52**,** 5162-70.

Leibing, T., Geraud, C., Augustin, I., Boutros, M., Augustin, H. G., Okun, J. G., Langhans, C. D., Zierow, J., Wohlfeil, S. A., Olsavszky, V., Schledzewski, K., Goerdt, S. & Koch, P. S. 2018. Angiocrine Wnt signaling controls liver growth and metabolic maturation in mice. *Hepatology,* 68**,** 707-722.

Leu, J. I., Crissey, M. A., Craig, L. E. & Taub, R. 2003. Impaired hepatocyte DNA synthetic response posthepatectomy in insulin-like growth factor binding protein 1-deficient mice with defects in C/EBP beta and mitogen-activated protein kinase/extracellular signal-regulated kinase regulation. *Mol Cell Biol,* 23**,** 1251-9.

Li, S., Mao, L., Zhao, F., Yan, J., Song, G., Luo, Q. & Li, Z. 2021. C19orf10 promotes malignant behaviors of human bladder carcinoma cells via regulating the PI3K/AKT and Wnt/beta-catenin pathways. *J Cancer,* 12**,** 4341-4354.

Li, W., Liang, X., Kellendonk, C., Poli, V. & Taub, R. 2002. STAT3 contributes to the mitogenic response of hepatocytes during liver regeneration. *J Biol Chem,* 277**,** 28411-7.

Liu, W., Jing, Z. T., Xue, C. R., Wu, S. X., Chen, W. N., Lin, X. J. & Lin, X. 2019. PI3K/AKT inhibitors aggravate death receptor-mediated hepatocyte apoptosis and liver injury. *Toxicol Appl Pharmacol,* 381**,** 114729.

Lorenz, L., Axnick, J., Buschmann, T., Henning, C., Urner, S., Fang, S., Nurmi, H., Eichhorst, N., Holtmeier, R., Bodis, K., Hwang, J. H., Mussig, K., Eberhard, D., Stypmann, J., Kuss, O., Roden, M., Alitalo, K., Haussinger, D. & Lammert, E. 2018. Mechanosensing by beta1 integrin induces angiocrine signals for liver growth and survival. *Nature,* 562**,** 128-132.

Mahadevan, V. 2020. Anatomy of the liver. *Surgery (Oxford),* 38**,** 427-431.

Mars, W. M., Kim, T. H., Stolz, D. B., Liu, M. L. & Michalopoulos, G. K. 1996. Presence of urokinase in serum-free primary rat hepatocyte cultures and its role in activating hepatocyte growth factor. *Cancer Res,* 56**,** 2837-43.

Martini, T., Naef, F. & Tchorz, J. S. 2023. Spatiotemporal Metabolic Liver Zonation and Consequences on Pathophysiology. *Annu Rev Pathol,* 18**,** 439-466.

Mcdonald, B., Mcavoy, E. F., Lam, F., Gill, V., De La Motte, C., Savani, R. C. & Kubes, P. 2008. Interaction of CD44 and hyaluronan is the dominant mechanism for neutrophil sequestration in inflamed liver sinusoids. *J Exp Med,* 205**,** 915-27.

Mcmurray, J. S. 2006. A new small-molecule Stat3 inhibitor. *Chem Biol,* 13**,** 1123-4.

Meng, B., Li, Y., Ding, Y., Xu, X., Wang, L., Guo, B., Zhu, B., Zhang, J., Xiang, L., Dong, J., Liu, M., Xiang, L. & Xiang, G. 2021. Myeloid-derived growth factor inhibits inflammation and alleviates endothelial injury and atherosclerosis in mice. *Sci Adv,* 7.

Michalopoulos, G. K. 2007. Liver regeneration. *J Cell Physiol,* 213**,** 286-300.

Michalopoulos, G. K. & Bhushan, B. 2021. Liver regeneration: biological and pathological mechanisms and implications. *Nat Rev Gastroenterol Hepatol,* 18**,** 40-55.

Michalopoulos, G. K. & Defrances, M. C. 1997. Liver regeneration. *Science,* 276**,** 60-6.

Mitchell, C. & Willenbring, H. 2008. A reproducible and well-tolerated method for 2/3 partial hepatectomy in mice. *Nat Protoc,* 3**,** 1167-70.

Miyaoka, Y. & Miyajima, A. 2013. To divide or not to divide: revisiting liver regeneration. *Cell Div,* 8**,** 8.

Moles, A., Murphy, L., Wilson, C. L., Chakraborty, J. B., Fox, C., Park, E. J., Mann, J., Oakley, F., Howarth, R., Brain, J., Masson, S., Karin, M., Seki, E. & Mann, D. A. 2014. A TLR2/S100A9/CXCL-2 signaling network is necessary for neutrophil recruitment in acute and chronic liver injury in the mouse. *J Hepatol,* 60**,** 782-91.

Møller, S. & Bernardi, M. 2013. Interactions of the heart and the liver. *Eur Heart J,* 34**,** 2804-11.

Motoi, S., Toyoda, H., Obara, T., Ohta, E., Arita, Y., Negishi, K., Moriya, K., Kuboi, Y., Soejima, M., Imai, T., Ido, A., Tsubouchi, H. & Kawano, T. 2019. Anti-Apoptotic Effects of Recombinant Human Hepatocyte Growth Factor on Hepatocytes Were Associated with Intrahepatic Hemorrhage Suppression Indicated by the Preservation of Prothrombin Time. *Int J Mol Sci,* 20.

Murata, S., Ohkohchi, N., Matsuo, R., Ikeda, O., Myronovych, A. & Hoshi, R. 2007. Platelets promote liver regeneration in early period after hepatectomy in mice. *World J Surg,* 31**,** 808-16.

Murtha-Lemekhova, A., Fuchs, J., Ghamarnejad, O., Nikdad, M., Probst, P. & Hoffmann, K. 2021. Influence of cytokines, circulating markers and growth factors on liver regeneration and post-hepatectomy liver failure: a systematic review and meta-analysis. *Sci Rep,* 11**,** 13739.

Nakai, H., Fuess, S., Storm, T. A., Muramatsu, S., Nara, Y. & Kay, M. A. 2005. Unrestricted hepatocyte transduction with adeno-associated virus serotype 8 vectors in mice. *J Virol,* 79**,** 214-24.

Nakamura, T. & Mizuno, S. 2010. The discovery of hepatocyte growth factor (HGF) and its significance for cell biology, life sciences and clinical medicine. *Proc Jpn Acad Ser B Phys Biol Sci,* 86**,** 588-610.

Nejak-Bowen, K., Orr, A., Bowen, W. C., Jr. & Michalopoulos, G. K. 2013. Conditional genetic elimination of hepatocyte growth factor in mice compromises liver regeneration after partial hepatectomy. *PLoS One,* 8**,** e59836.

Nishikawa, Y., Wang, M. & Carr, B. I. 1998. Changes in TGF-beta receptors of rat hepatocytes during primary culture and liver regeneration: increased expression of TGF-beta receptors associated with increased sensitivity to TGF-beta-mediated growth inhibition. *J Cell Physiol,* 176**,** 612-23.

Parmar, K. M., Larman, H. B., Dai, G., Zhang, Y., Wang, E. T., Moorthy, S. N., Kratz, J. R., Lin, Z., Jain, M. K., Gimbrone, M. A., Jr. & Garcia-Cardena, G. 2006. Integration of flow-dependent endothelial phenotypes by Kruppel-like factor 2. *J Clin Invest,* 116**,** 49-58.

Patijn, G. A., Lieber, A., Schowalter, D. B., Schwall, R. & Kay, M. A. 1998. Hepatocyte growth factor induces hepatocyte proliferation in vivo and allows for efficient retroviral-mediated gene transfer in mice. *Hepatology,* 28**,** 707-16.

Pauta, M., Rotllan, N., Fernandez-Hernando, A., Langhi, C., Ribera, J., Lu, M., Boix, L., Bruix, J., Jimenez, W., Suarez, Y., Ford, D. A., Baldan, A., Birnbaum, M. J., Morales-Ruiz, M. & Fernandez-Hernando, C. 2016. Akt-mediated foxo1 inhibition is required for liver regeneration. *Hepatology,* 63**,** 1660-74.

Pediaditakis, P., Lopez-Talavera, J. C., Petersen, B., Monga, S. P. & Michalopoulos, G. K. 2001. The processing and utilization of hepatocyte growth factor/scatter factor following partial hepatectomy in the rat. *Hepatology,* 34**,** 688-93.

Pichlmayr, R., Ringe, B., Gubernatis, G., Hauss, J. & Bunzendahl, H. 1988. [Transplantation of a donor liver to 2 recipients (splitting transplantation)--a new method in the further development of segmental liver transplantation]. *Langenbecks Arch Chir,* 373**,** 127-30.

Planas-Paz, L., Orsini, V., Boulter, L., Calabrese, D., Pikiolek, M., Nigsch, F., Xie, Y., Roma, G., Donovan, A., Marti, P., Beckmann, N., Dill, M. T., Carbone, W., Bergling, S., Isken, A., Mueller, M., Kinzel, B., Yang, Y., Mao, X., Nicholson, T. B., Zamponi, R., Capodieci, P., Valdez, R., Rivera, D., Loew, A., Ukomadu, C., Terracciano, L. M., Bouwmeester, T., Cong, F., Heim, M. H., Forbes, S. J., Ruffner, H. & Tchorz, J. S. 2016. The RSPO-LGR4/5-ZNRF3/RNF43 module controls liver zonation and size. *Nat Cell Biol,* 18**,** 467-79.

Poisson, J., Lemoinne, S., Boulanger, C., Durand, F., Moreau, R., Valla, D. & Rautou, P. E. 2017. Liver sinusoidal endothelial cells: Physiology and role in liver diseases. *J Hepatol,* 66**,** 212-227.

Polten, F., Reboll, M. R., Widera, C., Kempf, T., Bethmann, K., Gupta, P., Miglietta, J., Pekcec, A., Tillmanns, J., Bauersachs, J., Giannitsis, E., Pich, A. & Wollert, K. C. 2019. Plasma Concentrations of Myeloid-Derived Growth Factor in Healthy

Individuals and Patients with Acute Myocardial Infarction as Assessed by Multiple Reaction Monitoring-Mass Spectrometry. *Anal Chem,* 91**,** 1302-1308.

Porter, A. G. & Janicke, R. U. 1999. Emerging roles of caspase-3 in apoptosis. *Cell Death Differ,* 6**,** 99-104.

Preziosi, M., Okabe, H., Poddar, M., Singh, S. & Monga, S. P. 2018. Endothelial Wnts regulate β-catenin signaling in murine liver zonation and regeneration: A sequel to the Wnt–Wnt situation. *Hepatology Communications,* 2**,** 845-860.

Rafii, S., Butler, J. M. & Ding, B. S. 2016. Angiocrine functions of organ-specific endothelial cells. *Nature,* 529**,** 316-25.

Richman, R. A., Claus, T. H., Pilkis, S. J. & Friedman, D. L. 1976. Hormonal stimulation of DNA synthesis in primary cultures of adult rat hepatocytes. *Proc Natl Acad Sci U S A,* 73**,** 3589-93.

Roberts, A. B., Mccune, B. K. & Sporn, M. B. 1992. TGF-beta: regulation of extracellular matrix. *Kidney Int,* 41**,** 557-9.

Rocha, F. G. 2012. Liver blood flow. *Blumgart's Surgery of the Liver, Pancreas and Biliary Tract.*

Rogers, A. B. & Dintzis, R. Z. 2018. Hepatobiliary System. *Comparative Anatomy and Histology.*

Ross, M. A., Sander, C. M., Kleeb, T. B., Watkins, S. C. & Stolz, D. B. 2001. Spatiotemporal expression of angiogenesis growth factor receptors during the revascularization of regenerating rat liver. *Hepatology,* 34**,** 1135-48.

Russell, W. E., Coffey, R. J., Jr., Ouellette, A. J. & Moses, H. L. 1988. Type beta transforming growth factor reversibly inhibits the early proliferative response to partial hepatectomy in the rat. *Proc Natl Acad Sci U S A,* 85**,** 5126-30.

Sakamoto, T., Liu, Z., Murase, N., Ezure, T., Yokomuro, S., Poli, V. & Demetris, A. J. 1999. Mitosis and apoptosis in the liver of interleukin-6-deficient mice after partial hepatectomy. *Hepatology,* 29**,** 403-11.

Sakata, H., Takayama, H., Sharp, R., Rubin, J. S., Merlino, G. & Larochelle, W. J. 1996. Hepatocyte growth factor/scatter factor overexpression induces growth, abnormal development, and tumor formation in transgenic mouse livers. *Cell Growth Differ,* 7**,** 1513-23.

Sato, K., Hall, C., Glaser, S., Francis, H., Meng, F. & Alpini, G. 2016. Pathogenesis of Kupffer Cells in Cholestatic Liver Injury. *Am J Pathol,* 186**,** 2238-47.

Schindelin, J., Arganda-Carreras, I., Frise, E., Kaynig, V., Longair, M., Pietzsch, T., Preibisch, S., Rueden, C., Saalfeld, S., Schmid, B., Tinevez, J. Y., White, D. J., Hartenstein, V., Eliceiri, K., Tomancak, P. & Cardona, A. 2012. Fiji: an open-source platform for biological-image analysis. *Nat Methods,* 9**,** 676-82.

Schmidt, C., Bladt, F., Goedecke, S., Brinkmann, V., Zschiesche, W., Sharpe, M., Gherardi, E. & Birchmeier, C. 1995. Scatter factor/hepatocyte growth factor is essential for liver development. *Nature,* 373**,** 699-702.

Schmidt-Arras, D. & Rose-John, S. 2016. IL-6 pathway in the liver: From physiopathology to therapy. *Journal of Hepatology,* 64**,** 1403-1415.

Schmittgen, T. D. & Livak, K. J. 2008. Analyzing real-time PCR data by the comparative C(T) method. *Nat Protoc,* 3**,** 1101-8.

Schmucker, D. L. & Sanchez, H. 2011. Liver regeneration and aging: a current perspective. *Curr Gerontol Geriatr Res,* 2011**,** 526379.

Schoen, J. M., Wang, H. H., Minuk, G. Y. & Lautt, W. W. 2001. Shear stress-induced nitric oxide release triggers the liver regeneration cascade. *Nitric Oxide,* 5**,** 453-64.

Schon, H. T. & Weiskirchen, R. 2014. Immunomodulatory effects of transforming growth factor-beta in the liver. *Hepatobiliary Surg Nutr,* 3**,** 386-406.

Seirup, M., Sengupta, S., Swanson, S., Mcintosh, B. E., Collins, M., Chu, L. F., Cheng, Z., Gorkin, D. U., Duffin, B., Bolin, J. M., Argus, C., Stewart, R. & Thomson, J. A. 2022. Rapid changes in chromatin structure during dedifferentiation of primary hepatocytes in vitro. *Genomics,* 114**,** 110330.

Shetty, S., Lalor, P. F. & Adams, D. H. 2018. Liver sinusoidal endothelial cells - gatekeepers of hepatic immunity. *Nat Rev Gastroenterol Hepatol,* 15**,** 555-567.

Shiota, G., Rhoads, D. B., Wang, T. C., Nakamura, T. & Schmidt, E. V. 1992. Hepatocyte growth factor inhibits growth of hepatocellular carcinoma cells. *Proc Natl Acad Sci U S A,* 89**,** 373-7.

Shiota, G., Wang, T. C., Nakamura, T. & Schmidt, E. V. 1994. Hepatocyte growth factor in transgenic mice: Effects on hepatocyte growth, liver regeneration and gene expression. *Hepatology,* 19**,** 962-972.

Si-Tayeb, K., Lemaigre, F. P. & Duncan, S. A. 2010. Organogenesis and development of the liver. *Dev Cell,* 18**,** 175-89.

Sibulesky, L. 2013. Normal liver anatomy. *Clin Liver Dis (Hoboken),* 2**,** S1-S3.

Sim, R., Yang, C. & Yang, Y. Y. 2024. Chemical Proteomics and Morphological Profiling Revealing MYDGF as a Target for Synthetic Anticancer Macromolecules. *Biomacromolecules.*

Sokabe, T., Yamamoto, K., Ohura, N., Nakatsuka, H., Qin, K., Obi, S., Kamiya, A. & Ando, J. 2004. Differential regulation of urokinase-type plasminogen activator expression by fluid shear stress in human coronary artery endothelial cells. *Am J Physiol Heart Circ Physiol,* 287**,** H2027-34.

Soldatow, V. Y., Lecluyse, E. L., Griffith, L. G. & Rusyn, I. 2013. In vitro models for liver toxicity testing. *Toxicol Res (Camb),* 2**,** 23-39.

Sorensen, K. K., Simon-Santamaria, J., Mccuskey, R. S. & Smedsrod, B. 2015. Liver Sinusoidal Endothelial Cells. *Compr Physiol,* 5**,** 1751-74.

Sparrelid, E., Johansson, H., Gilg, S., Nowak, G., Ellis, E. & Isaksson, B. 2018. Serial Assessment of Growth Factors Associated with Liver Regeneration in Patients Operated with Associating Liver Partition and Portal Vein Ligation for Staged Hepatectomy. *Eur Surg Res,* 59**,** 72-82.

Stanger, B. Z. 2015. Cellular homeostasis and repair in the mammalian liver. *Annu Rev Physiol,* 77**,** 179-200.

Stolz, D. B., Mars, W. M., Petersen, B. E., Kim, T. H. & Michalopoulos, G. K. 1999. Growth factor signal transduction immediately after two-thirds partial hepatectomy in the rat. *Cancer Res,* 59**,** 3954-60.

Strain, A. J., Ismail, T., Tsubouchi, H., Arakaki, N., Hishida, T., Kitamura, N., Daikuhara, Y. & Mcmaster, P. 1991. Native and recombinant human hepatocyte growth factors are highly potent promoters of DNA synthesis in both human and rat hepatocytes. *J Clin Invest,* 87**,** 1853-7.

Straub, C., Pazdrak, K., Young, T. W., Stafford, S. J., Wu, Z., Wiktorowicz, J. E., Haag, A. M., English, R. D., Soman, K. V. & Kurosky, A. 2009. Toward the proteome of the human peripheral blood eosinophil. *PROTEOMICS – Clinical Applications,* 3**,** 1151-1173.

Su, A. I., Guidotti, L. G., Pezacki, J. P., Chisari, F. V. & Schultz, P. G. 2002. Gene expression during the priming phase of liver regeneration after partial hepatectomy in mice. *Proc Natl Acad Sci U S A,* 99**,** 11181-6.

Sunagozaka, H., Honda, M., Yamashita, T., Nishino, R., Takatori, H., Arai, K., Yamashita, T., Sakai, Y. & Kaneko, S. 2011. Identification of a secretory protein c19orf10 activated in hepatocellular carcinoma. *Int J Cancer,* 129**,** 1576-85.

Tajima, H., Matsumoto, K. & Nakamura, T. 1991. Hepatocyte growth factor has potent anti-proliferative activity in various tumor cell lines. *FEBS Lett,* 291**,** 229-32.

Takagi, H., Sharp, R., Hammermeister, C., Goodrow, T., Bradley, M. O., Fausto, N. & Merlino, G. 1992. Molecular and genetic analysis of liver oncogenesis in transforming growth factor alpha transgenic mice. *Cancer Res,* 52**,** 5171-7.

Talarmin, H., Rescan, C., Cariou, S., Glaise, D., Zanninelli, G., Bilodeau, M., Loyer, P., Guguen-Guillouzo, C. & Baffet, G. 1999. The mitogen-activated protein kinase kinase/extracellular signal-regulated kinase cascade activation is a key signalling pathway involved in the regulation of G(1) phase progression in proliferating hepatocytes. *Mol Cell Biol,* 19**,** 6003-11.

Tao, Y., Wang, M., Chen, E. & Tang, H. 2017. Liver Regeneration: Analysis of the Main Relevant Signaling Molecules. *Mediators Inflamm,* 2017**,** 4256352.

Taub, R. 2004. Liver regeneration: from myth to mechanism. *Nat Rev Mol Cell Biol,* 5**,** 836-47.

Tesoriere, A., Dinarello, A. & Argenton, F. 2021. The Roles of Post-Translational Modifications in STAT3 Biological Activities and Functions. *Biomedicines,* 9.

Tomiya, T., Tani, M., Yamada, S., Hayashi, S., Umeda, N. & Fujiwara, K. 1992. Serum hepatocyte growth factor levels in hepatectomized and nonhepatectomized surgical patients. *Gastroenterology,* 103**,** 1621-4.

Trefts, E., Gannon, M. & Wasserman, D. H. 2017. The liver. *Curr Biol,* 27**,** R1147-R1151.

Tsuchida, T., Murata, S., Matsuki, K., Mori, A., Matsuo, M., Mikami, S., Okamoto, S., Ueno, Y., Tadokoro, T., Zheng, Y. W. & Taniguchi, H. 2019. The Regenerative Effect of Portal Vein Injection of Liver Organoids by Retrorsine/Partial Hepatectomy in Rats. *Int J Mol Sci,* 21.

Tulin, E. E., Onoda, N., Nakata, Y., Maeda, M., Hasegawa, M., Nomura, H. & Kitamura, T. 2001. SF20/IL-25, a novel bone marrow stroma-derived growth factor that binds to mouse thymic shared antigen-1 and supports lymphoid cell proliferation. *J Immunol,* 167**,** 6338-47.

Tulin, E. E., Onoda, N., Nakata, Y., Maeda, M., Hasegawa, M., Nomura, H. & Kitamura, T. 2003. SF20/IL-25, a novel bone marrow stroma-derived growth factor that binds to mouse thymic shared antigen-1 and supports lymphoid cell proliferation. *J Immunol,* 170**,** 1593.

Uehara, Y., Minowa, O., Mori, C., Shiota, K., Kuno, J., Noda, T. & Kitamura, N. 1995. Placental defect and embryonic lethality in mice lacking hepatocyte growth factor/scatter factor. *Nature,* 373**,** 702-5.

Urner, S., Kelly-Goss, M., Peirce, S. M. & Lammert, E. 2018. Mechanotransduction in Blood and Lymphatic Vascular Development and Disease. *Adv Pharmacol,* 81**,** 155-208.

Vekemans, K. & Braet, F. 2005. Structural and functional aspects of the liver and liver sinusoidal cells in relation to colon carcinoma metastasis. *World J Gastroenterol,* 11**,** 5095-102.

Vollmar, B. & Menger, M. D. 2009. The hepatic microcirculation: mechanistic contributions and therapeutic targets in liver injury and repair. *Physiol Rev,* 89**,** 1272-1275.

Wang, J., Ma, R., Wang, Y., Zhang, S., Wang, J., Zheng, J., Xue, W. & Ding, X. 2023. rhMYDGF Alleviates I/R-induced Kidney Injury by Inhibiting Inflammation and Apoptosis via the Akt Pathway. *Transplantation,* 107**,** 1729-1739.

Wang, L., Li, Y., Guo, B., Zhang, J., Zhu, B., Li, H., Ding, Y., Meng, B., Zhao, H., Xiang, L., Dong, J., Liu, M., Zhang, J., Xiang, L. & Xiang, G. 2020a. Myeloid-Derived Growth Factor Promotes Intestinal Glucagon-Like Peptide-1 Production in Male Mice With Type 2 Diabetes. *Endocrinology,* 161.

Wang, P., Mariman, E., Keijer, J., Bouwman, F., Noben, J. P., Robben, J. & Renes, J. 2004. Profiling of the secreted proteins during 3T3-L1 adipocyte differentiation leads to the identification of novel adipokines. *Cell Mol Life Sci,* 61**,** 2405-17.

Wang, S., Pacher, P., De Lisle, R. C., Huang, H. & Ding, W. X. 2016. A Mechanistic Review of Cell Death in Alcohol-Induced Liver Injury. *Alcohol Clin Exp Res,* 40**,** 1215-23.

Wang, X., Mao, J., Zhou, T., Chen, X., Tu, H., Ma, J., Li, Y., Ding, Y., Yang, Y., Wu, H. & Tang, X. 2021. Hypoxia-induced myeloid derived growth factor promotes hepatocellular carcinoma progression through remodeling tumor microenvironment. *Theranostics,* 11**,** 209-221.

Wang, Y., Li, Y., Feng, J., Liu, W., Li, Y., Liu, J., Yin, Q., Lian, H., Liu, L. & Nie, Y. 2020b. Mydgf promotes Cardiomyocyte proliferation and Neonatal Heart regeneration. *Theranostics,* 10**,** 9100-9112.

Wang, Y., Zhang, Y., Li, J., Zhao, R., Long, X., Li, C., Liu, W., Chen, W. & Shi, B. 2022. Role of Mydgf in the regulation of hypoxia/reoxygenation-induced apoptosis in cardiac microvascular endothelial cells. *In Vitro Cell Dev Biol Anim,* 58**,** 669-678.

Webber, E. M., Godowski, P. J. & Fausto, N. 1994. In vivo response of hepatocytes to growth factors requires an initial priming stimulus. *Hepatology,* 19**,** 489-97.

Weeraphan, C., Diskul-Na-Ayudthaya, P., Chiablaem, K., Khongmanee, A., Chokchaichamnankit, D., Subhasitanont, P., Svasti, J. & Srisomsap, C. 2012.

Effective enrichment of cholangiocarcinoma secretomes using the hollow fiber bioreactor culture system. *Talanta,* 99**,** 294-301.

Weiler, T., Du, Q., Krokhin, O., Ens, W., Standing, K., El-Gabalawy, H. & Wilkins, J. A. 2007. The identification and characterization of a novel protein, c19orf10, in the synovium. *Arthritis Res Ther,* 9**,** R30.

Wen, X., Jiao, L. & Tan, H. 2022. MAPK/ERK Pathway as a Central Regulator in Vertebrate Organ Regeneration. *Int J Mol Sci,* 23.

Wen, Z., Zhong, Z. & Darnell, J. E. 1995. Maximal activation of transcription by statl and stat3 requires both tyrosine and serine phosphorylation. *Cell,* 82**,** 241-250.

Wisse, E. 1970. An electron microscopic study of the fenestrated endothelial lining of rat liver sinusoids. *J Ultrastruct Res,* 31**,** 125-50.

Worsdorfer, P., Dalda, N., Kern, A., Kruger, S., Wagner, N., Kwok, C. K., Henke, E. & Ergun, S. 2019. Generation of complex human organoid models including vascular networks by incorporation of mesodermal progenitor cells. *Sci Rep,* 9**,** 15663.

Xie, G., Song, Y., Li, N., Zhang, Z., Wang, X., Liu, Y., Jiao, S., Wei, M., Yu, B., Wang, Y., Wang, H. & Qu, A. 2022. Myeloid peroxisome proliferator-activated receptor alpha deficiency accelerates liver regeneration via IL-6/STAT3 pathway after 2/3 partial hepatectomy in mice. *Hepatobiliary Surg Nutr,* 11**,** 199-211.

Xu, J., Ma, H., Shi, L., Zhou, H., Cheng, Y., Tong, J., Meng, B., Xu, X., He, K., Ding, S., Zhang, J., Yue, L. & Xiang, G. 2023a. Inflammatory Cell-Derived MYDGF Attenuates Endothelial LDL Transcytosis to Protect Against Atherogenesis. *Arterioscler Thromb Vasc Biol,* 43**,** e443-e467.

Xu, J., Song, Y., Ding, S., Duan, W., Xiang, G. & Wang, Z. 2023b. Myeloid-derived growth factor and its effects on cardiovascular and metabolic diseases. *Cytokine Growth Factor Rev*.

Xu, X., Li, Y., Shi, L., He, K., Sun, Y., Ding, Y., Meng, B., Zhang, J., Xiang, L., Dong, J., Liu, M., Zhang, J., Xiang, L. & Xiang, G. 2022. Myeloid-derived growth factor (MYDGF) protects bone mass through inhibiting osteoclastogenesis and promoting osteoblast differentiation. *EMBO Rep,* 23**,** e53509.

Xue, F., Takahara, T., Yata, Y., Kuwabara, Y., Shinno, E., Nonome, K., Minemura, M., Takahara, S., Li, X., Yamato, E. & Watanabe, A. 2003. Hepatocyte growth factor gene therapy accelerates regeneration in cirrhotic mouse livers after hepatectomy. *Gut,* 52**,** 694-700.

Yagi, S., Hirata, M., Miyachi, Y. & Uemoto, S. 2020. Liver Regeneration after Hepatectomy and Partial Liver Transplantation. *Int J Mol Sci,* 21.

Yamaguchi, H. & Wang, H. G. 2001. The protein kinase PKB/Akt regulates cell survival and apoptosis by inhibiting Bax conformational change. *Oncogene,* 20**,** 7779-86.

Yanagita, K., Nagaike, M., Ishibashi, H., Niho, Y., Matsumoto, K. & Nakamura, T. 1992. Lung may have an endocrine function producing hepatocyte growth factor in response to injury of distal organs. *Biochem Biophys Res Commun,* 182**,** 802-9.

Yang, S., Li, H. W., Tian, J. Y., Wang, Z. K., Chen, Y., Zhan, T. T., Ma, C. Y., Feng, M., Cao, S. F., Zhao, Y., Li, X., Ren, J., Liu, Q., Jin, L. Y., Wang, Z. Q., Jiang, W. Y., Zhao, Y. X., Zhang, Y. & Liu, X. 2023. Myeloid-derived growth factor suppresses VSMC dedifferentiation and attenuates postinjury neointimal formation in rats by activating S1PR2 and its downstream signaling. *Acta Pharmacol Sin*.

Yu, Z., Kastenmuller, G., He, Y., Belcredi, P., Moller, G., Prehn, C., Mendes, J., Wahl, S., Roemisch-Margl, W., Ceglarek, U., Polonikov, A., Dahmen, N., Prokisch, H., Xie, L., Li, Y., Wichmann, H. E., Peters, A., Kronenberg, F., Suhre, K., Adamski, J., Illig, T. & Wang-Sattler, R. 2011. Differences between human plasma and serum metabolite profiles. *PLoS One,* 6**,** e21230.

Zarnegar, R., Defrances, M. C., Kost, D. P., Lindroos, P. & Michalopoulos, G. K. 1991. Expression of hepatocyte growth factor mRNA in regenerating rat liver after partial hepatectomy. *Biochem Biophys Res Commun,* 177**,** 559-65.

Zeilinger, K., Freyer, N., Damm, G., Seehofer, D. & Knospel, F. 2016. Cell sources for in vitro human liver cell culture models. *Exp Biol Med (Maywood),* 241**,** 1684-98.

Zerrad-Saadi, A., Lambert-Blot, M., Mitchell, C., Bretes, H., Collin De L'hortet, A., Baud, V., Chereau, F., Sotiropoulos, A., Kopchick, J. J., Liao, L., Xu, J., Gilgenkrantz, H. & Guidotti, J. E. 2011. GH receptor plays a major role in liver regeneration through the control of EGFR and ERK1/2 activation. *Endocrinology,* 152**,** 2731-41.

Zhan, P., Zhang, Y., Shi, W., Liu, X., Qiao, Z., Wang, Z., Wang, X., Wu, J., Tang, W., Sun, Y., Zhang, Y., Zhen, J., Shang, J., Liu, M. & Yi, F. 2022. Myeloid-derived growth factor deficiency exacerbates mitotic catastrophe of podocytes in glomerular disease. *Kidney Int,* 102**,** 546-559.

Zhang, H., Pu, W., Tian, X., Huang, X., He, L., Liu, Q., Li, Y., Zhang, L., He, L., Liu, K., Gillich, A. & Zhou, B. 2016. Genetic lineage tracing identifies endocardial origin of liver vasculature. *Nat Genet,* 48**,** 537-43.

Zhang, W. & Liu, H. T. 2002. MAPK signal pathways in the regulation of cell proliferation in mammalian cells. *Cell Res,* 12**,** 9-18.

Zhang, X. J., Olsavszky, V., Yin, Y., Wang, B., Engleitner, T., Ollinger, R., Schledzewski, K., Koch, P. S., Rad, R., Schmid, R. M., Friess, H., Goerdt, S., Huser, N., Geraud, C., Von Figura, G. & Hartmann, D. 2020. Angiocrine Hepatocyte Growth Factor Signaling Controls Physiological Organ and Body Size and Dynamic Hepatocyte Proliferation to Prevent Liver Damage during Regeneration. *Am J Pathol,* 190**,** 358-371.

Zhao, L., Feng, S., Wang, S., Fan, M., Jin, W., Li, X., Wang, C. & Yang, Y. 2020. Production of bioactive recombinant human myeloid-derived growth factor in Escherichia coli and its mechanism on vascular endothelial cell proliferation. *J Cell Mol Med,* 24**,** 1189-1199.

Zhao, Y., Ye, W., Wang, Y.-D. & Chen, W.-D. 2022. HGF/c-Met: A Key Promoter in Liver Regeneration. *Frontiers in Pharmacology,* 13.

9. Supplementary information

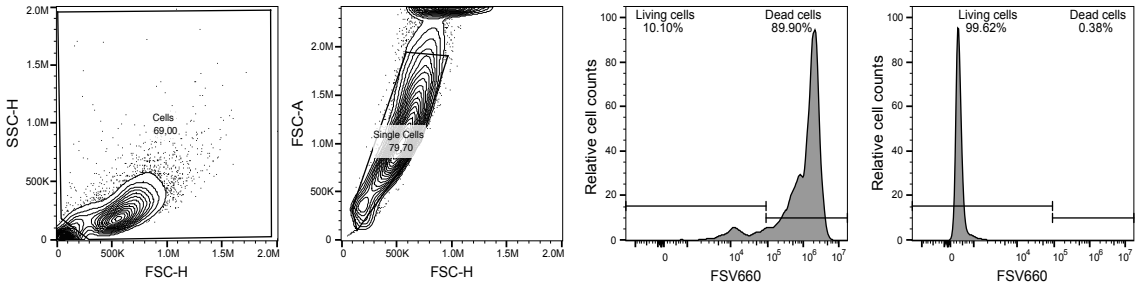

Supplementary Figure 1: Gating criteria for flow cytometric analysis related to Figure 5.

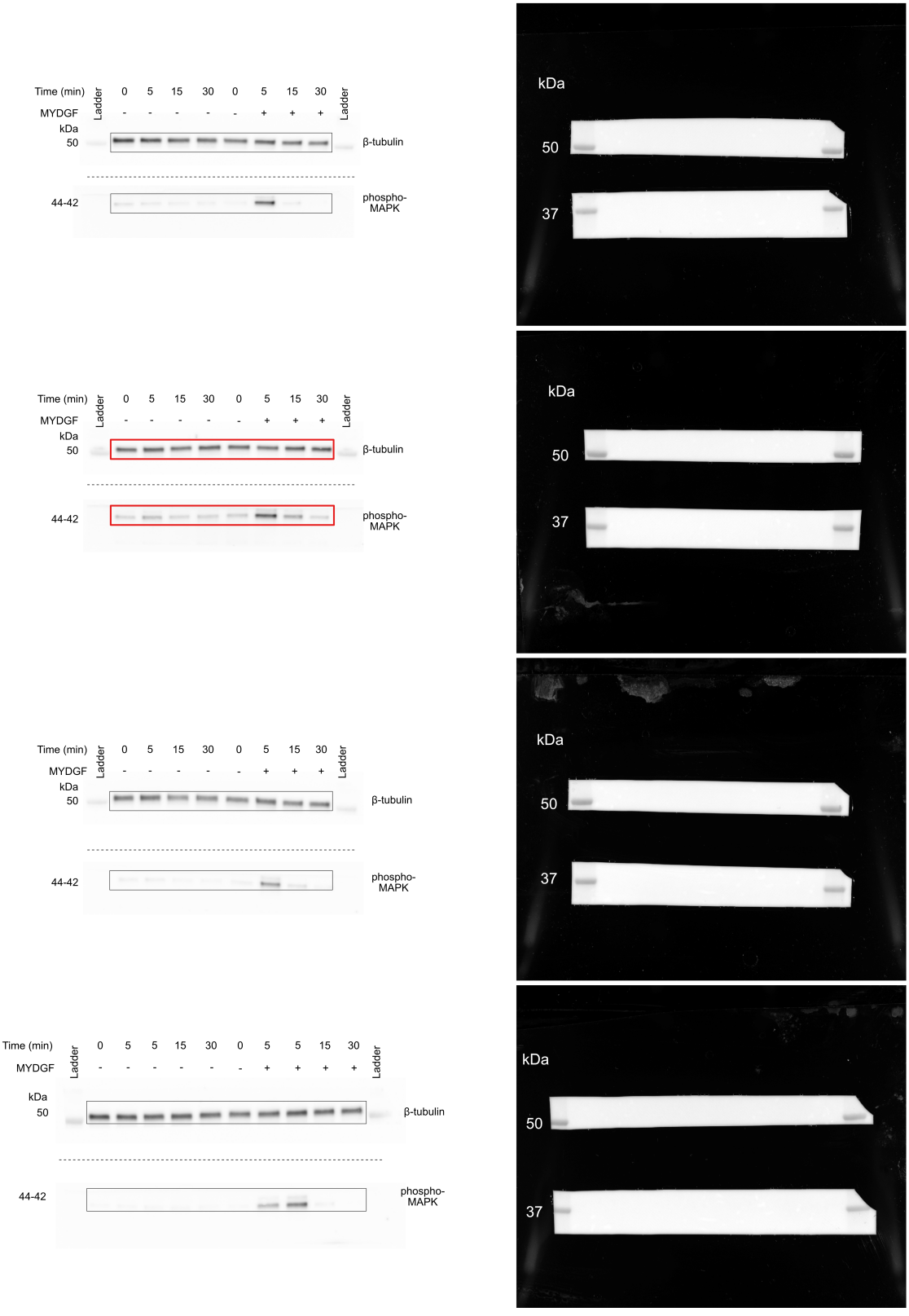

Supplementary Figure 2: Uncropped Western blots plus colorimetric images related to Figure 11a, b.
Detected proteins and molecular weights in kilodalton (kDa) are shown, and bands marked with black boxes were used for analysis, while bands additionally marked with a red box are shown in the figure.

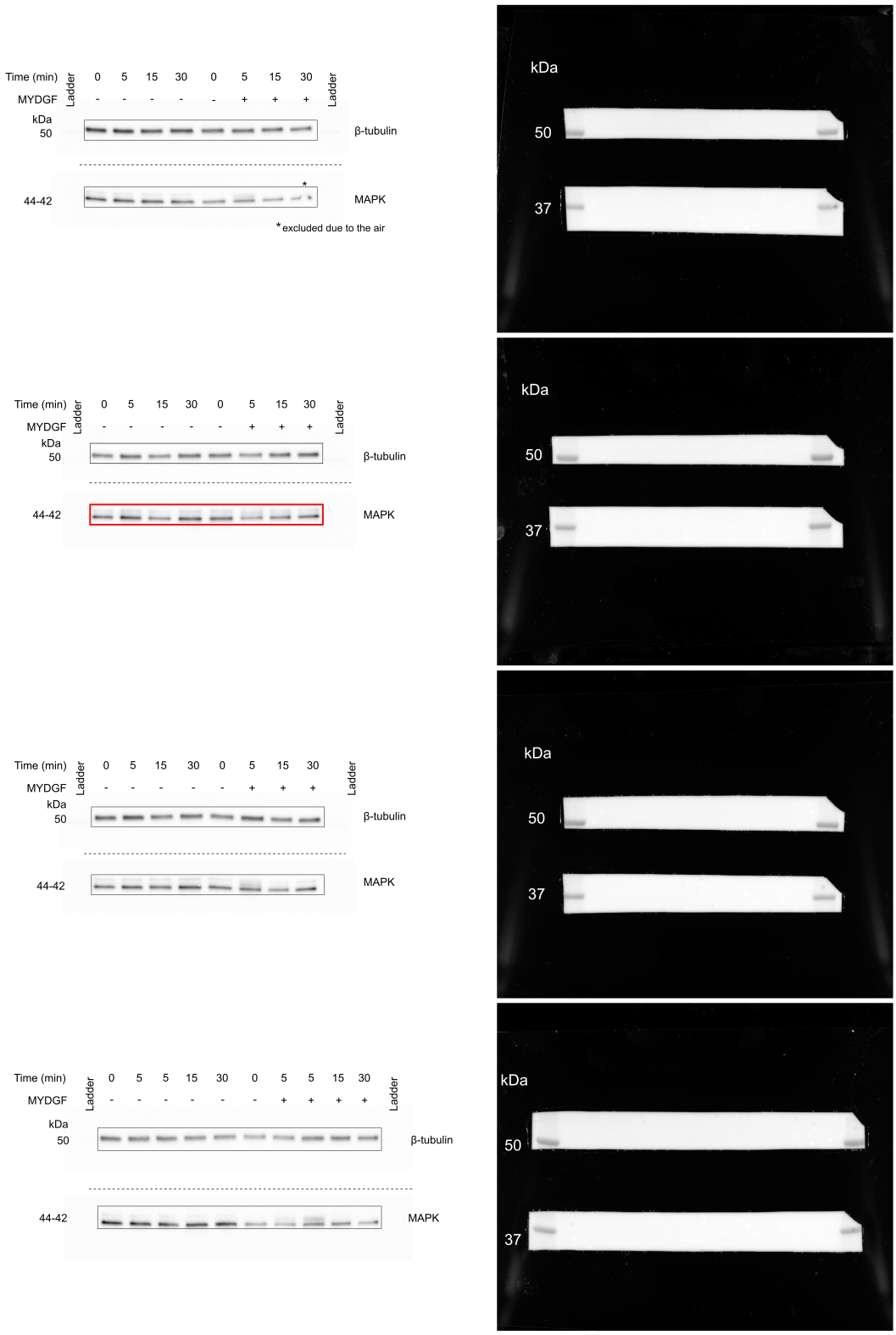

Supplementary Figure 3: Uncropped Western blots plus colorimetric images related to Figure 11a, b.
Detected proteins and molecular weights in kilodalton (kDa) are shown, and bands marked with black boxes were used for analysis, while bands additionally marked with a red box are shown in the figure.

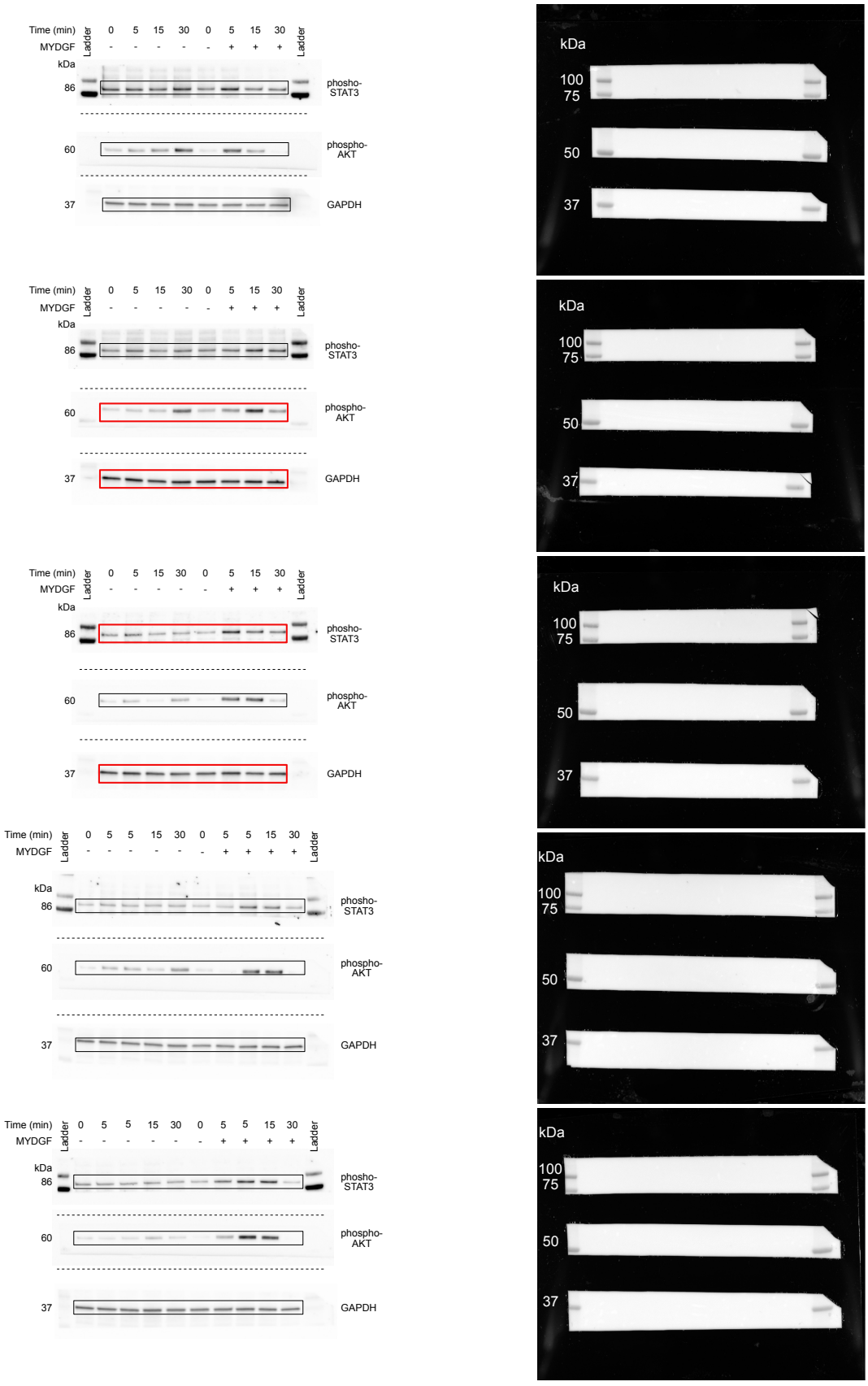

Supplementary Figure 4: Uncropped Western blots plus colorimetric images related to Figure 11c-f.
Detected proteins and molecular weights in kilodalton (kDa) are shown, and bands marked with black boxes were used for analysis, while bands additionally marked with a red box are shown in the figure.

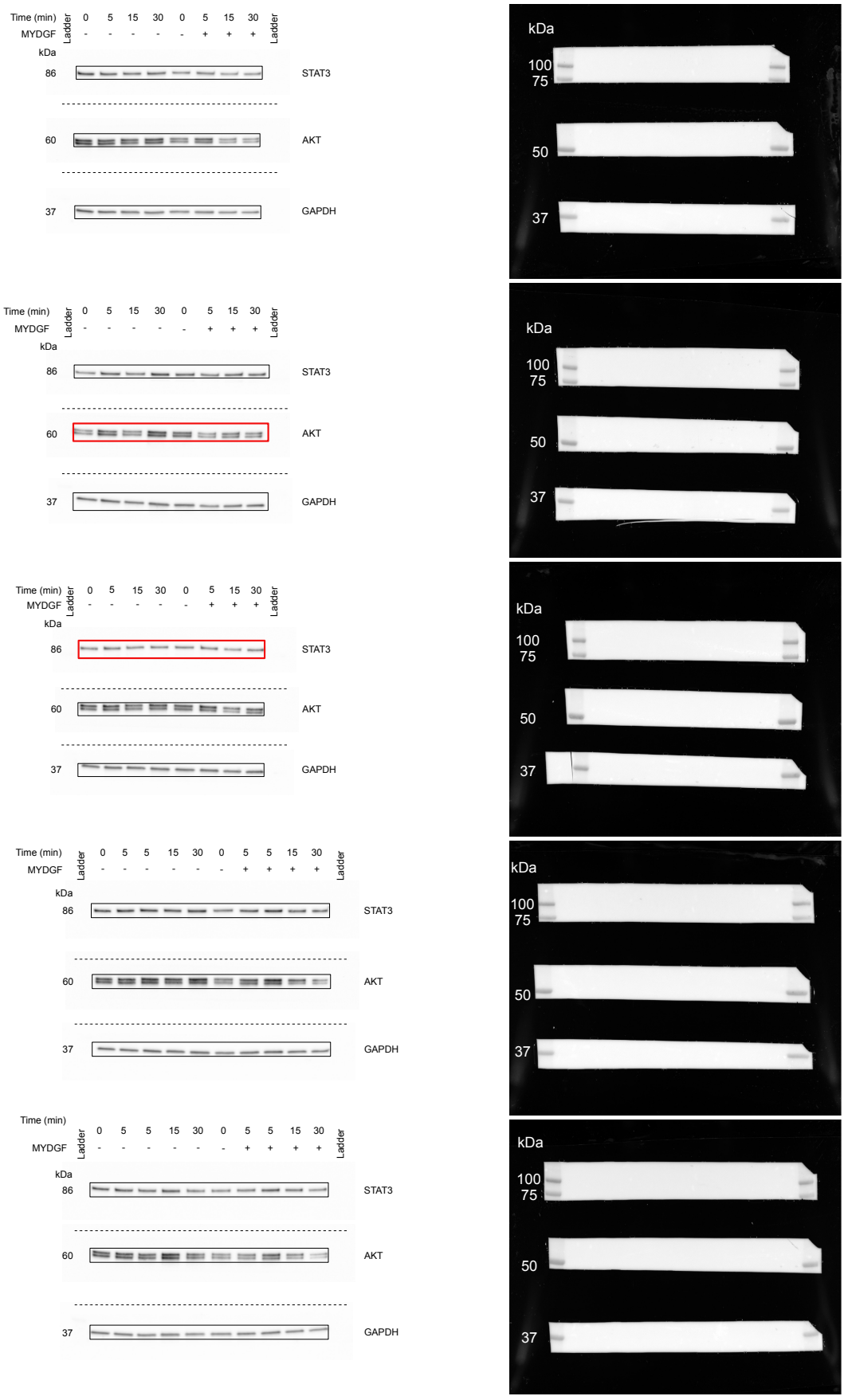

Supplementary Figure 5: Uncropped Western blots plus colorimetric images related to Figure 11c-f.
Detected proteins and molecular weights in kilodalton (kDa) are shown, and bands marked with black boxes were used for analysis, while bands additionally marked with a red box are shown in the figure.

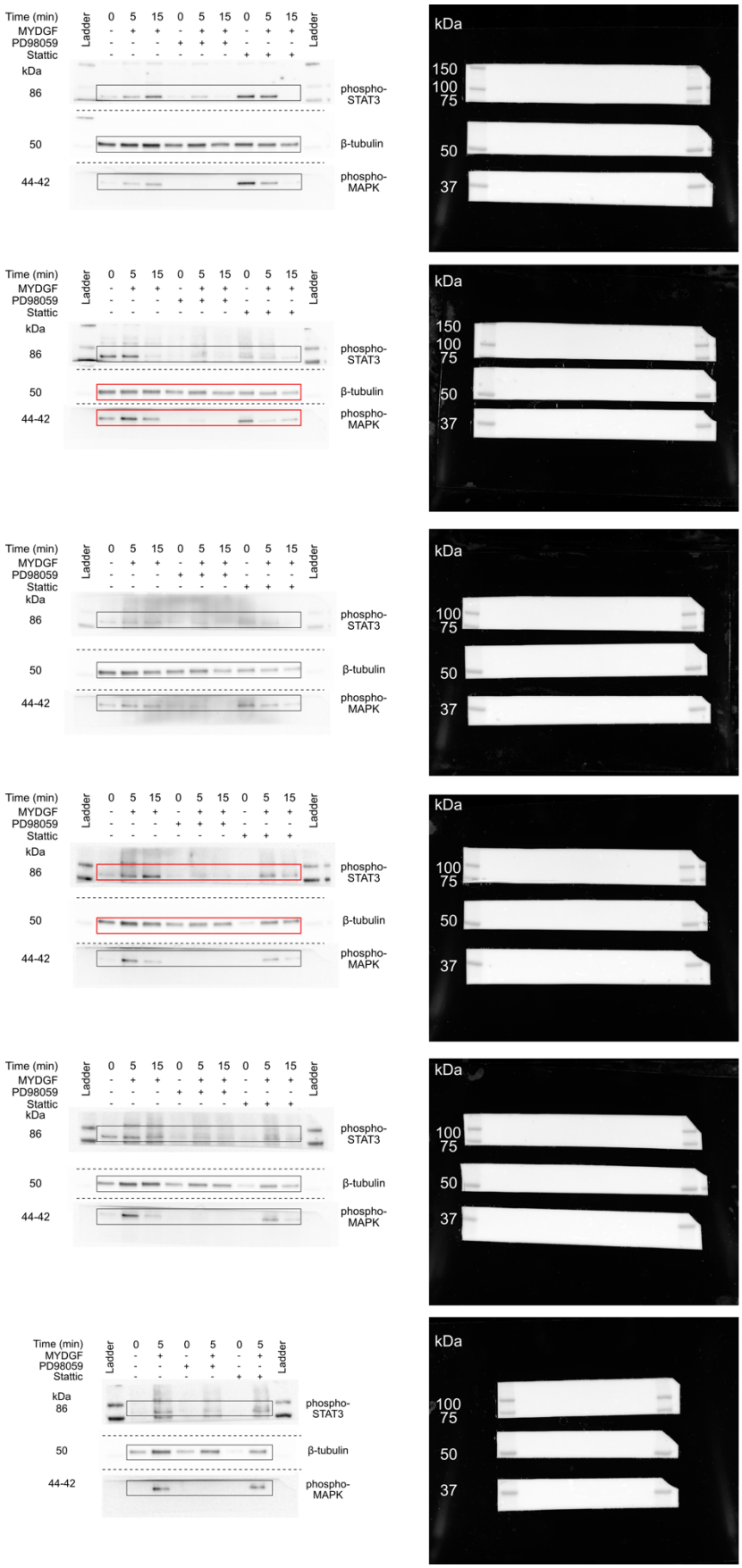

Supplementary Figure 6: Uncropped Western blots plus colorimetric images related to Figure 12.
Detected proteins and molecular weights in kilodalton (kDa) are shown, and bands marked with black boxes were used for analysis, while bands additionally marked with a red box are shown in the figure.

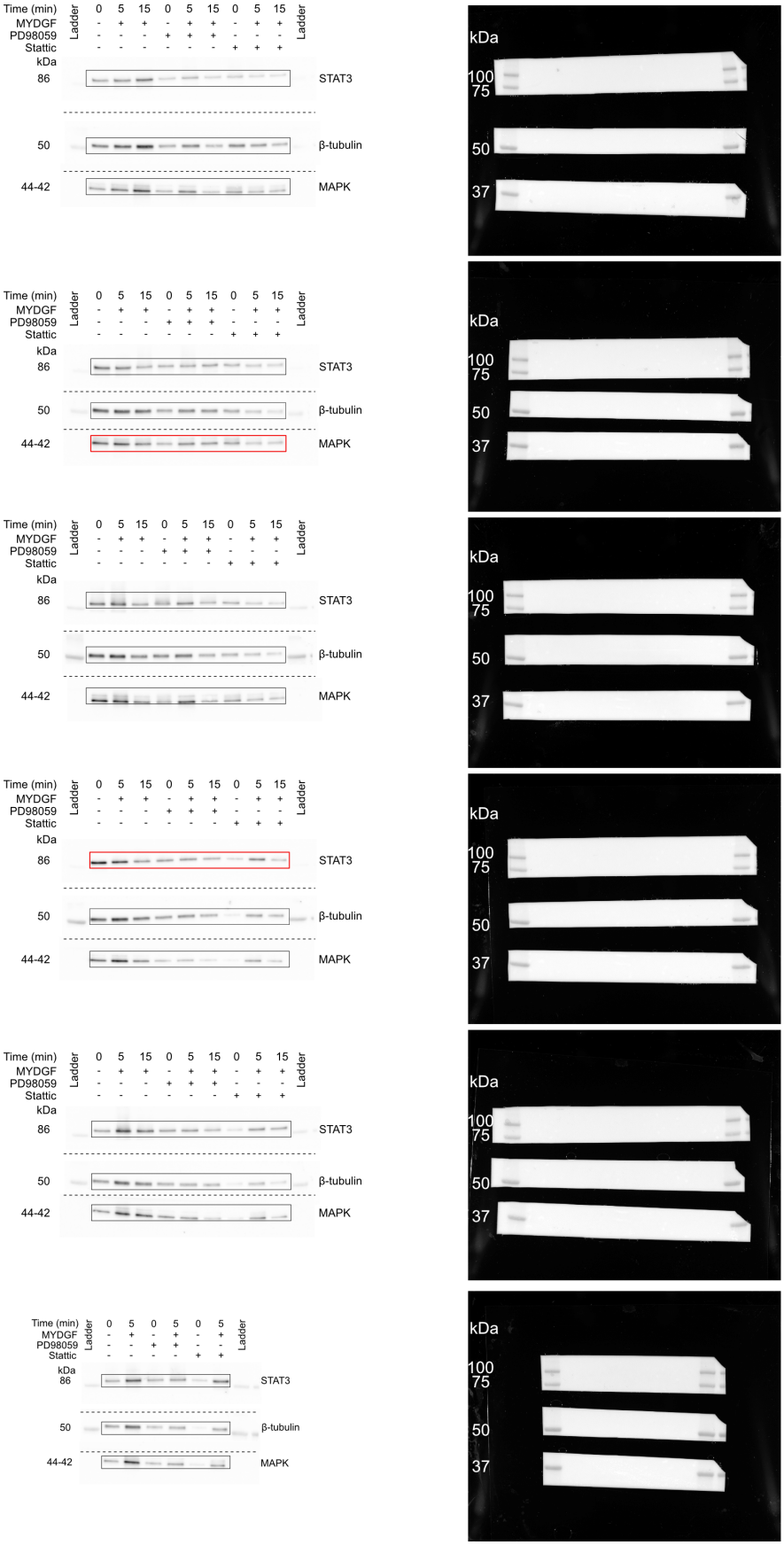

Supplementary Figure 7: Uncropped Western blots plus colorimetric images related to Figure 12.
Detected proteins and molecular weights in kilodalton (kDa) are shown, and bands marked with black boxes were used for analysis, while bands additionally marked with a red box are shown in the figure.

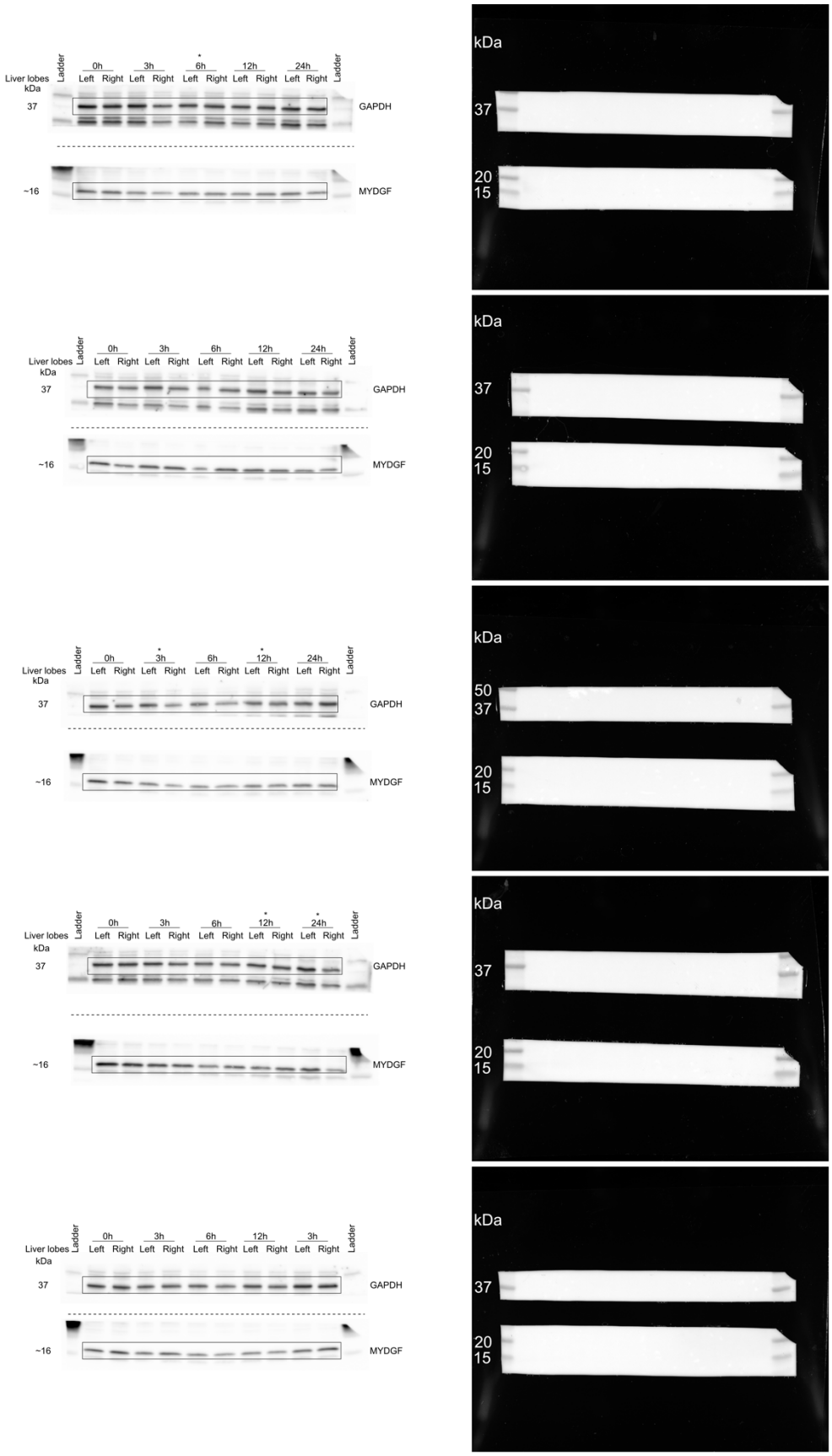

*Mice with improperly perfused (light brown) livers and hemorrhages in the livers were excluded from further analysis.

Supplementary Figure 8: Uncropped Western blots plus colorimetric images related to Figure 15b.
Detected proteins and molecular weights in kilodalton (kDa) are shown, and bands marked with black boxes were used for analysis.

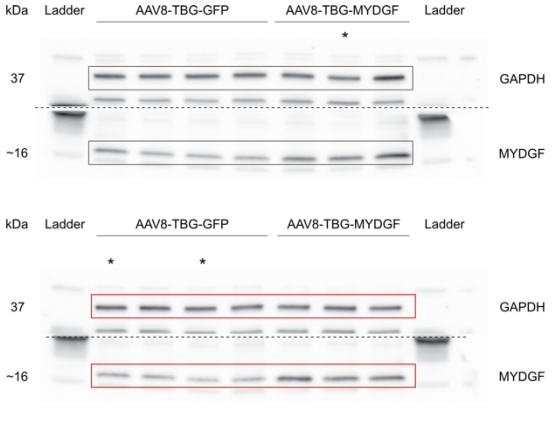

*Mice with improperly perfused (light brown) livers and hemorrhages in the livers were excluded from further analysis.

Supplementary Figure 9: Uncropped Western blots plus colorimetric images related to Figure 18.
Detected proteins and molecular weights in kilodalton (kDa) are shown, and bands marked with black boxes were used for analysis, while bands additionally marked with a red box are shown in the figure.

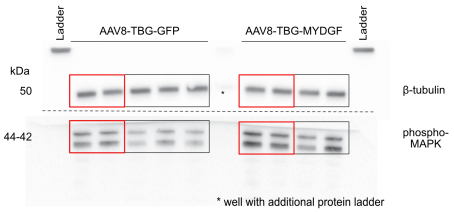

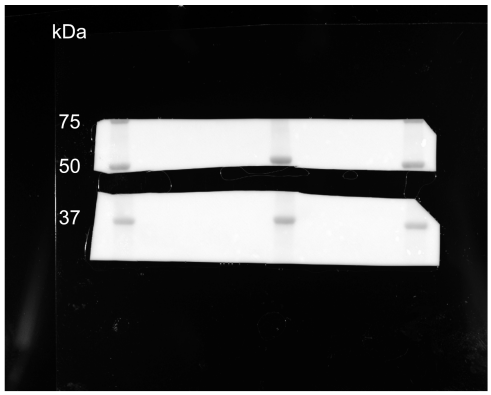

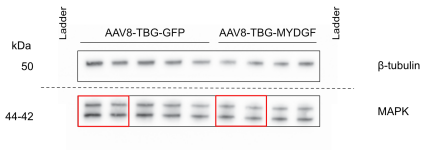

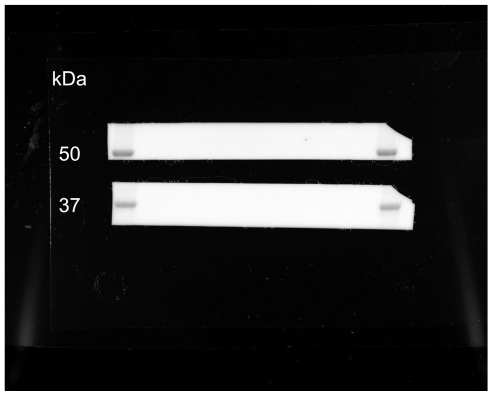

Supplementary Figure 10: Uncropped Western blots plus colorimetric images related to Figure 22a.
Detected proteins and molecular weights in kilodalton (kDa) are shown, and bands marked with black boxes were used for analysis, while bands additionally marked with a red box are shown in the figure.

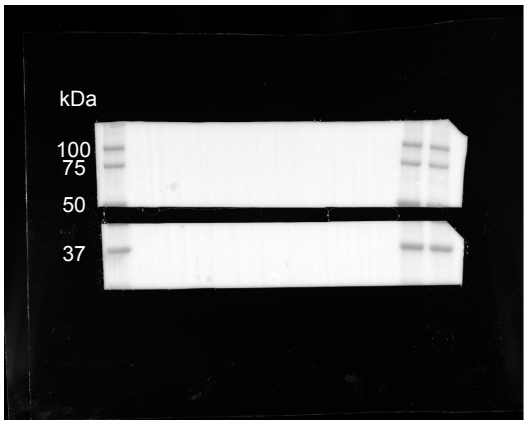

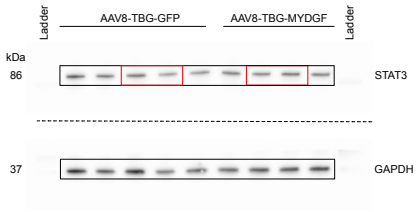

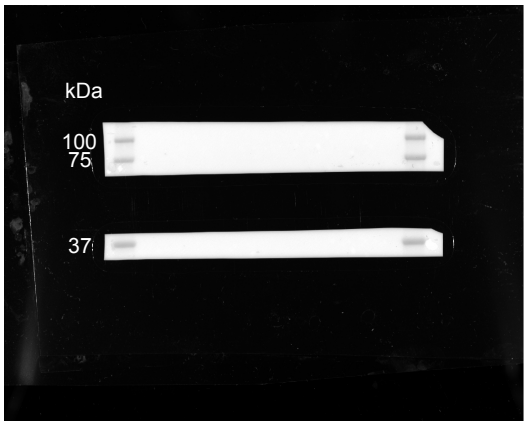

Supplementary Figure 11: Uncropped Western blots plus colorimetric images related to Figure 22b.
Detected proteins and molecular weights in kilodalton (kDa) are shown and bands marked with black boxes were used for analysis, while bands additionally marked with a red box are shown in the figure.

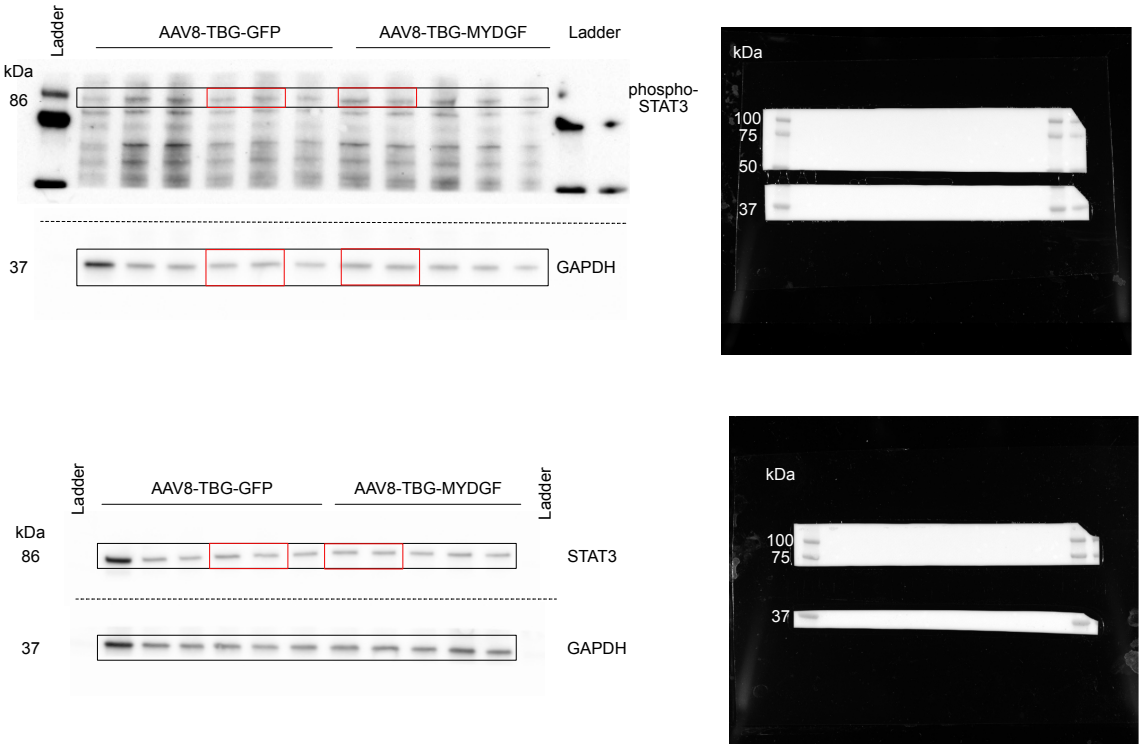

Supplementary Figure 12: Uncropped Western blots plus colorimetric images related to Figure 22c.
Detected proteins and molecular weights in kilodalton (kDa) are shown, and bands marked with black boxes were used for analysis, while bands additionally marked with a red box are shown in the figure.

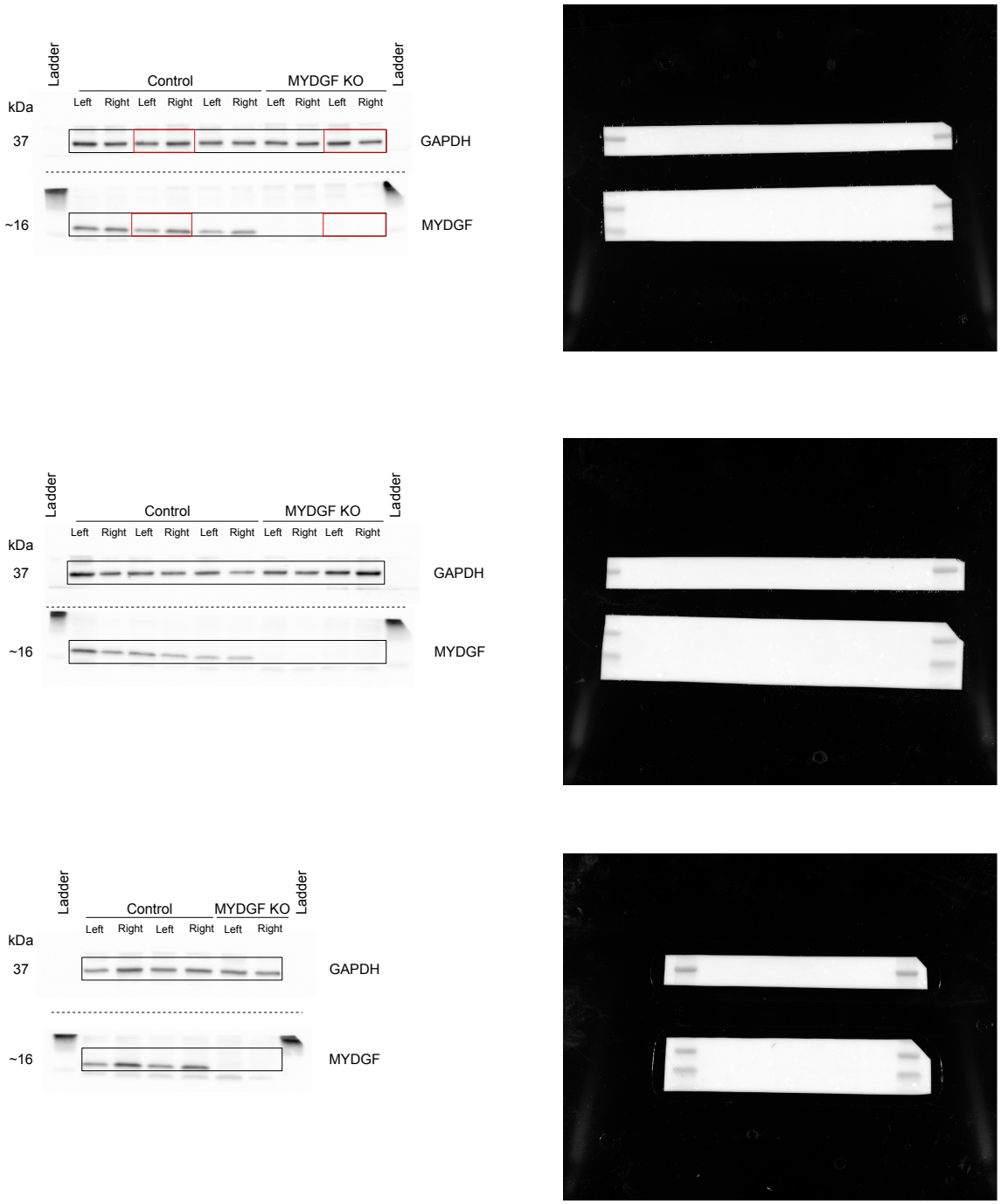

Supplementary Figure 13: Uncropped Western blots plus colorimetric images related to Figure 23.
Detected proteins and molecular weights in kilodalton (kDa) are shown, and bands marked with black boxes were used for analysis, while bands additionally marked with a red box are shown in the figure.

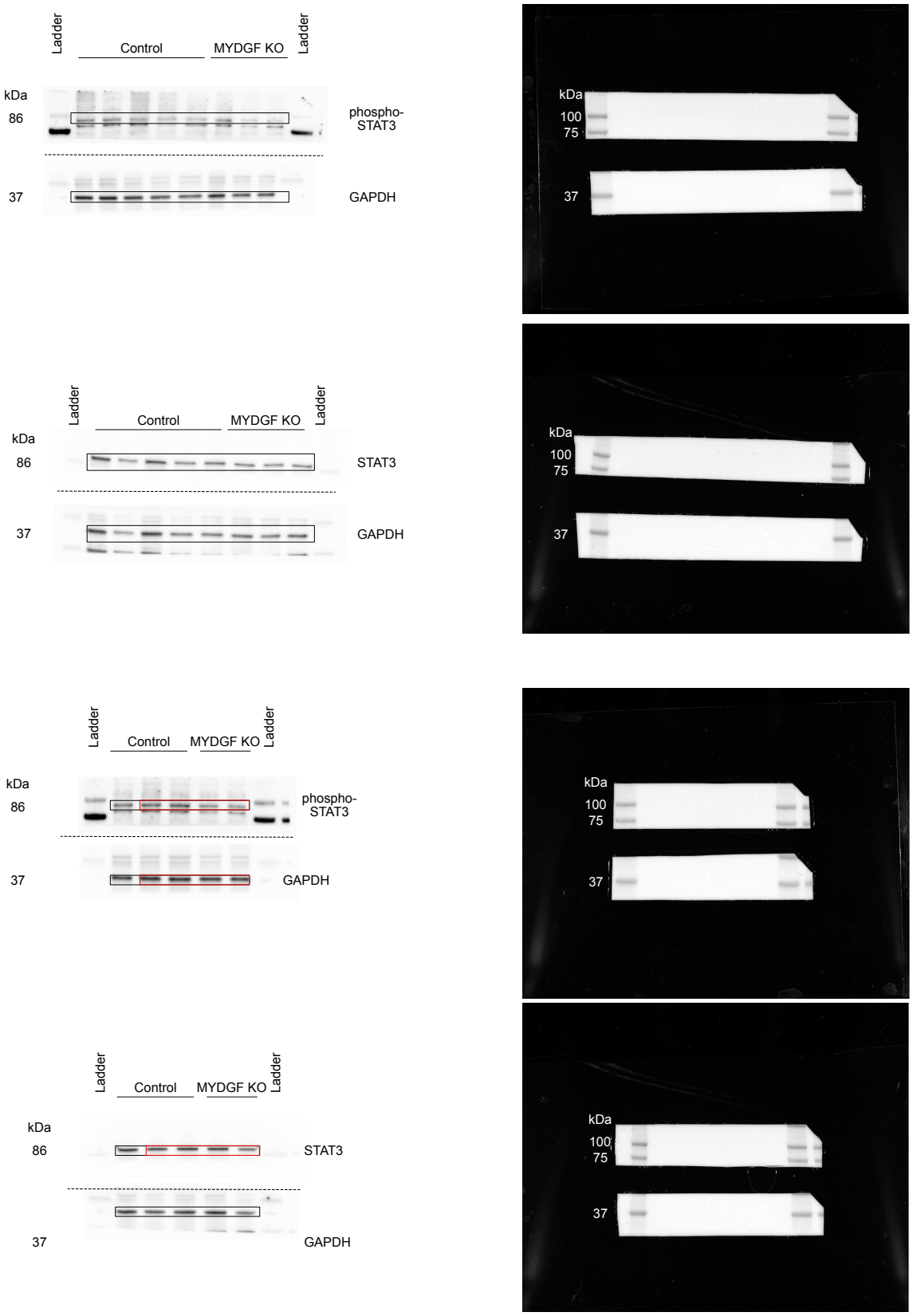

Supplementary Figure 14: Uncropped Western blots plus colorimetric images related to Figure 26.
Detected proteins and molecular weights in kilodalton (kDa) are shown, and bands marked with black boxes were used for analysis, while bands additionally marked with a red box are shown in the figure.

10. Publication licenses

49 Spadina Ave. Suite 200
Toronto ON M5V 2J1 Canada
www.biorender.com

Confirmation of Publication and Licensing Rights

March 12th, 2024
Science Suite Inc.

Subscription:	*Student Plan*
Agreement number:	*YI26KG38DI*
Journal name:	*PhD thesis Paula Follert Heinrich Heine University*

To whom this may concern,

This document is to confirm that Paula Follert has been granted a license to use the BioRender content, including icons, templates and other original artwork, appearing in the attached completed graphic pursuant to BioRender's Academic License Terms. This license permits BioRender content to be sublicensed for use in journal publications.

All rights and ownership of BioRender content are reserved by BioRender. All completed graphics must be accompanied by the following citation: "Created with BioRender.com".

BioRender content included in the completed graphic is not licensed for any commercial uses beyond publication in a journal. For any commercial use of this figure, users may, if allowed, recreate it in BioRender under an Industry BioRender Plan.

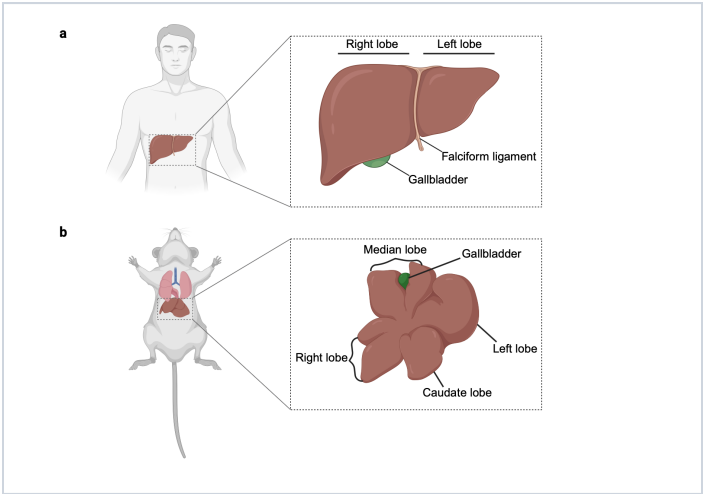

For any questions regarding this document, or other questions about publishing with BioRender refer to our BioRender Publication Guide, or contact BioRender Support at support@biorender.com.

Publication license for Figure 1

49 Spadina Ave. Suite 200
Toronto ON M5V 2J1 Canada
www.biorender.com

Confirmation of Publication and Licensing Rights

March 21st, 2024
Science Suite Inc.

Subscription:	*Student Plan*
Agreement number:	*KP26LP4A2H*
Journal name:	*PhD thesis Paula Follert Heinrich Heine University*

To whom this may concern,

This document is to confirm that Paula Follert has been granted a license to use the BioRender content, including icons, templates and other original artwork, appearing in the attached completed graphic pursuant to BioRender's Academic License Terms. This license permits BioRender content to be sublicensed for use in journal publications.

All rights and ownership of BioRender content are reserved by BioRender. All completed graphics must be accompanied by the following citation: "Created with BioRender.com".

BioRender content included in the completed graphic is not licensed for any commercial uses beyond publication in a journal. For any commercial use of this figure, users may, if allowed, recreate it in BioRender under an Industry BioRender Plan.

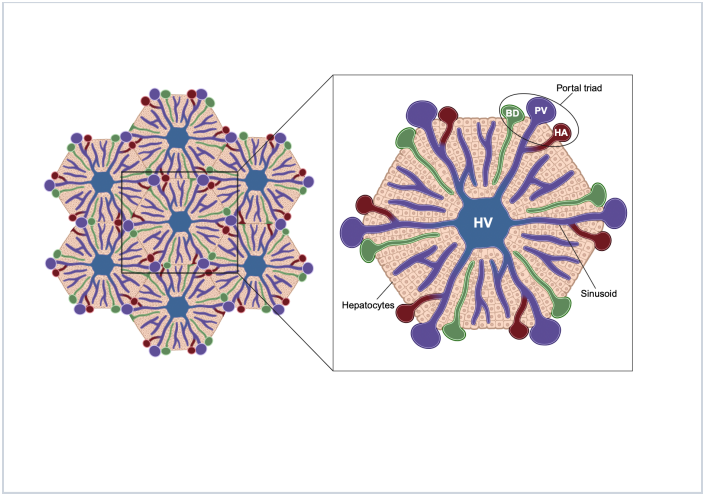

For any questions regarding this document, or other questions about publishing with BioRender refer to our BioRender Publication Guide, or contact BioRender Support at support@biorender.com.

Publication license for Figure 2

49 Spadina Ave. Suite 200
Toronto ON M5V 2J1 Canada
www.biorender.com

Confirmation of Publication and Licensing Rights

March 22nd, 2024
Science Suite Inc.

Subscription:	*Student Plan*
Agreement number:	*FI26LUM0E7*
Journal name:	*PhD thesis Paula Follert Heinrich Heine University*

To whom this may concern,

This document is to confirm that Paula Follert has been granted a license to use the BioRender content, including icons, templates and other original artwork, appearing in the attached completed graphic pursuant to BioRender's Academic License Terms. This license permits BioRender content to be sublicensed for use in journal publications.

All rights and ownership of BioRender content are reserved by BioRender. All completed graphics must be accompanied by the following citation: "Created with BioRender.com".

BioRender content included in the completed graphic is not licensed for any commercial uses beyond publication in a journal. For any commercial use of this figure, users may, if allowed, recreate it in BioRender under an Industry BioRender Plan.

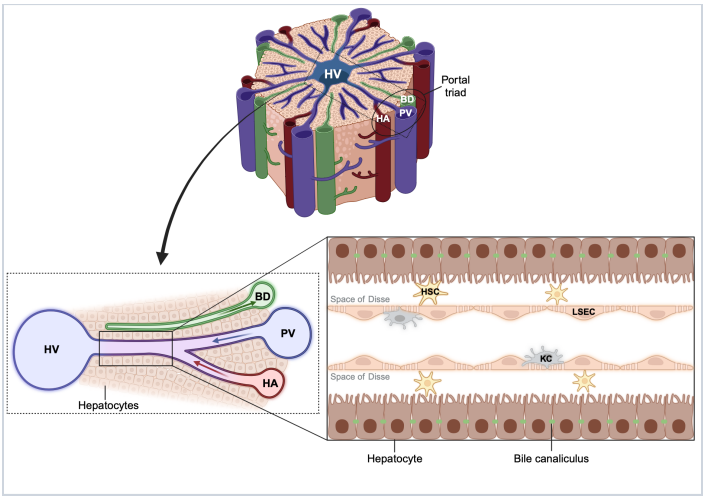

For any questions regarding this document, or other questions about publishing with BioRender refer to our BioRender Publication Guide, or contact BioRender Support at support@biorender.com.

Publication license for Figure 3

49 Spadina Ave. Suite 200
Toronto ON M5V 2J1 Canada
www.biorender.com

Confirmation of Publication and Licensing Rights

March 18th, 2024
Science Suite Inc.

Subscription:	*Student Plan*
Agreement number:	*UJ26L9QOHK*
Journal name:	*PhD thesis Paula Follert Heinrich Heine University*

To whom this may concern,

This document is to confirm that Paula Follert has been granted a license to use the BioRender content, including icons, templates and other original artwork, appearing in the attached completed graphic pursuant to BioRender's Academic License Terms. This license permits BioRender content to be sublicensed for use in journal publications.

All rights and ownership of BioRender content are reserved by BioRender. All completed graphics must be accompanied by the following citation: "Created with BioRender.com".

BioRender content included in the completed graphic is not licensed for any commercial uses beyond publication in a journal. For any commercial use of this figure, users may, if allowed, recreate it in BioRender under an Industry BioRender Plan.

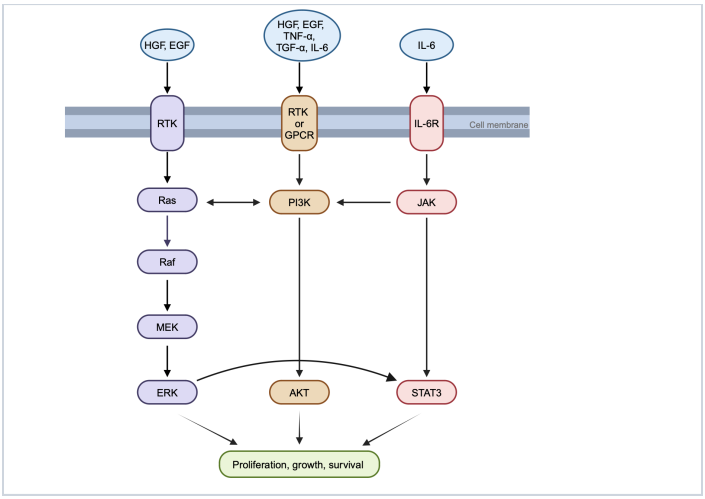

For any questions regarding this document, or other questions about publishing with BioRender refer to our BioRender Publication Guide, or contact BioRender Support at support@biorender.com.

Publication license for Figure 4

11. Acknowledgment

Zuerst möchte ich mich ganz herzlich bei meinem Doktorvater Prof. Dr. Eckhard Lammert bedanken. Vielen Dank Ecki, dass du mir die Möglichkeit gegeben hast meine Promotion bei dir im Labor zu absolvieren. Danke, dass du mir während meiner gesamten Promotionszeit immer mit deinen Ratschlägen zur Seite standest und mich in allen Situationen unterstützt hast.

Vielen Dank auch an Prof. Dr. Axel Gödecke, dass er sich als Zweitgutachter meiner Arbeit angenommen hat. Danke Axel für die tolle Zeit bei dir im IRTG 1902 und, dass du immer für uns alle ein offenes Ohr hattest!

Auch ein herzliches Dankeschön an Sandra, Janett und Kathryn für die tolle Organisation des IRTG's 1902!

Zudem möchte ich mich bei dem ganzen jetzigen und ehemaligen Lab-Lammert Team für die tolle gemeinsame Zeit bedanken! Ihr seid ein wirklich tolles Team und es macht jeden Tag aufs Neue Spaß zur Arbeit zu kommen.
Esther, dir möchte ich zudem für deine organisatorische Hilfe danken!

Daniel, dir gilt ein besonders Dankeschön für deine großzügige Hilfsbereitschaft und die wissenschaftliche Unterstützung während meiner gesamten Promotion.

Andrea und Barbara, vielen Dank, dass ihr mich beim Picken der zahlreichen Organoide immer tatkräftig unterstützt habt! Silke, dir vielen Dank für deine technische Unterstützung bei den Tieren!

Linda, bei dir möchte ich mich vor allem ganz herzlich für die tolle gemeinsame Zusammenarbeit bedanken! Danke, dass ich Teil deines Herzensprojektes werden durfte und dieses auch zu meinem wurde.

Philip und Sydney bei euch möchte ich mich für die vielen gemeinsamen wissenschaftlichen und nicht-wissenschaftlichen Diskussion innerhalb, sowie außerhalb des Labors bedanken, die meinen Arbeitsalltag immer sehr bereichert haben!
Danke, dass ihr mich immer unterstützt!

Auch bei meinen Freunden, die mich während meines gesamten Studiums begleitet haben, möchte ich mich bedanken! Besonders dir Stephan möchte ich für die vielen tollen Jahre der gemeinsamen Freundschaft danken! Das gemeinsame Studium hat diese Freundschaft erst ermöglicht!

Zudem möchte ich bei meiner Schwester Antonia Follert für das Anhören unzähliger wissenschaftlicher Probleme und den tollen mentalen Support in den letzten Jahren bedanken. Du bist eine wundervolle Schwester!

Vor allem möchte ich mich auch ganz herzlich bei meinem Freund Dennis Monßen für die liebevolle Unterstützung während meiner Promotionszeit bedanken! Danke, dass du alle Höhen und Tiefen mit mir durchgestanden hast und immer für mich da warst. Ohne Dich hätte ich die ein oder andere Situation und mentale Krise bestimmt nicht so gut meistern können!

Zum Schluss möchte ich mich aus tiefstem Herzen bei meinen Eltern Harald Reiterer und Rita Follert bedanken. Vielen Dank, dass ihr es mir ermöglicht habt dieses Studium zu absolvieren und immer an mich geglaubt habt!
Ihr seid die besten und liebevollsten Eltern die man sich nur wünschen kann!

12. Declaration

Ich, Paula Follert, versichere an Eides statt, dass die vorliegende Dissertation von mir selbstständig und ohne unzulässige fremde Hilfe unter Beachtung der „Grundsätze zur Sicherung guter wissenschaftlicher Praxis an der Heinrich-Heine-Universität Düsseldorf“ erstellt worden ist.

Düsseldorf, 26. März 2024 Paula Follert